NATIONAL TRANSPORTATION SAFETY BOARD

Office of Research and Engineering
Materials Laboratory Division
Washington, D.C. 20594

July 26, 2022

MATERIALS LABORATORY FACTUAL REPORT Report No. 20-062

A. ACCIDENT INFORMATION

Place	:	Camp Dwyer, Afghanistan
Date	:	April 20, 2020
Vehicle	:	Sikorsky S-61N, N908CH
NTSB No.	:	DCA20LA100
Investigator	:	Dan Bower, AS-10

B. COMPONENTS EXAMINED

Five fractured composite main rotor blades

C. DETAILS OF THE EXAMINATION

On 20 April 2020, at approximately 0800 local time, a Sikorsky S-61N, N908CH, experienced a loss of control in flight and rolled on its side during an emergency landing at Camp Dwyer, Afghanistan. The three crew members onboard were seriously injured, and the helicopter sustained substantial damage. The flight was operating under the provisions of 14 CFR Part 135 as a cargo flight under contract to the Department of Defense.

In accordance with ICAO Annex 13, the National Transportation Safety Board (NTSB) accepted delegation of the investigation from the Afghanistan Civil Aviation Authority.

The fractured main rotor blades were sent to the NTSB Training Center in Ashburn, Virginia for examination by the NTSB Materials Laboratory, Office of Aviation Safety, and representative party members from the operator (Construction Helicopters Inc. doing business as CHI Aviation), the aircraft design authority (Sikorsky Aircraft), the main rotor blade design authority (Carson Helicopters, Inc.), and the Federal Aviation Administration. The group exam took place on October 14, 2020, after initial reconstruction efforts were conducted by the NTSB. Follow-on work scope was established for the NTSB to conduct following the group examination. Table I lists the group examination attendees.

Figure 1 shows the two crates received that contained the main rotor blade pieces immediately after opening. During the examination, the pieces of the main rotor blades were reconstructed to aid in the overall visual inspection and subsequent examination procedures. Due to the degree of fragmentation, not all pieces recovered from the accident site were able to be confidently reconstructed. Figure 2 shows an overall photograph of the reconstructed main rotor blades as viewed from the lower surface looking inboard from tip to root. Figure 3 shows component fragments that were recovered but not able to be confidently reconstructed.

The accident aircraft was outfitted with a main rotor blade set which consisted of five composite blades mounted to the rotor hub via a metallic flanged cuff. From review of engineering drawings and discussions with the main rotor blade design authority, the composite main rotor blade design was predominantly a fiber reinforced polymeric composite construction. Each main rotor blade consisted of a molded and cured D-shaped hollow spar constructed from carbon-fiber and fiberglass reinforced epoxy pre-impregnated uni-directional tape and woven textile materials. The aft surface of the spar was bonded to a machined aramid/phenolic honeycomb core afterbody with a foaming epoxy splice adhesive material. The upper and lower blade skins were constructed from woven fiberglass/epoxy prepreg material with copper mesh embedded under an epoxy surfacing film which was molded into thin sheets and cured. The pre-cured skins were bonded to the upper and lower surfaces of the spar, core afterbody, and trailing-edge mating surfaces using a supported epoxy film adhesive. The construction was consistent with an airfoil-shaped secondarily bonded composite sandwich structure[1]. A C-shaped nickel-based leading-edge cap was bonded to the nose of the spar and overlap areas on the upper and lower blade skins using a paste adhesive material and scrim cloth. The leading-edge cap covered approximately 70% of the blade span extending to the tip and was comprised of two-pieces which overlapped at closer to the tip end. Tungsten weights were embedded locally within the rotor blade, some of which were integrated during bonding operations and others were assembled after bonding operations, based on balancing procedures. The main rotor blade skins were finished with a paint scheme of white topcoat with two sets of two thin red stripes oriented chordwise and a set of two chordwise red patches at the blade tip. The topcoat scheme was mirrored on the upper and lower blade skins. Figure 4 shows a schematic of the main rotor blade for reference.

Throughout this report, the individual main rotor blades that were examined are referred to by the color nomenclature system developed by Sikorsky Aircraft as shown in figure 5. The main rotor blade order is Red, Black, White, Yellow, Blue as viewed from the pilot seat with blades passing by the observer from right-to-left (counterclockwise rotation as viewed from above). For example, the term “red blade” used in the following report, refers to the blade that was assembled in the red blade position on the aircraft. The blades were received from the accident site disassembled from the rotor hub with identification information corresponding to the color position labeled on the interior of the flanged cuff.

Following the reconstruction, all blades exhibited a higher degree of fragmentation near the blade tip with portions of the leading-edge cap separated, consistent with impact damage under powered rotation. There were three primary chordwise spar/afterbody fracture locations discernable from the fragmented tip observed along the spans of the red and black blades, five along the white blade, two along the yellow blade, and four along the blue blade. The primary chordwise spar/afterbody fracture locations are summarized in Table II. Detailed observations for each fracture location and other general observations are presented following the maintenance summary below for each blade.

[1] A secondarily bonded composite sandwich structure refers to pre-cured fiber-reinforced polymeric detail components assembled and bonded together using heat and pressure/vacuum activated thermoset adhesive materials. The construction, similar in nature to a sandwich, typically consists of thin skin panels bonded to a less dense core material designed to optimize strength, stiffness, and weight properties. As opposed to a co-cured structure in which detail components are simultaneously cured and bonded or co-bonded structures where a combination of pre-cured and uncured components are assembled and simultaneously bonded and cured.

1. Maintenance Summary

The accident main rotor blades, P/N 163-101-1, were installed on the accident helicopter (N908CH) under the provisions of Federal Aviation Administration (FAA) Supplemental Type Certificate (STC) No. SR01585NY held by Carson Helicopters, Inc ("Carson"). According to aircraft records, the main rotor blades were installed onto N908CH on July 27, 2016, at an aircraft total time (ATT) of 35,298.9 flight hours. Table III shows the component total times (CTT) of each blade at the time of installation onto N908CH.

The component log cards for the 'red' main rotor blade, S/N CHI-0385, and the 'blue' main rotor blade, S/N CHI-0386, showed they were removed for computed tomography (CT) scan inspection in March 2009. According to Carson, the CT scan focused generally on the back wall of the spar and was accomplished for all blades manufactured around that timeframe.

The Instructions for Continued Airworthiness (ICA) for the Carson main rotor blades, Manual No. CHI-MR-ICA, contained airworthiness limitations as well as mandatory inspections and their intervals. The inspections included a daily visual inspection, a recurrent 150-hour visual inspection, and a recurrent 1250-hour visual and coin tap inspection. These recurrent inspections were incorporated into the operator's continuous airworthiness maintenance program (CAMP). Within the CAMP, the 150-hour inspection was incorporated under out-of-phase check card (OPC)-38 and the 1250-hour inspection was incorporated under OPC-67.

For the accident helicopter, the latest flight log page provided to investigators was dated April 19, 2020 (the day before the accident), which contained a sign-off for the main rotor blade daily visual inspection. No defects or comments were noted in the discrepancy section of the log dated April 19, 2020. The aircraft total time (ATT) at the time of the daily visual inspection on April 19, 2020, was 38,492.8 flight hours. The ATT at the end of the day on April 19, 2020, was 38,495.2 flight hours.

The last OPC-38 inspection was performed on March 26, 2020, at an ATT of 38,432.6 flight hours with no defects noted. The last OPC-67 inspection was performed on February 26, 2020, at an ATT of 38,335.3 flight hours with no defects noted.

2. Red Blade Examination

The root portion of the red blade was received attached to the metallic blade cuff by 10 bolts secured with slotted nuts and split/cotter pins and all appeared to be fastened. Just outboard of the blade cuff were three placards bonded to the lower skin surface which contained identification information as shown in figure 6. As the blade transitioned from the narrow root section to the full blade width, there were red characters on the lower skin side which contained the following identification information:

"P/N 163-101-1 REV Q
S/N CHI-0385
MFG DAS 09/08

WT 226.72 LB CG BS 174.18
MODEL SIKORSKY S-61 SERIES
TCDS 1H15 & H2EA”

The blade was fractured and separated generally chordwise through the spar and afterbody at approximate blade station (BS) locations 236, 281 – 306, and 333 – 349 as shown in figures 7, 8, and 9, respectively.

Away from the spar and afterbody fracture locations, the blade skin was largely disbonded from the spar and honeycomb core afterbody surface but had not liberated from the blade. Areas of the trailing edge interface, leading-edge cap interface, and root cuff were still intact which held large portions of the skins in place.

On the lower blade skin, inboard of BS 236 spar fracture, were three distinct areas of branched cracking observed approximately 33, 66, and 109 inches inboard of the fracture location, which converged approximately two to three inches from the trailing edge. These branched cracks spread out toward the leading edge at an approximate 70 – 80-degree angle, creating a triangular shaped flap with the attached ligament oriented approximately parallel to the span axis. There were smaller branched cracks observed terminating along the larger primary cracks. These triangular shaped flap features were observed on the lower and upper blade skins at approximately the same blade station locations. Figure 10 shows the two inboard branched crack sites observed on the lower skin.

The nickel alloy leading edge cap exhibited a flat, chordwise fracture surface along the entire profile on the inboard piece of the BS 236 fracture. Figure 11 shows closer photographs of the upper and lower side of the inboard leading edge cap fracture surface as reconstructed. The outboard fracture surface of the leading-edge cap was generally torn, deformed, and exhibited slanted fracture surfaces consistent with shear lips due to overstress separation. An approximately 4 ¼ inch long section of the lower outboard leading edge cap fracture surface was deformed and bent away from the blade but was flatter in appearance. This area was later confirmed to be the mating fracture surface to the inboard side of the leading-edge cap. This flat fracture surface was excised from the blade and examined in more detail and results are discussed later in this report.

The BS 236 blade fracture, shown in figure 7, exhibited fiber pull-out at the leading edge of the spar and was relatively flat chordwise, over the mid to aft spar region where extensive chordwise translaminar fracture features were observed. Extensive interlaminar and intralaminar fracture features were observed extending into the blade away from the primary fracture surfaces. An approximate 4 – 5-foot section of the blade skins and honeycomb core afterbody spanning the spar fracture was completely separated from the blade. The skin remnants that were reconstructed exhibited primarily adhesive failure from the spar and afterbody with localized areas of bonded honeycomb core remnants (indicative of fracture within the core near the bonded joint interface). The adhesive layer was visible on the spar surface and intact honeycomb core. Portions of honeycomb core near the splice joint remained bonded to the aft wall of the spar which indicated failure of the afterbody took place primarily within the honeycomb core material transverse to the ribbon direction along the span with evidence of node bond separation along the chordwise direction. The blade fracture features were consistent with aft bending loading at the time of fracture.

Another blade fracture, shown in figure 8, was observed further outboard at approximate blade station BS 281 – 306. The fracture surface exhibited a fibrous appearance with extensive pull-out around the leading edge of the spar, extending further around the lower side of the spar compared to the upper side. A relatively flat translaminar chordwise fracture surface with interlaminar and intralaminar features extending into the spar was observed along the mid and aft spar. The section of leading-edge cap where spar damage and fracture were observed was completely separated and not recovered or able to be reconstructed except for a small, mangled piece that separated from the inboard side of the blade fracture. This piece of leading-edge cap retained portions of the spar, scrim cloth, and adhesive used to bond the cap to the spar. Where still attached, inboard and outboard of the blade fracture, the fractured edges of the leading-edge cap were deformed, buckled, and exhibited slanted shear lip features, consistent with tearing due to overstress. The honeycomb core afterbody spanning the fracture location was separated but, mostly recovered and reconstructed. Outboard of the fracture, sections of core near the splice joint remained bonded to the aft surface of the spar which indicated failure of the afterbody took place primarily within the honeycomb core material transverse to the ribbon direction. Inboard of the fracture, fibrous sections of the aft wall of the spar were pulled away toward the trailing edge and spar material remained attached to the core splice joint on the afterbody piece which indicated failure of the spar drove separation of the inboard section of afterbody. The blade fracture features observed were consistent with aft bending loading at the time of fracture.

Figure 9 shows the tip portion of the blade outboard of approximate BS 333. This area was heavily fragmented through the spar, skin, and core afterbody, which exhibited extensive node bond separation. The leading-edge cap was fractured and deformed/buckled/wrinkled at this location and was not recovered or able to be reconstructed. Scratched and marred areas of paint emanated from the leading-edge cap bond surface. The degree of fragmentation and crushed condition of the spar, afterbody, and adjacent leading-edge cap in this region was consistent with leading-edge impact damage.

Figure 12 shows a view of the reconstructed red blade as viewed from tip-to-root of the upper surface (top) and the lower surface (bottom).

3. Black Blade Examination

The root portion of the black blade was received attached to the metallic blade cuff by 10 bolts secured with slotted nuts and split/cotter pins and all appeared to be fastened. Just outboard of the blade cuff were three small placards bonded to the lower skin surface which contained identification information as shown in figure 13. As the blade transitioned from the narrow root section to the full blade width, there were red characters on the lower skin side which contained the following identification information:

“P/N 163-101-1 REV R
S/N CHI-0729
MFG DAS 07/11
WT 227.06 LB CG BS 173.94
MODEL SIKORSKY S-61 SERIES

TCDS 1H15 & H2EA”

The blade was fractured and separated through the spar and afterbody at approximate blade stations BS 213 - 217, BS 296, and BS 354 as shown in figures 14, 15, and 16, respectively.

Away from the spar and afterbody fracture locations, the blade skin was largely disbonded from the spar and honeycomb core surface but had not liberated from the blade. Areas of the trailing edge interface, leading-edge cap interface, and root cuff were still intact which held large portions of the skins in place.

On the lower blade skin, inboard of the BS 215 spar fracture, there were two distinct areas of branched cracking observed approximately 36 and 112 inches inboard of the fracture location, which converged approximately two to four inches from the trailing edge. These branched cracks spread out toward the leading edge at an approximate 70 – 80-degree angle, creating a triangular shaped flap with the attached ligament oriented approximately parallel to the span axis. There were smaller branched cracks observed terminating along the larger primary cracks. A similar diagonal crack in the blade skin was observed spanning outboard from leading edge to trailing edge approximately 48 inches inboard from the spar fracture. Further outboard, a similar triangular shaped flap feature was observed converging at approximate blade station 259 on both the upper and lower blade skins. These triangular shaped flap features and diagonal cracks were observed on the upper and lower blade skins at approximately the same blade station locations. Figure 17 shows a photograph of the branched crack site and similar diagonal crack, indicated by yellow arrows, just inboard of the BS 215 blade fracture on the upper blade surface.

The nickel alloy leading edge cap was intact, attached, and relatively undamaged from its inboard edge to the inboard blade fracture, where it was fractured and separated. The inboard side of the fractured leading-edge cap was spread open and peeled away from the spar and blade skins. The leading-edge cap on the mating outboard side of the blade fracture was similarly deformed, predominantly on the upper side of the blade. The deformation was consistent with an aft bending load at fracture. The fracture surface exhibited a slanted appearance over a tortuous pathway around the leading-edge cap, consistent with shear lip features formed as a result of overstress separation.

The BS 215 blade fracture, shown in figure 14, exhibited fiber pull-out at the leading edge of the spar and was relatively flat chordwise, over the mid to aft spar region, where extensive chordwise translaminar fracture features were observed. Extensive interlaminar and intralaminar fracture features were observed extending into the blade away from the primary fracture surfaces. The blade skins were cracked and separated locally at the blade fracture, but no substantial portions of the afterbody were fragmented. There was evidence of mixed mode adhesive and cohesive separation between the blade skins, spar, and core afterbody in this region. On the lower surface of the outboard portion of the blade, just outboard of the fracture at the trailing-edge, was a section of missing afterbody and lower skin with adjacent witness marks consisting of dark gray/green parallel scratches which emanated outboard toward the trailing edge.

The BS 296 blade fracture surface, shown in figure 15, exhibited a fibrous morphology on the leading edge and a relatively flat, translaminar, chordwise fracture surface, with interlaminar and intralaminar features extending into the spar, along the mid and aft spar. A 10 – 12-inch section of the leading-edge cap was separated at the blade fracture location but was recovered. The recovered piece was deformed and torn and retained portions of the spar, scrim cloth, and adhesive used to bond the cap to the spar. Where still attached, the inboard section of leading-edge cap was crushed inward at the highlight immediately adjacent to the fracture surface and buckling, tearing, and peeling deformation was observed. Outboard of this blade fracture, the upper and lower blade skins, and a portion of the afterbody had separated. The skins had separated along the spar-to-afterbody splice joint until midway through the inboard thick red stripe near the tip where it shifted diagonally outboard toward the trailing-edge. The honeycomb core was separated from the spar for approximately 12 inches outboard of the blade fracture and sections of core material near the splice joint remained bonded to the aft surface of the spar, which indicated failure of the afterbody took place primarily within the honeycomb core material transverse to the ribbon direction. The blade fracture features observed were consistent with aft bending and impact loads at fracture and overstress separation of the leading-edge cap.

The tip section of the blade outboard of approximate blade station BS 354, shown in figure 16, was heavily fragmented through the spar, skin, and core afterbody. The outboard leading-edge cap was separated and not recovered or able to be reconstructed except for a small piece from the area where the outboard leading-edge cap overlapped the inboard leading-edge cap. This small section of leading-edge cap was deformed and buckled, and fracture surfaces were consistent with overstress separation. The surface where the outboard leading-edge cap was bonded exhibited evidence of cohesive failure within the adhesive. Scratched and marred areas of paint on the blade skins emanated from the leading-edge side. The fibrous condition of the spar, and degree of fragmentation of the afterbody in this region was consistent with a leading-edge impact event.

Figure 18 shows a view of the reconstructed black blade as viewed from tip-to-root of the upper surface (top) and the lower surface (bottom).

4. White Blade Examination

The white blade was received separated from the cuff. The 10 bolts had sheared completely on the lower side. Five of the inboard-most slotted nuts with a portion of bolt were retained in the cuff. All bolt heads on the upper surface of blade had sheared off and were not recovered except the two outboard-most bolt heads and portions of the shanks were retained in the blade root. Figure 19 shows a spanwise view (looking inboard) of the blade cuff positioned next to the blade root, upper surface. The upper surface of the cuff flange exhibited fastener pull-out at the two outboard holes (yellow brackets) with deformation up and away from the blade surface and toward the trailing edge, consistent with upward and aft bending loads on the blade root.

Just outboard of the blade cuff attachment interface were two small placards bonded to the lower skin surface which contained identification information as shown in figure 20. Between these two placards was an area where a third placard had apparently been present.

As the blade transitioned from the narrow root section to the full blade width, there were red characters on the lower skin side which contained the following identification information:

"P/N 163-101-1 REV R
S/N CHI-0742
MFG DAS 08/11
WT 227.48 LB CG BS 173.62
MODEL SIKORSKY S-61 SERIES
TCDS 1H15 & H2EA"

The lower surface of the root exhibited an area of parallel scratches that were dark gray/green/brown in appearance as shown in figure 21. The scratches were most prevalent on the leading and trailing edge sides over approximately 3 – 4 feet of the blade span from the root end. The scratch pattern had a slight radius of curvature consistent with rotation about an axis inboard of the root cuff attachment.

The blade was fractured and partially separated through the spar and leading-edge cap at approximate blade station BS 148, and completely separated through the spar and afterbody at approximate blade stations BS 228, BS 263 – 276, BS 299 – 307, and BS 347. Figures 22 – 26 document these locations, respectively.

The leading-edge cap was partially separated from the inboard edge, indicated by red arrows in figures 21 and 22, to approximate blade station BS 148, indicated by the black arrow in figure 22, where it was partially fractured, deformed, and buckled. The spar exhibited fiber crushing damage at this location but had not fractured completely. The lower aft edge was battered and dimpled with an adjacent area of dark gray scratches on the lower skin emanating outward towards the trailing edge as shown in figure 22. The leading-edge cap was predominantly intact and adhered to the spar from this area until just inboard of the first complete blade fracture at approximate BS 228, where the cap was fractured and completely separated from the blade. The fracture surfaces were tortuous, deformed, and exhibited shear lip features consistent with overstress separation.

The mating section of leading-edge cap was recovered which was approximately five feet long and spanned the BS 228 spar fracture location, as shown partially reconstructed in figure 23. The outer surface was marred with scratches and dents and the piece was generally buckled, bent aft, and flared open the location where it overlapped the primary spar fracture, consistent with aft bending loading and impact damage. The inner surface had retained local areas of spar material, scrim cloth, and adhesive and was consistent with a cohesive separation.

On the lower blade skin, inboard of the BS 228 spar fracture, there were three distinct areas of branched cracking observed approximately 48, 88, and 140 inches inboard of the fracture location, which converged approximately two to four inches from the trailing edge. These branched cracks spread out toward the leading edge at an approximate 70 – 80-degree angle, creating a triangular shaped flap with the attached ligament oriented approximately parallel to the span axis. There were smaller branched cracks observed terminating along the larger primary cracks. These triangular shaped flap features were observed on the lower and upper blade skins at approximately the same blade station

locations. The inboard and middle locations are highlighted by yellow arrows in figures 21 and 22, respectively.

The BS 228 blade fracture, shown in figure 23, exhibited fiber pull-out at the leading edge of the spar and was relatively flat chordwise over the mid to aft spar region, where extensive chordwise translaminar fracture features were observed. Extensive interlaminar and intralaminar fracture features were observed extending into the blade away from the primary fracture surfaces. These fracture features were consistent with aft bending loading at the time of fracture.

Outboard of this blade fracture to approximate BS 307, as shown in figures 23, 24, and 25, majority of the upper and lower blade skins, honeycomb core afterbody, and leading-edge cap had separated and fragmented. Failure of the afterbody was observed primarily in the honeycomb core as remnants were observed bonded to the aft wall of the spar. Recovered blade skin pieces exhibited mixed adhesive and core failure modes. The exposed leading edge of the spar where the cap had separated exhibited evidence of cohesive failure of the adhesive/scrim cloth layer as well as spar material separation. The blade fracture features observed were consistent with aft bending and impact loads at fracture.

The BS 263 blade fracture, shown in figure 24, exhibited a fibrous morphology over a span of approximately 13 inches, indicated by the black bracket, at the leading edge through the mid-spar where relatively flat chordwise translaminar fracture features were observed through the aft spar. Extensive interlaminar and intralaminar fracture features were observed extending into the blade away from the primary fracture surfaces. These fracture features were consistent with aft bending loading at the time of fracture.

The BS 300 blade fracture, shown in figure 25, exhibited a predominantly translaminar fracture morphology traversing outboard through the spar from the leading edge along an approximate 8-inch span, with more fibrous features observed at the leading edge. The leading-edge cap outboard of this fracture location was still attached to the blade along the leading-edge highlight, but was deformed, torn, and peeled away from the blade adjacent to the fracture.

The outboard leading-edge cap detail was separated from the spar at the overlap joint with the inboard detail but was still attached to a piece of fractured spar adjacent to the tip weight fitting near BS 347 as shown in figure 26 indicated by black arrows. This section of the outboard leading-edge cap detail was deformed, twisted, torn, and buckled where it had separated from the blade. The outboard edge of the leading-edge cap at the tip weight fitting was separated and there was no leading-edge cap recovered or able to be reconstructed outboard of the tip weight fitting along the swept blade tip. At the blade tip, the spar was crushed and delaminated. The core afterbody and blade skin was fragmented and tattered. The blade skin surface exhibited dark green areas where paint had been removed. The scarred surface appearance, degree of fragmentation, crushed condition of the spar, and leading-edge cap deformation where recovered was all consistent with leading edge impact damage.

A piece of blade skin with portions of honeycomb core remnants adhered was received from the accident site with a hole marked “suspect” using blue masking tape. Upon reconstruction, this piece was identified as a portion of the lower skin of the White blade with the hole located at approximate blade station 281, approximately 9 inches from the trim tab trailing edge. The hole measured approximately 0.6 inch by 0.3 inch. This feature was examined further, and observations are detailed later in this report.

Figure 27 shows a view of the reconstructed white blade as viewed from tip-to-root of the upper surface (top) and the lower surface (bottom).

5. Yellow Blade Examination

The root portion of the yellow blade was received attached to the metallic blade cuff by 10 bolts secured with slotted nuts and split/cotter pins and all appeared to be fastened. Just outboard of the blade cuff were three small placards bonded to the lower skin surface which contained identification information as shown in figure 28. As the blade transitioned from the narrow root section to the full blade width, there were red characters on the lower skin side which contained the following identification information:

“P/N 163-101-1 REV Q
S/N CHI-0357
MFG DAS 07/08
WT 227.81 LB CG BS 173.34
MODEL SIKORSKY S-61 SERIES
TCDS 1H15 & H2EA”

A section of the leading-edge cap, approximately five feet long from the inboard edge to a chordwise fracture, was recovered that had completely separated from the blade as shown partially reconstructed in figure 29. The recovered section was flared open, buckled, and bent slightly aft at the location where it overlapped a primary spar fracture at BS 153. There was no notable scarring or impact damage observed on the outer surface. The inner surface retained local portions of spar material, scrim cloth, and adhesive and was consistent with predominantly cohesive failure at separation. There was an irregular shaped hole feature, approximately 1.5 – 2.5 inches in diameter, on the upper surface just inboard of the spar fracture location which exhibited tearing and inward deformation around the periphery as indicated by the arrow. There was no evidence of a through-hole in the corresponding area of the spar nor any visible scrape-like witness marks around the hole periphery on the outer surface. The bond surface of the leading-edge cap around this feature contained remnants of adhered spar plies. This was consistent with deformation and tearing during separation and inconsistent with puncture of a foreign object.

The blade was fractured and separated through the spar and afterbody at approximate blade stations BS 153 and BS 332 – 336 shown in figures 30 and 32, respectively.

The BS 153 blade fracture, shown in figure 30, exhibited fiber pull-out at the leading edge of the spar, followed by slanted ply separation oriented along internal +/- 45° ply levels, and was relatively flat chordwise, over the mid to aft spar region, where chordwise translaminar fracture features were observed. Extensive interlaminar and intralaminar

fracture features were observed extending into the blade away from the primary fracture surfaces. A section of honeycomb core after-body approximately 12 inches in length, which spanned the blade fracture, was not recovered or able to be reconstructed. Remnants of honeycomb core were observed adhered to the aft surface of the spar which indicated failure occurred within the honeycomb core. The spar fracture features, separated section of afterbody, deformation/separation of the leading-edge cap were all consistent with an aft bending load at fracture.

The upper and lower blade skins from near the inboard end of the leading-edge cap to the first primary spar fracture was disbonded from the blade and fragmented into multiple pieces about a triangular branched crack feature which converged approximately 23 inches inboard of the spar fracture as shown in figure 31. The skin separation from the spar and afterbody was predominantly adhesive in nature with film adhesive remaining on the spar and afterbody side of the interface.

On the lower blade skin, there were five distinct areas of branched cracking observed on the approximately 23 inches inboard, and 14, 50, 74, and 104 inches outboard of the BS 153 blade fracture location that converged approximately two to four inches from the trailing edge. These branched cracks spread out toward the leading edge at an approximate 70 – 80-degree angle, creating a triangular shaped flap with the attached ligament oriented approximately parallel to the span axis. There were smaller branched cracks observed terminating along the larger primary cracks. These triangular shaped flap features were observed on the lower and upper blade skins at approximately the same blade station locations, except at the feature furthest outboard, only a single diagonal crack spanning outboard from leading-edge to trailing edge was observed. The two branched crack features observed furthest inboard are indicated by yellow arrows in figures 30 and 31. The branched crack features observed furthest outboard are indicated by yellow arrows in figure 32, which shows a complete view of the upper surface of the outboard blade fragment below the red and yellow inset views showing the corresponding features on the lower blade surface. A trapezoidal shaped branched crack feature with similar orientation to the triangular features was also observed on the upper skin converging at the trim tab approximately 143 - 149 inches from the BS 153 blade fracture location as indicated in figure 32 by a red arrow. A closer view of this area is shown in the top left (green boxed) image.

The section of rotor blade from approximate blade station BS 164 to approximate blade station BS 332 between the spar fracture locations was mostly unfragmented except for the immediate vicinity of the blade fractures and the branched crack patterns documented herein.

The outboard spar fracture at approximate blade station BS 332, shown in figure 33, exhibited a crushed appearance and predominantly fibrous morphology with splinters projecting outboard approximately 25 inches from the torn leading-edge cap. The leading-edge cap at this location, shown in figure 34 indicated by a yellow arrow, was crushed inward and flattened at the highlight where a dark gray witness mark was evident with localized tearing observed around this mark. There were no additional outboard leading-edge cap pieces recovered or able to be reconstructed. The rotor blade tip section was fragmented and areas of the spar and afterbody were not recovered or able to be confidently reconstructed. These features at the blade tip section were consistent with impact loading at

fracture. The angled crack features present on the upper and lower blade skins and primary spar fracture surface morphologies were consistent with aft bending loading at fracture.

Figure 35 shows a view of the reconstructed yellow blade as viewed from tip-to-root of the upper surface (top) and the lower surface (bottom).

6. Blue Blade Examination

The blue blade was received folded about prominent partial spar fractures inside of the shipping crate as the crate was not long enough to contain the entire blade fragment. Some fibers and ply levels and the leading-edge cap remained continuous through the blade fracture locations. After removal from the crate, the blade was carefully unfolded approximately 180° about the BS 177 spar fracture and laid out to facilitate the reconstruction effort.

The root portion of the blue blade was received attached to the metallic blade cuff by 10 bolts secured with slotted nuts and split/cotter pins and all appeared to be fastened. Just outboard of the blade cuff were three small placards bonded to the lower skin surface which contained identification information as shown in figure 36. As the blade transitioned from the narrow root section to the full blade width, there were red characters on the lower skin side which contained the following identification information:

“P/N 163-101-1 REV Q
S/N CHI-0386
MFG DAS 09/08
WT 226.95 LB CG BS 174.02
MODEL SIKORSKY S-61 SERIES
TCDS 1H15 & H2EA”

The leading-edge cap was fractured at approximate blade station BS 125, as indicated by a white arrow in figure 37, and exhibited a rough and deformed morphology with shear lip features consistent with overstress tearing. The aft edge of the leading-edge cap had peeled away from the lower skin and was deformed and buckled but still partially adhered to the spar leading-edge inboard and outboard of the fracture. There were broken fibers from the spar protruding through the torn leading-edge cap, but the blade was not completely separated at this location.

The blade was most notably fractured through the spar and afterbody at approximate blade stations BS 177, BS 277, and BS 325 as shown in figures 38, 39, and 40, respectively.

The BS 177 blade fracture, shown in figure 38, exhibited a fibrous morphology on the leading edge which protruded from the deformed and torn leading-edge cap. Through the rest of the spar, the fracture was relatively flat chordwise and predominantly translaminar. Some fibers and plies were still continuous through this fracture and the spar was not completely separated which allowed the blade to be delivered in a folded configuration. For approximately 16 inches inboard of this blade fracture, the leading-edge cap exhibited dents, gouges, and smeared metal on the lower surface with a scratch pattern oriented aft and slightly outboard from the highlight. This was consistent with leading edge impact damage.

Between the BS 125 partial leading-edge cap fracture and the BS 177 blade fracture, the lower blade skin was fragmented into two pieces that exhibited evidence of translaminar skin failure, interlaminar skin failure, and disbond from the spar and honeycomb core afterbody. The upper blade skin in this area was largely intact except for a diagonal translaminar crack traversing outboard from the leading-edge cap near the partial fracture at BS 125 through the trailing-edge.

At the blade fracture at approximate blade station BS 277, shown in figure 39 indicated by a white arrow, the leading-edge cap was fractured, deformed, and exhibited several smaller tears and buckle lines emanating from the fracture surface. The leading-edge cap was compressed inward at the highlight near the fracture surface, splayed open, and peeled away from the lower skin along several inches inboard where the leading-edge cap was still attached. The leading-edge cap outboard of this fracture was not recovered or able to be reconstructed except for two small, mangled pieces from near the leading-edge cap overlap joint and tip weight fitting.

The spar was heavily fragmented from the BS 277 blade fracture and outboard. The lower portion of the spar remained partially attached to the inboard section of the blade and spanned to approximate blade station BS 325. Extensive interlaminar, intralaminar, and translaminar fracture features were observed, and the spar was fractured transverse to the chord plane along the blade span. The blade fracture at approximate blade station BS 325 (outboard end of red bracket in figure 39) was predominantly flat chordwise and translaminar along the aft inner ply levels of the lower spar section. An approximately 48-inch section of the upper portion of the spar, shown adjacent to the reconstructed blade and indicated by a red bracket in figure 39, was received from the accident site labeled as “these pieces came from inside the tail boom.” Pieces of the honeycomb core afterbody that were recovered and able to be reconstructed in this area exhibited evidence of failure through the core, cohesive failure within the core splice joint at the core-to-spar interface, and mixed adhesive and core failure at the core-to-skin interface. The lower skin was largely not recovered or able to be confidently reconstructed in this area. A piece of the upper skin from this area, shown with the internal side visible and indicated by a red arrow in figure 39, was received from the accident site labeled as “these pieces came from inside the tail boom.” The inboard edge of this piece corresponded with approximate blade station BS 260 and the outboard edge of the piece corresponded to approximate blade station BS 307. This piece of upper skin was tattered with partial tears along an approximately 45° orientation relative to spanwise direction with areas of chipped topcoat and irregular and rectangular shaped regions of missing skin. Figure 40 shows upper surface views of blade fractures BS 277 (right) and BS 325 (left) with the upper spar piece and upper skin piece partially reconstructed. The condition of the rotor blade from approximate blade stations BS 277 to BS 325 was consistent with an impact event with the airframe.

On the lower blade skin, there were three distinct areas of branched cracking observed approximately 85 inches inboard and 42 inches outboard of the BS177 fracture location and approximately 15 inches inboard of the BS 277 fracture location that converged approximately 1 – 3 inches from the trailing edge. These branched cracks spread out toward the leading edge at an approximate 70 – 80-degree angle, creating a triangular shaped flap with the attached ligament oriented approximately parallel to the span axis. There were smaller branched cracks observed terminating along the larger primary cracks. These

triangular shaped flap features were observed on the lower and upper blade skins at approximately the same blade station locations except for the outboard location which corresponded to the upper skin piece labeled “these pieces came from inside the tail boom.” These branched crack features are shown in figure 41 indicated by yellow arrows. These features were consistent with aft bending loading.

Figure 42 shows a view of the reconstructed blue blade as viewed from tip-to-root of the upper surface (top) and the lower surface (bottom).

7. Red Blade Leading-Edge Cap Flat Fracture – BS 236

A closer examination of the flat fracture surfaces of the red blade leading edge cap at approximate BS 236 blade fracture location was performed with the aid of a 4X – 80X zoom stereomicroscope. Figure 43 shows a view of the lower surface of the BS 236 blade fracture with the mating inboard and outboard leading-edge cap flat fracture surfaces indicated by yellow arrows. A closer view of the inboard fracture surface is shown in figure 44 after removal from the loosely adhered spar. The adjacent surface exhibited remnants of spar plies, adhesive, and scrim cloth. Figure 45 shows forward and aft views of the mating outboard flat leading-edge cap fracture surface on the lower blade surface, bracketed by yellow arrows, which also displayed remnants of spar plies, adhesive, and scrim cloth at the bonded interface.

A digital microscope was used to further examine the fracture surface which revealed a predominantly smeared morphology. Faint curved crack arrest marks were observed. Figure 46 shows digital microscope images of the two inset areas labeled in figure 44, with the direction of crack propagation indicated with yellow arrows based on the curvature of the crack arrest marks, which are oriented approximately vertically along the fracture surface bracketed in red in the images. The arrest marks originated from interconnected internal voids approximately 0.015 inch by 0.008 inch in area on the upper surface, approximately 0.6 inch from the trailing edge of the leading-edge cap, indicated by the black arrow in figure 44. Figure 47 shows optical (top) and scanning electron microscope (bottom) images of the origin area, with radial marks observed emanating in opposite directions from the corners of the internal voids. The crack progression marks continued from this area in both directions, to the upper aft edge and around the highlight along the lower surface toward the lower aft edge, as indicated by yellow areas in figures 44, 46, and 47. Figure 48 shows progressively closer secondary electron images of typical crack arrest marks observed on the fracture surface, as indicated by red arrows. The yellow arrow indicated the progressive crack propagation direction. Extensive smearing was observed, and no conclusive evidence of fatigue striations were observed.

Energy dispersive x-ray spectroscopy (EDS) was performed at the origin area for compositional analysis. Figure 49 shows a compositional mapping and the associated spectrum that was acquired. Nickel was prevalent on the fracture surface with streaks rich in silicon and oxygen obscuring part of the origin, consistent with glass fibers. A layer rich in carbon and oxygen was observed along the top of the image which corresponded to the inner surface of the leading-edge cap where spar ply remnants were present.

The adhesive layer between leading edge cap and spar exhibited a relatively flat, smeared appearance on the same plane as the leading-edge cap fracture. Loose tows of scrim cloth were observed locally near the leading-edge cap fracture surface where adhesive had cracked and separated.

The adjacent inner surface to the fracture, as shown in figure 50, exhibited remnants of oppositely oriented spar plies, adhesive, and scrim cloth still adhered, consistent with cohesive failure within the spar and adhesive layers. Figure 51 shows a tilted secondary electron image of the adjacent inner surface of the leading-edge cap where the fracture surface is just out of view in the lower right corner of the image. Most of the fracture features on the adhesive layer were obliterated, however there were visible fiber tracks left from the separated unidirectional carbon fibers with river line features spanning the resin between tracks, consistent with a peel dominated overstress fracture mode.[2] Some areas of separated spar plies exhibited a smooth and shiny appearance, while others exhibited a rough and duller appearance as indicated in figure 50. These areas and other areas of the spar layers which were peeled back at natural inter/intralaminar separations were examined using scanning electron microscopy. Figure 52 shows secondary electron images of the boundary (yellow dashed line) between a smooth and shiny appearing area (right side, left image) and a rough and dull appearing area (left side, left image). The smooth, shiny area was fiber dominated and the rough, dull area was resin dominated with visible fiber tracks. A closer view is shown in the right image of figure 52 where river lines and textured microflow features were observed on the resin fracture surfaces and hackle and shear cusp features[3] were observed spanning between fibers, consistent with mixed-mode peel and shear overstress fracture.

The upper blade skin which spanned the BS 236 blade fracture was not recovered or able to be reconstructed. The lower blade skin was intact at the flat leading-edge cap crack station location as seen in figure 43, which indicated the leading-edge cap crack did not progress into the lower blade skin.

8. Yellow Blade Film Adhesive Measurements at Blade Fracture – BS 153

Transverse sections to the blade span were collected from the yellow blade upper skin, lower skin, and trailing edge section in the vicinity of the spar fracture at approximate blade station 153 to measure the film adhesive thickness. Surveyed areas included locations where adhesive failure was observed between the skin and afterbody, as well as locations where core failure was observed, and the skin remained bonded to a portion of the honeycomb core afterbody. The average thickness was measured using a digital microscope as the smallest distance observed between a honeycomb-core cell-wall and the adhesive boundary, or mating face sheet, as applicable, and was approximately 0.005 inch for areas which exhibited predominantly adhesive separation and approximately 0.004 inch for areas

[2] Fiber tracks and river lines are fracture features observed on polymers and polymer matrix composites.
Greenhalgh, Emile. 2009. Failure Analysis and Fractography of Polymer Composites. Cambridge, England: Woodhead Publishing.

[3] River lines, textured microflow, shear cusps, and hackles are fracture features observed on polymers and polymer matrix composites.
Greenhalgh, Emile. 2009. Failure Analysis and Fractography of Polymer Composites. Cambridge, England: Woodhead Publishing.

which were intact or still bonded to a portion of the core afterbody. The coefficients of variation for the measurements were 33% and 32%, respectively and measurements ranged from 0.001 – 0.009 inch. Representative digital microscope images are shown in figure 53.

The adhesive layer thickness at the trailing edge section was approximately 0.044 inch where one skin had separated, and 0.038 inch where upper and lower skins had both separated. Representative digital microscope images are shown in figure 53.

Rounded fillets of adhesive were generally observed between honeycomb core cell walls and the skin-to-core bond interface.

The afterbody bond surfaces where adhesive separation of the blade skin was observed were examined with the aid of a 4X – 80X zoom stereomicroscope and digital microscope. The film adhesive (green in color) generally remained on the honeycomb core side of the interface. There were two distinct appearances observed, one resembling a 5-harness satin style textile pattern, and the other resembling a plain weave style textile pattern. Figure 54 shows a view of the blade skin side of the interface (left image) and the honeycomb core/film adhesive side of the interface (right image). The dashed lines in each image highlight the boundary between the two different fracture surface appearances observed. The 5-harness satin weave pattern of the glass fibers from the skin, and corresponding imprint on the film adhesive retained on the afterbody is shown on the left of each image, respectively, while the corresponding plain weave patterns are shown in the right of each image oriented approximately 45° relative to the 5-harness satin weave pattern. This was consistent with blade skin separation taking place between the surface of the precured blade skin and film adhesive as well as the glass fiber-matrix interface. There was no evidence of the presence of a plain weave ply in the construction, consistent with a removable surface preparation ply typically used when manufacturing pre-cured composite details for subsequent bonding.

9. White Blade Skin Hole Examination

A piece of blade skin with portions of honeycomb core remnants adhered was received from the accident site with a hole marked “suspect” using blue masking tape. Upon reconstruction, this piece was identified as a portion of the lower skin of the white blade with the hole located at approximate blade station 281, approximately 9 inches from the trim tab trailing edge. The hole measured approximately 0.6 inch by 0.3 inch. Figure 55 shows views from the outer surface (left) and inner surface (right) with the hole marked by a red arrow. Figure 56 shows closer views of the hole feature from the outer surface (left) and the inner surface (right).

As viewed from the outer (lower) surface, a fan-like pattern of scratched and chipped paint was observed spreading from the leading-edge side of the skin, just inboard of the hole, to the trailing edge, outboard of the hole, consistent with impact damage from multiple pieces of foreign debris. Scratched and chipped white paint revealed a dark green colored primer material beneath the paint and deeper chips revealed the lighter green film adhesive layer. The surface surrounding the hole exhibited similar paint chipping, predominantly on the leading-edge side of the hole. Torturous translaminar branched cracks were observed

emanating from the hole which were arrested at other skin cracks or within the skin, consistent with secondary crack paths.

As viewed from the inner surface of the lower skin, Local ply separation was observed surrounding the hole and the translaminar cracks as evidenced by a lighter yellow-white appearance.

The hole edges were viewed using SEM, however sample charging and instability made features difficult to interpret. EDS was used to examine chemical composition around the hole edge, but signal counts were relatively low. Primary peaks of silicon, oxygen, and carbon were observed, consistent with fiberglass/epoxy composite materials.

A portion of the blue blade upper skin found inside the tail boom cavity at the accident site, shown in figure 57, also contained several hole features which were examined. The outer surface of the skin (left) exhibited similar characteristics to the white blade, including scratches, chipped paint, translaminar branched cracks emanating from the holes, and local ply separation around holes and cracks on the inner surface (right), consistent with impact damage from foreign debris.

Michael Meadows
Materials Engineer

Table I: Group members present during component exam

Group Member	Organization
Michael Meadows	NTSB, RE-30
Chihoon Shin	NTSB, AS-40
Daniel Bower	NTSB, AS-10
Todd Gentry	FAA
Paris D'Avanzo	Construction Helicopters Inc.
Keith Hughes	Construction Helicopters Inc.
Clayton Carson	Carson Helicopters, Inc.
Rod Manogue	Carson Helicopters, Inc.
Kenneth Deyo	Sikorsky Aircraft
Dave Blair	Sikorsky Aircraft

Table II: Approximate main rotor blade station (BS) values of reported spar fracture locations

Blade ID Color → / Fracture Index [1] ↓	Red	Black	White	Yellow	Blue
Frac 1	236	213 - 217	148 [2]	153	126 [2]
Frac 2	281 - 306	296	228	332 - 336	177
Frac 3	333 - 349	354	263 - 276	[4]	277 [3]
Frac 4	[4]	[4]	299 - 307		325 [3]
Frac 5			347		[4]
Frac 6			[4]		
[1] Fracture index numbers are sequenced from root end to tip end					
[2] Partial spar fractures					
[3] Spanning piece from upper spar surface found in tail boom					
[4] Tip end was substantially fragmented					

Table III: Accident vehicle main rotor blade service times

Blade Color	S/N	CTT at Install	CTT on April 19, 2020
Red	S/N CHI-0385	83.5 hours	3,279.8 hours
Black	S/N CHI-0729	15.9 hours	3,212.2 hours
White	S/N CHI-0742	15.9 hours	3,212.2 hours
Yellow	S/N CHI-0357	67.2 hours	3,263.5 hours
Blue	S/N CHI-0386	133.4 hours	3,329.7 hours

Figure 1: Photograph showing the two crates as received after opening.

Figure 2: Photograph of lower surface of blades as reconstructed with primary blade fracture locations identified with arrows. Blade identification colors from left-to-right are yellow, blue, red, black, white. The scale highlighted by a yellow box is 12 inches in length.


b


c

Figure 3: Photograph showing pieces of a) afterbody and spar fragments, b) the leading-edge cap, c) blade skin fragments, and d) miscellaneous pieces from the airframe that were recovered from the accident site but unable to be confidently reconstructed.

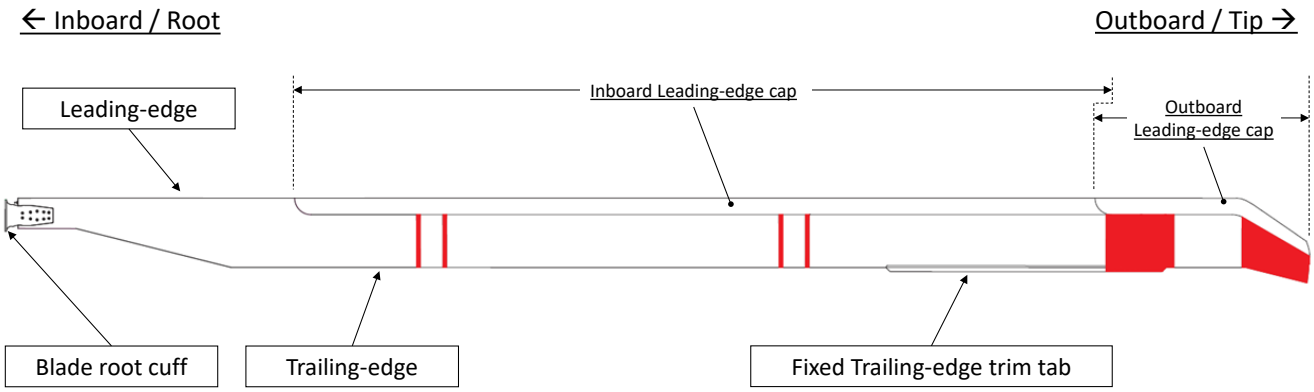

Figure 4: Schematic of a main rotor blade from the accident vehicle. Not to scale. Adapted from Carson Helicopters Inc. provided schematic.

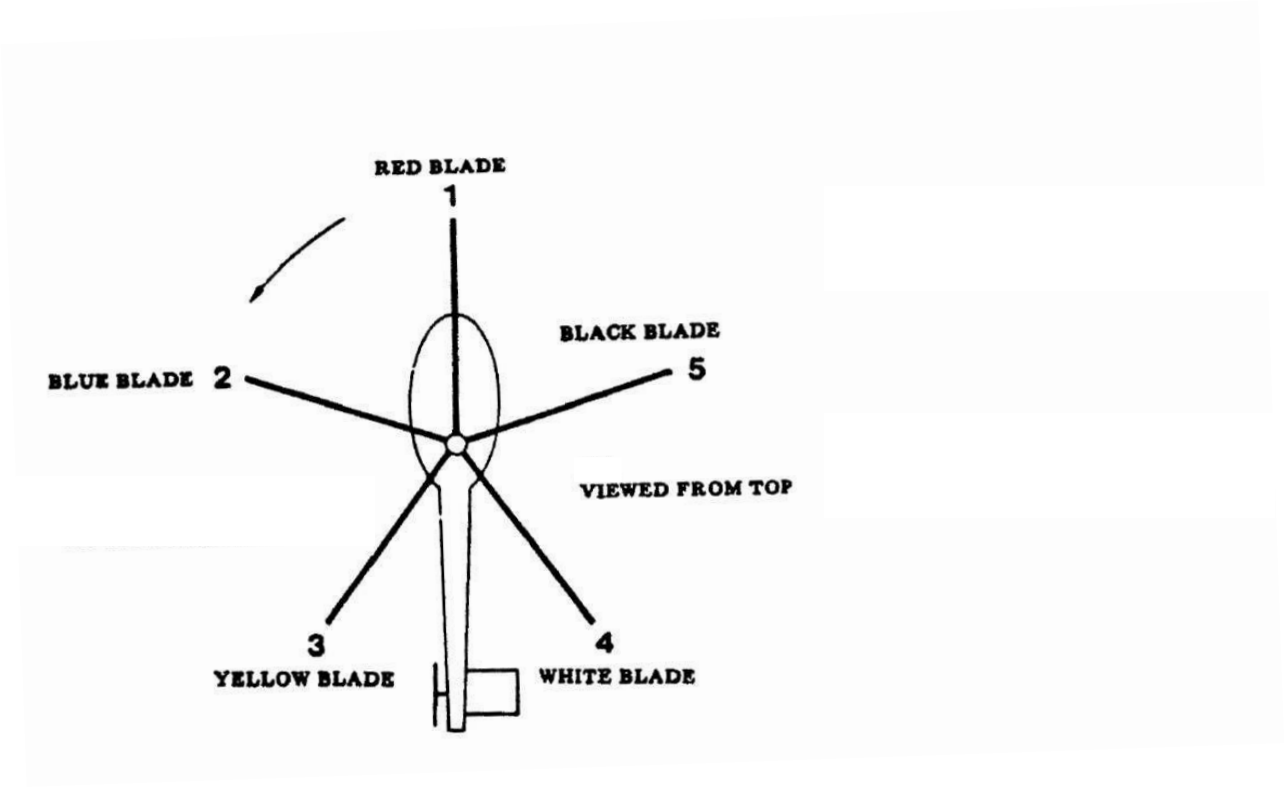

Figure 5: Schematic of the main rotor blade sequence and naming convention. Not to scale. Adapted from Sikorsky Aircraft provided schematic.

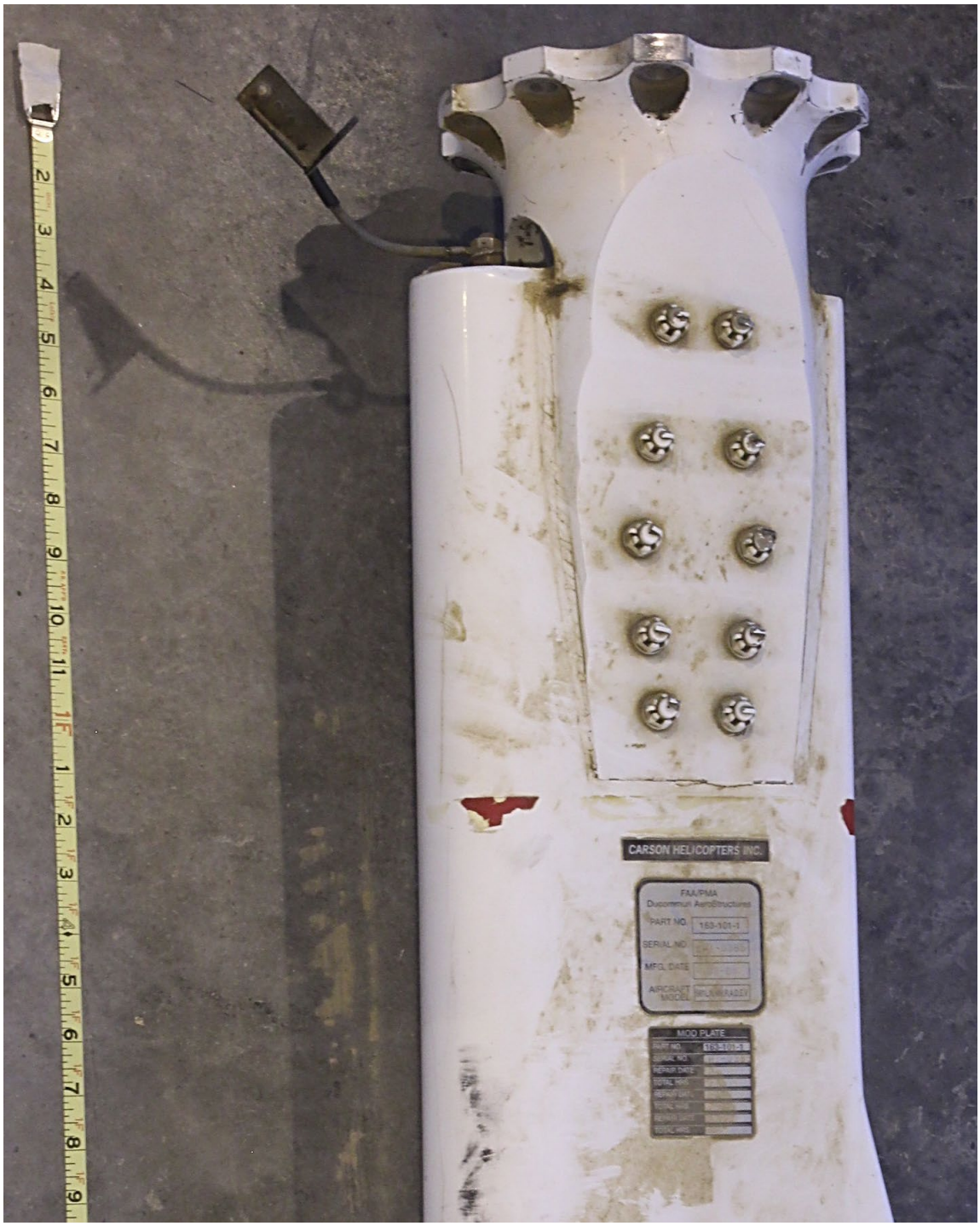

Figure 6: Photograph of the red blade identification placards and lower surface of the attached blade cuff.

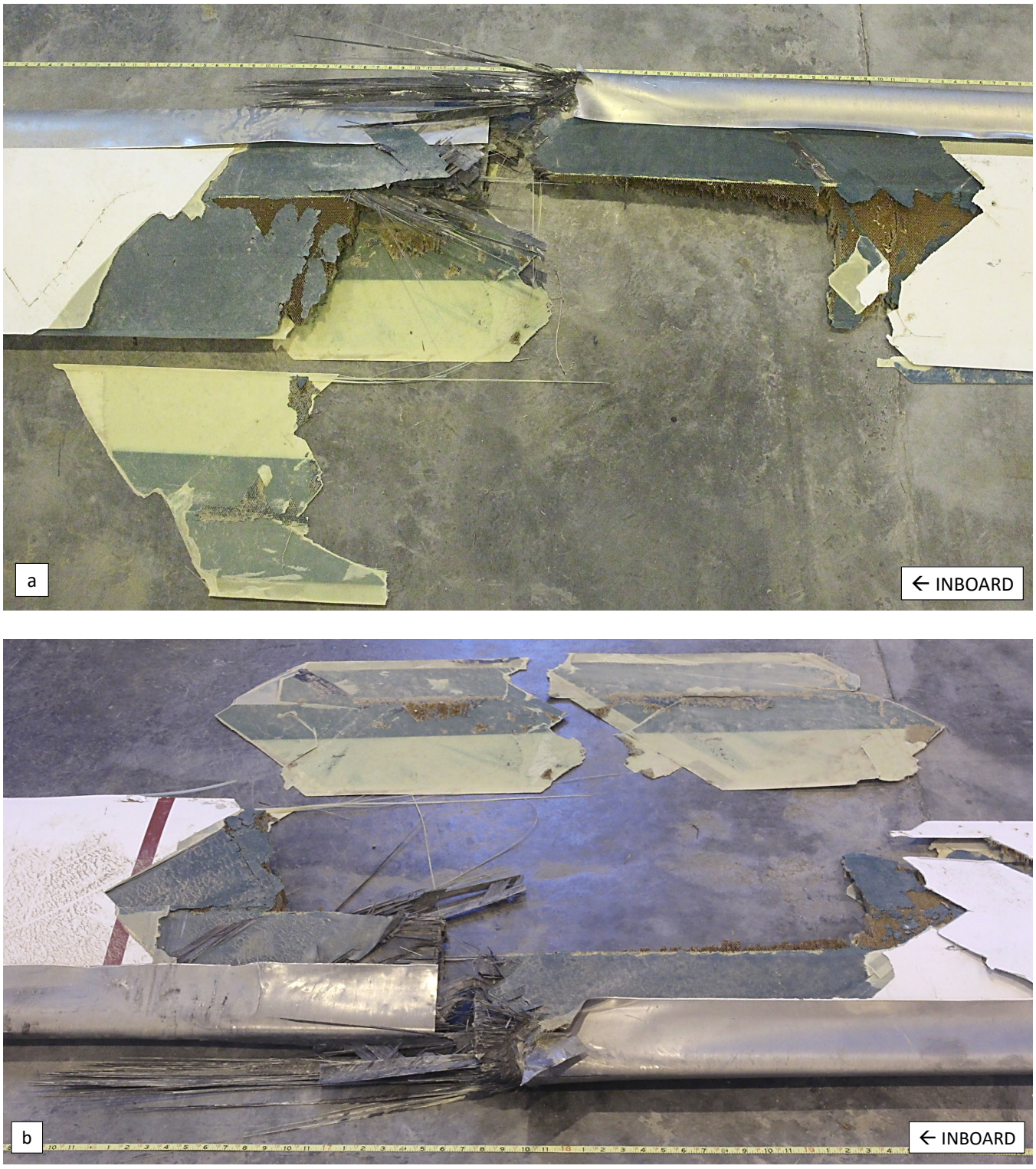

Figure 7: Photograph of the red blade BS 236 fracture location a) upper surface and b) lower surface

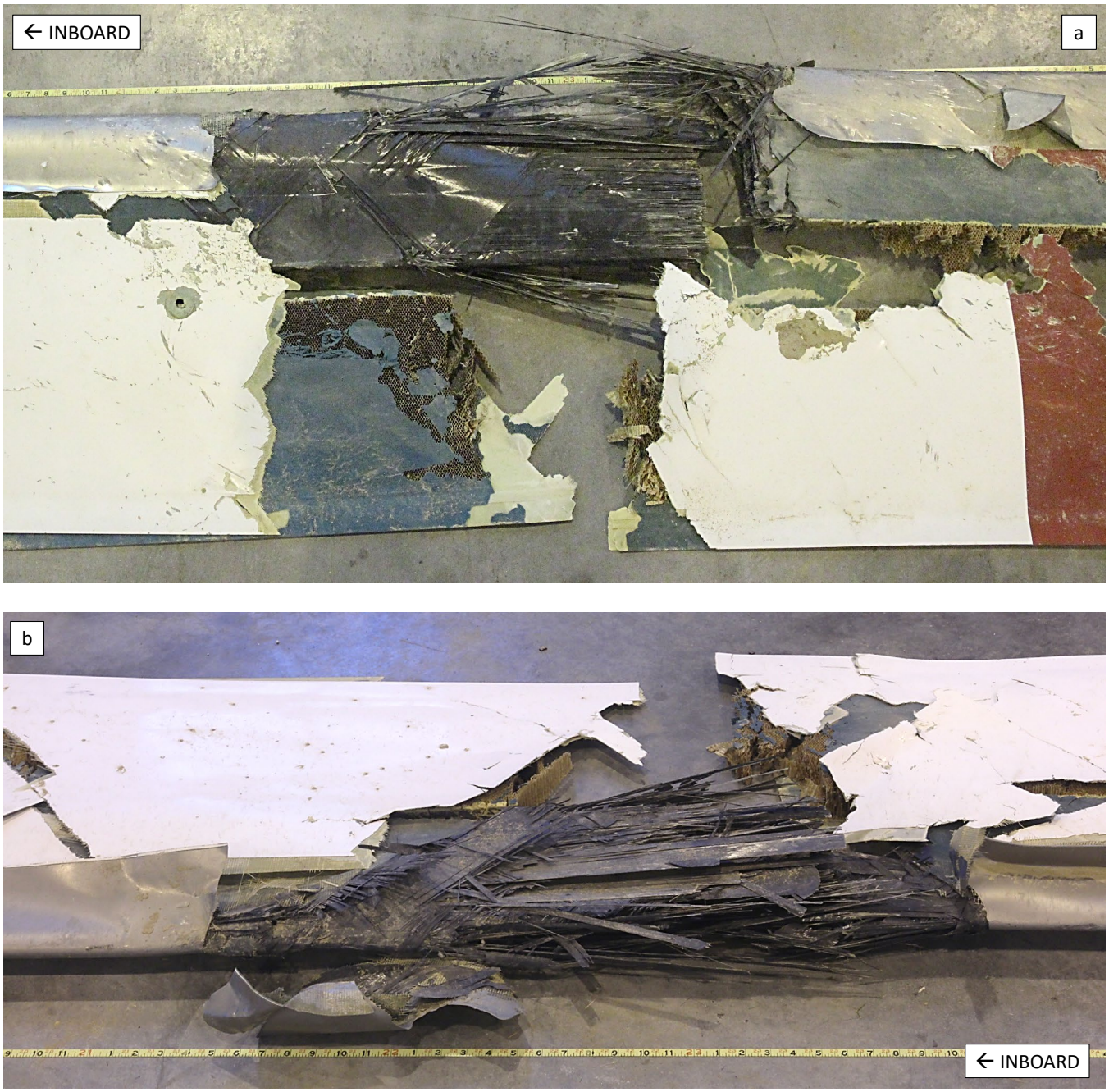

Figure 8: Photograph of the red blade BS 281 – 306 fracture location a) upper surface and b) lower surface

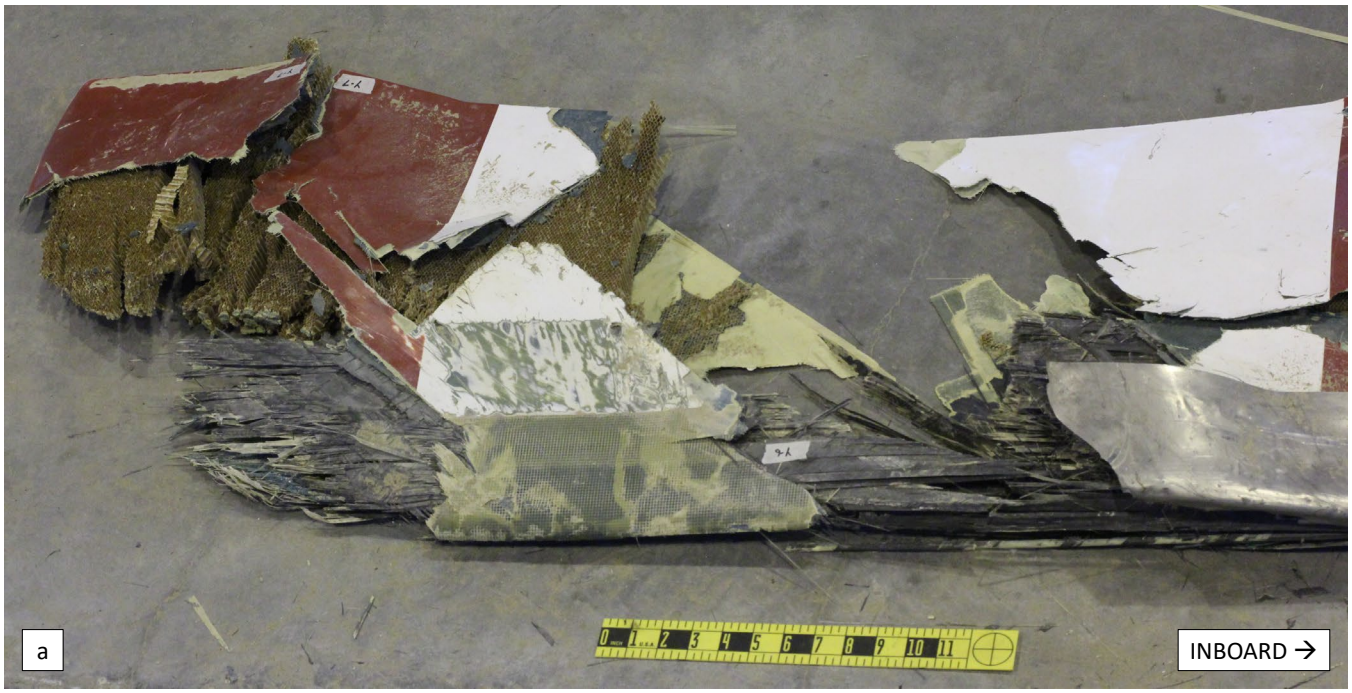

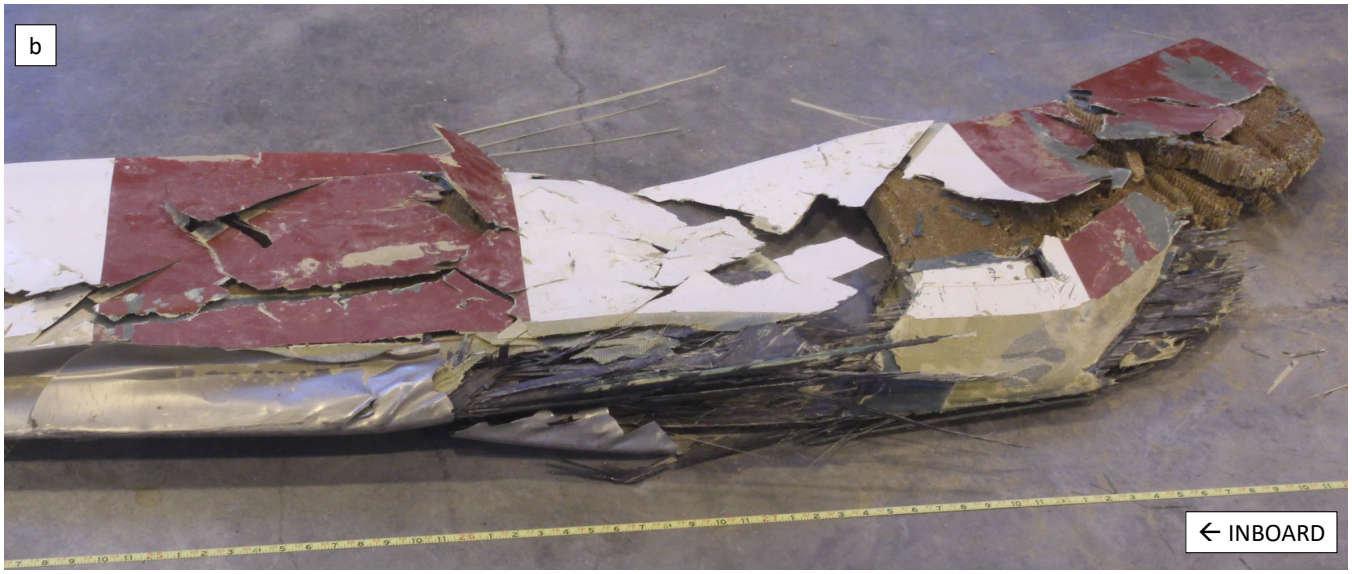

Figure 9: Photograph of the red blade BS 333 – 349 fracture location a) upper surface and b) lower surface

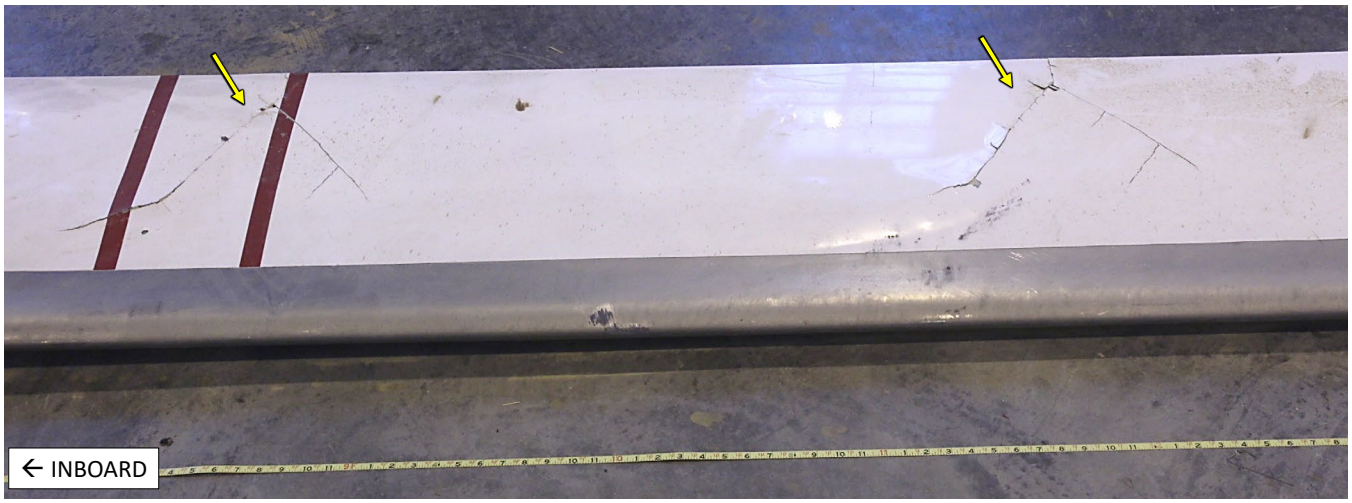

Figure 10: Photograph of inboard branched cracking sites, indicated by yellow arrows, observed on the red blade, lower skin.

Figure 11: Photograph of the red blade leading-edge cap flat fracture at BS 236 as reconstructed viewed from the lower surface (left) and upper surface (right).

Figure 12: Photograph of the reconstructed red blade upper surface (top image) and lower surface (bottom image) viewed from tip to root.

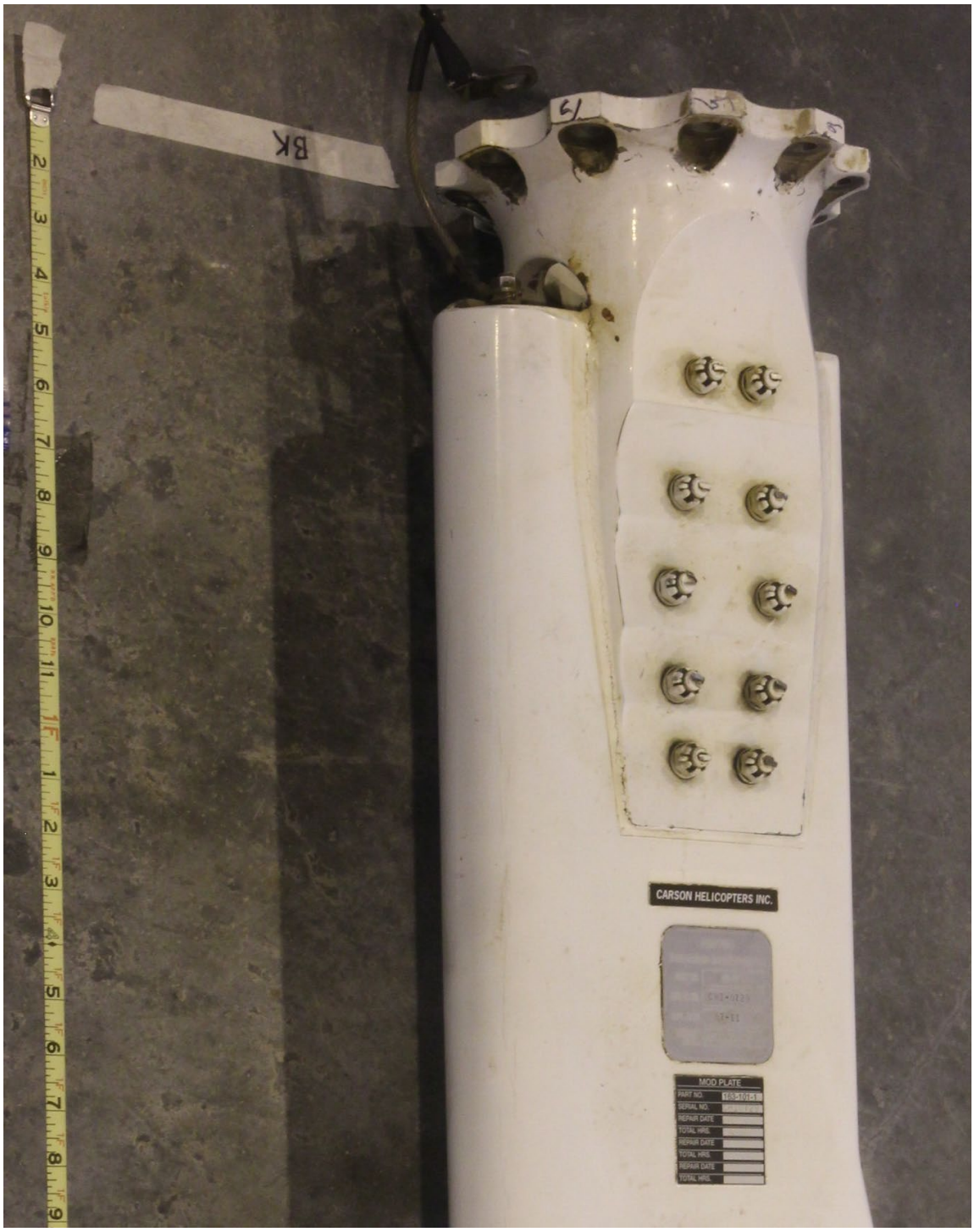

Figure 13: Photograph of the black blade identification placards and lower surface of the attached blade cuff.

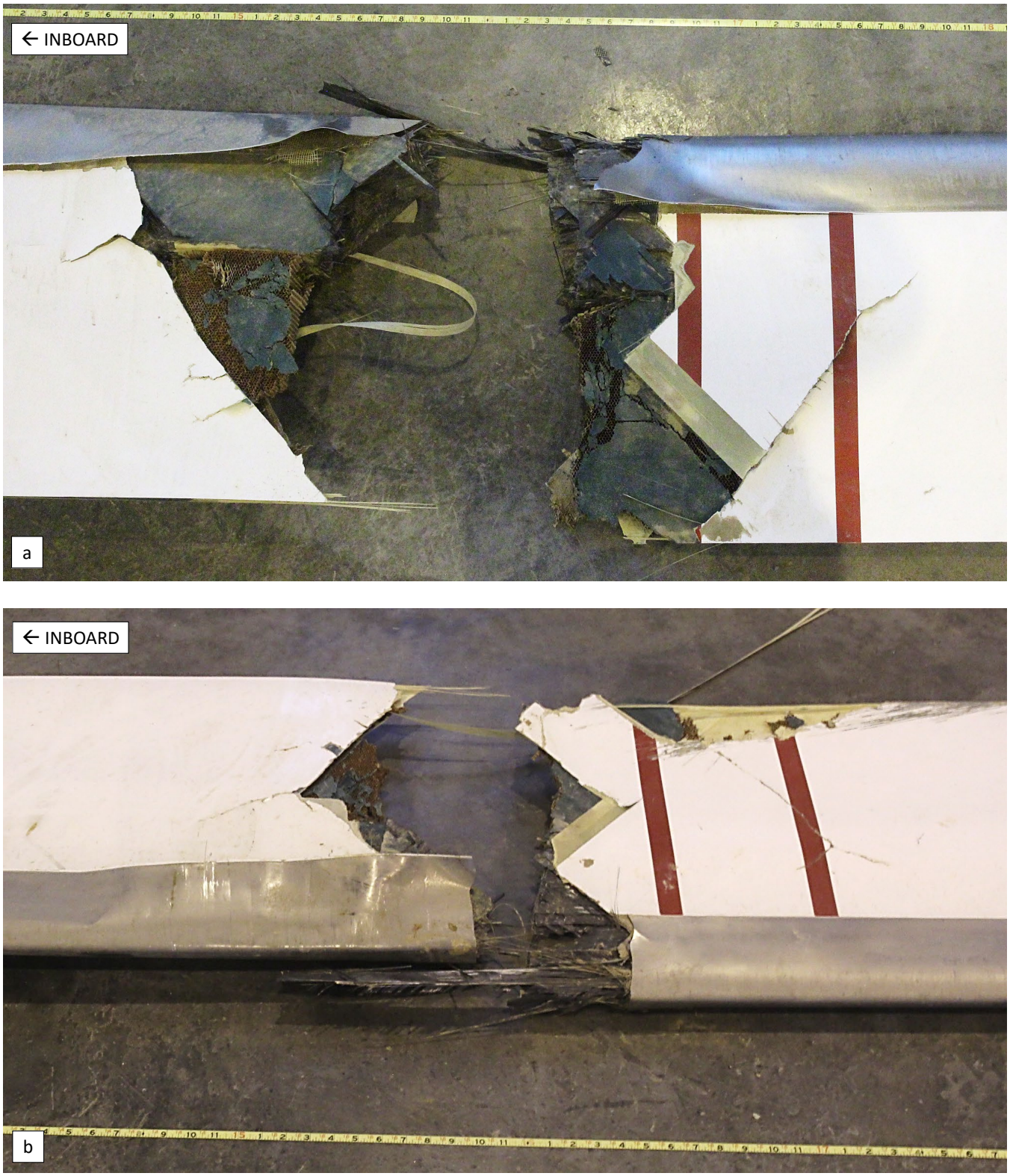

Figure 14: Photograph of the black blade BS 213 – 217 fracture location a) upper surface and b) lower surface

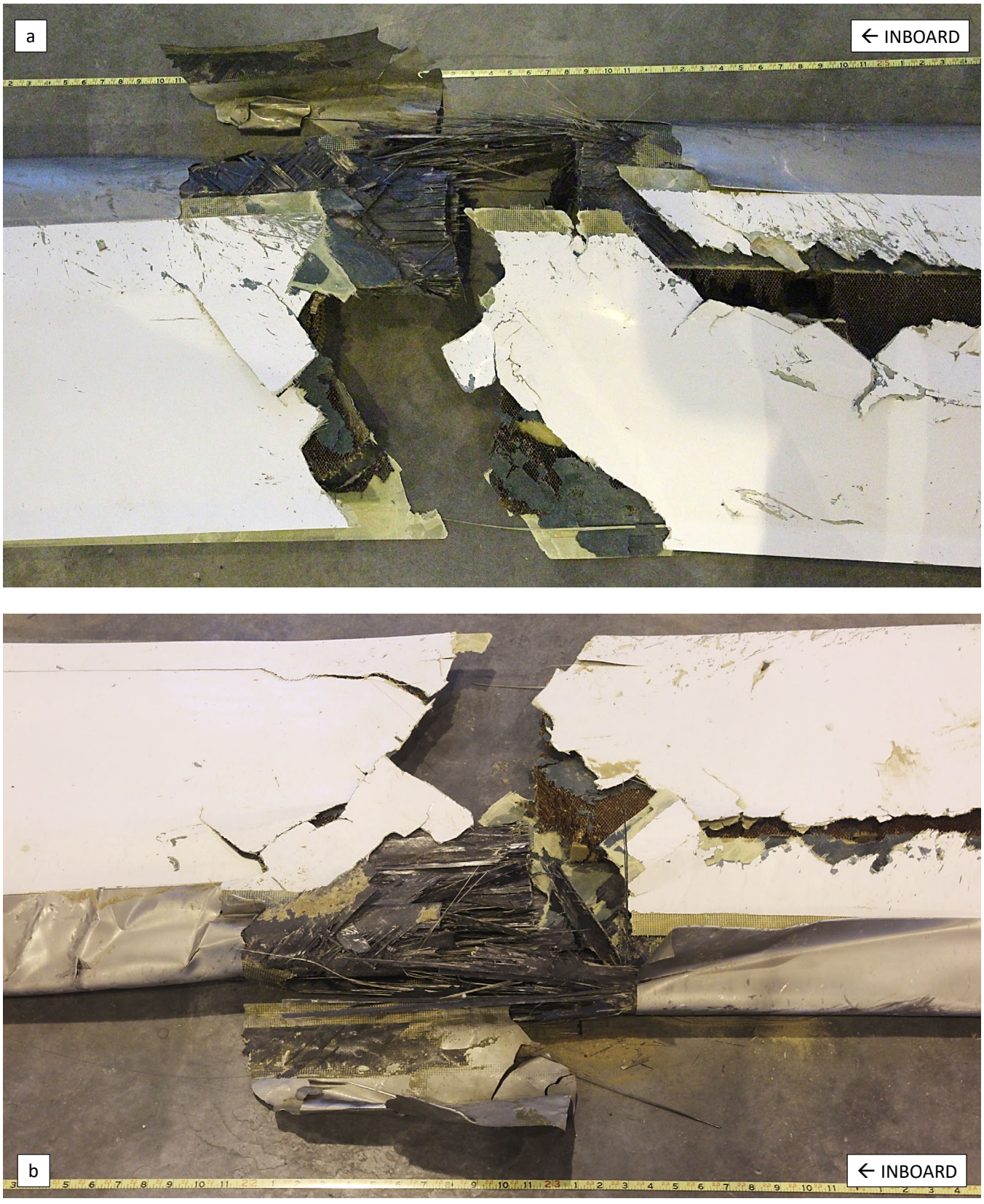

Figure 15: Photograph of the black blade BS 296 fracture location a) upper surface and b) lower surface

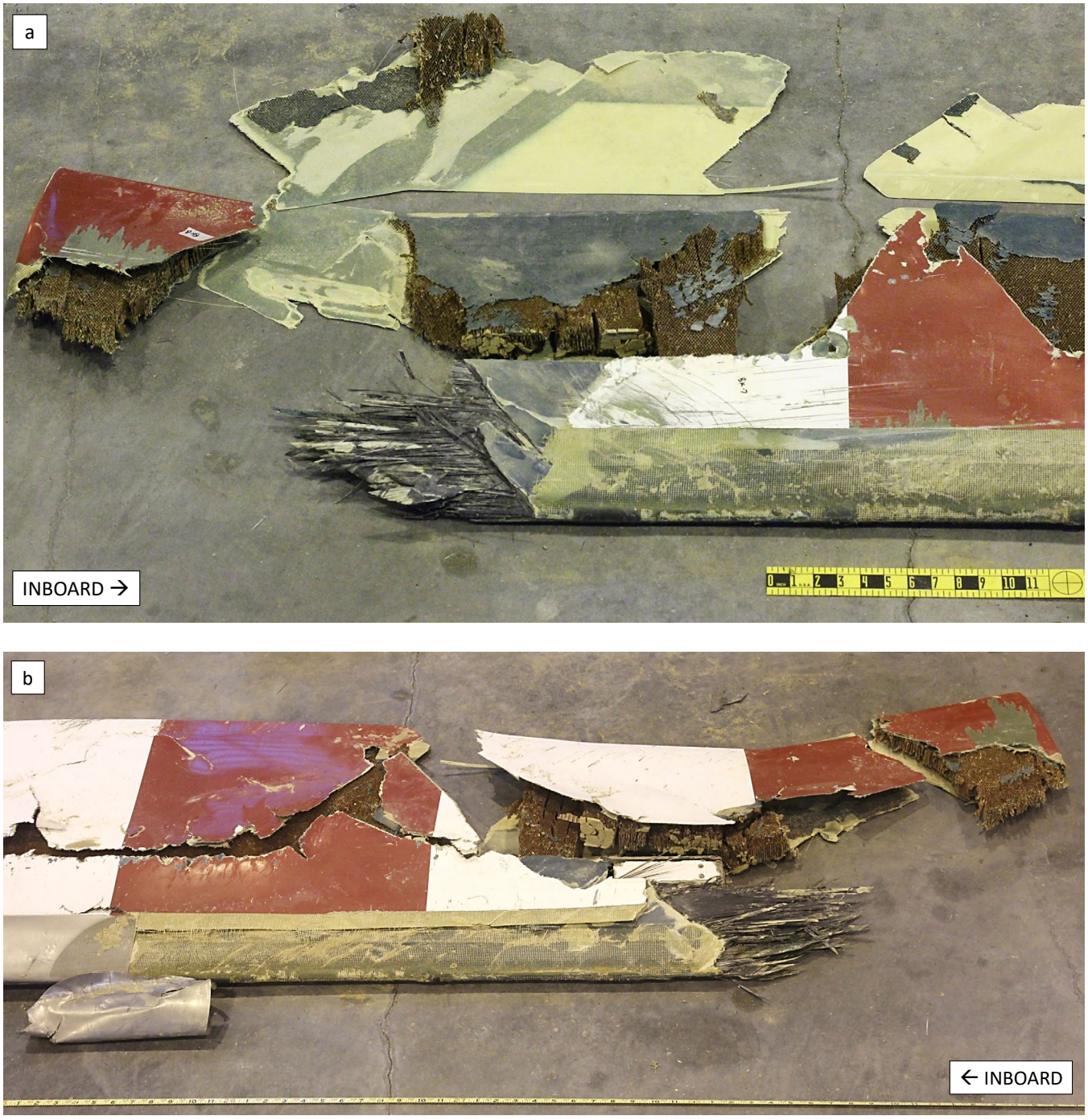

Figure 16: Photograph of the black blade BS 354 fracture location a) upper surface and b) lower surface

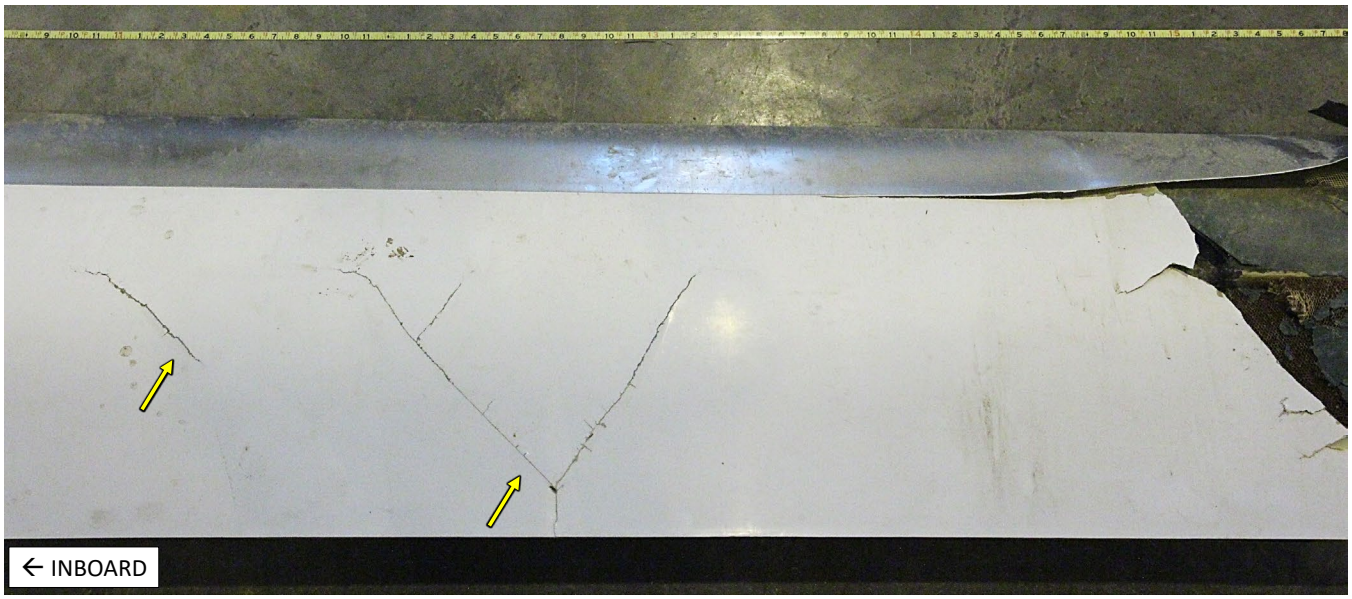

Figure 17: Photograph of branched cracking sites, indicated by yellow arrows, observed on the black blade, upper skin, just inboard of the BS 215 fracture location.

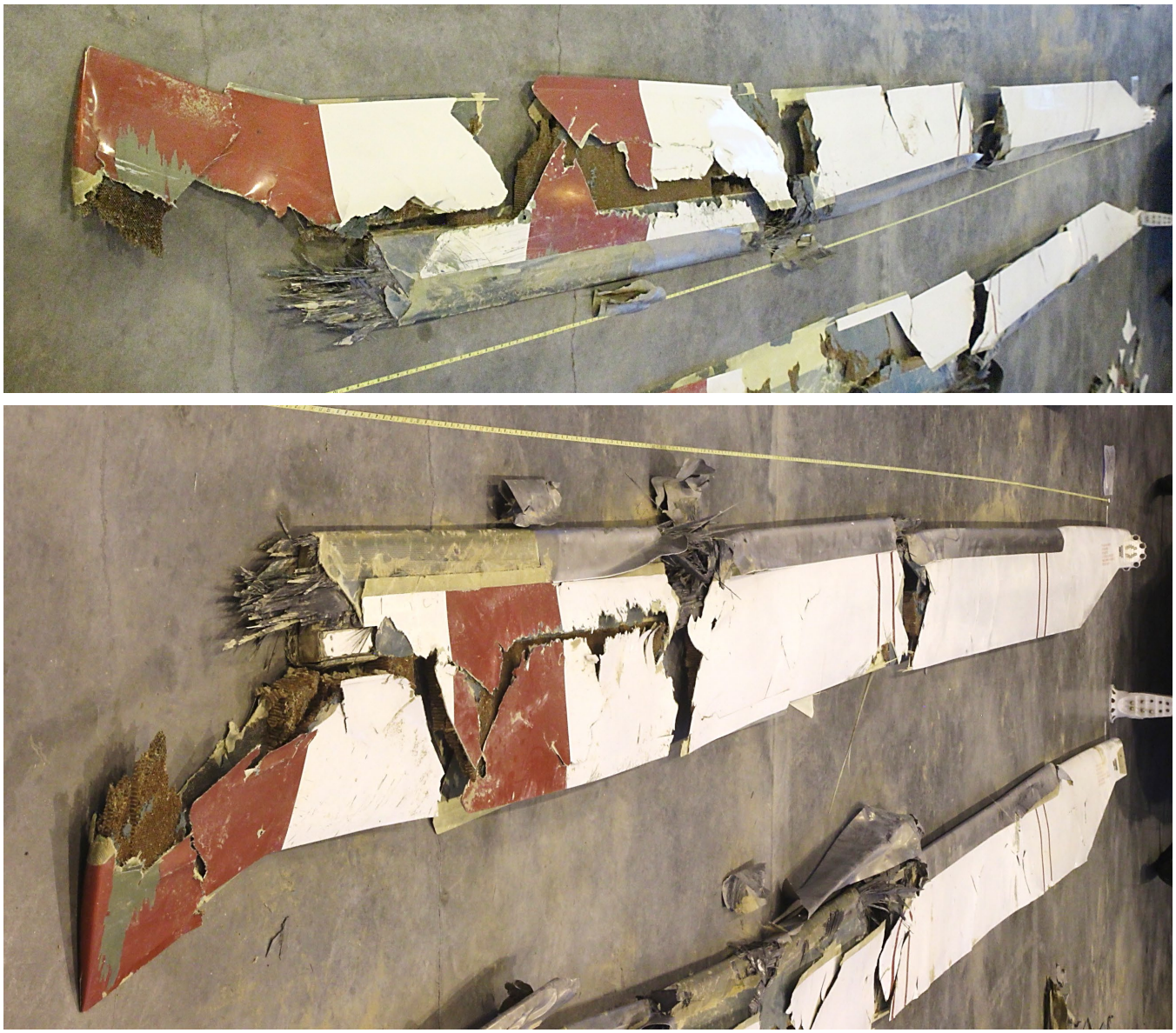

Figure 18: Photograph of the reconstructed black blade upper surface (top image) and lower surface (bottom image) viewed from tip to root.

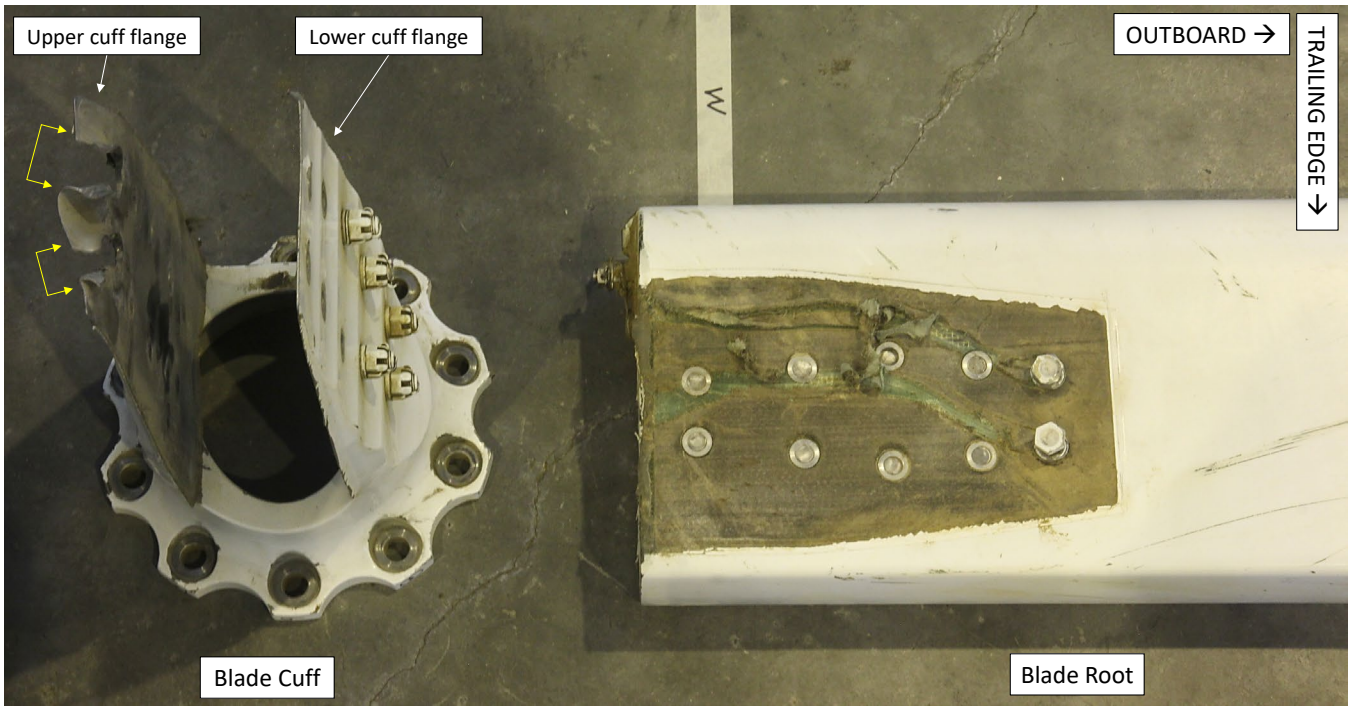

Figure 19: Photograph of the separated white blade cuff (spanwise view looking inboard) positioned next to the blade root, upper surface. Yellow brackets indicate deformation and fastener pullout observed on the upper cuff flange at the outboard fastener locations.

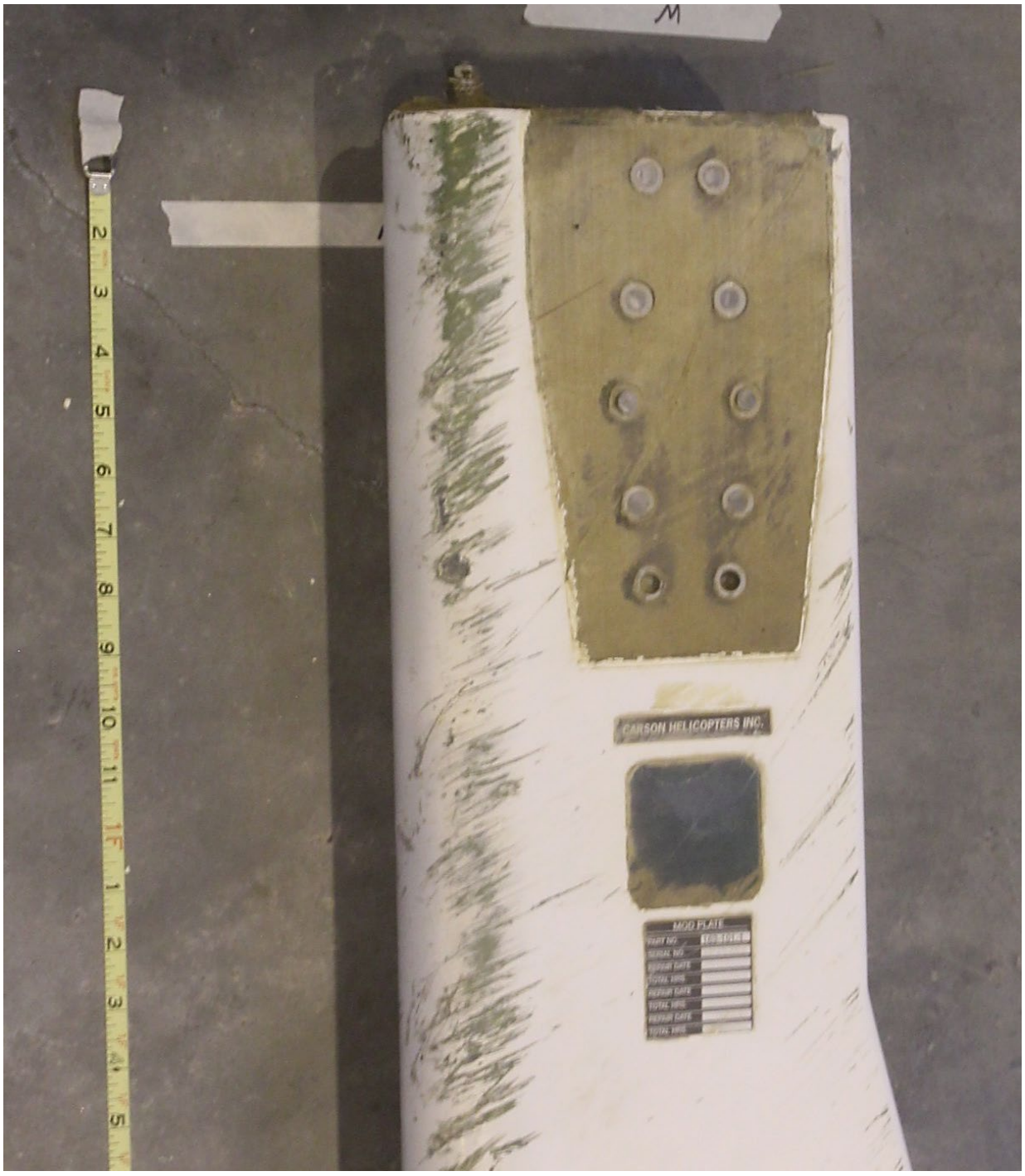

Figure 20: Photograph of the white blade identification placards and lower surface of the blade root where the blade cuff was separated.

Figure 21: A photograph of the lower surface of the white blade root looking outboard. Parallel curved scratches were observed on the inboard end. A branched crack feature is indicated by a yellow arrow and leading-edge cap separation is indicated between red arrows.

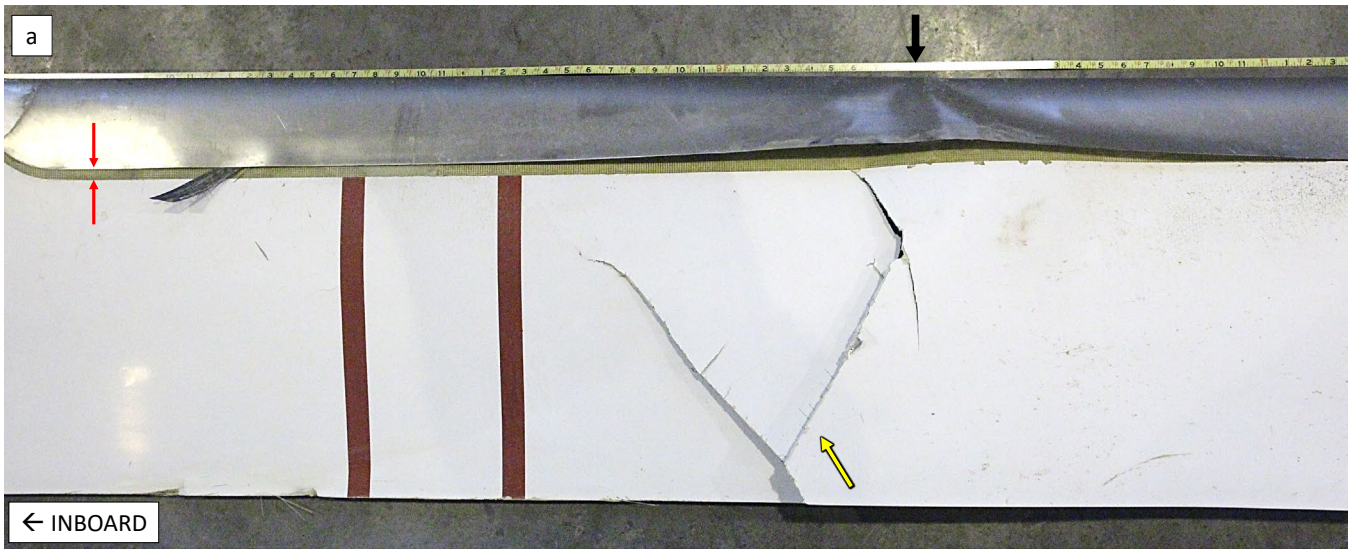

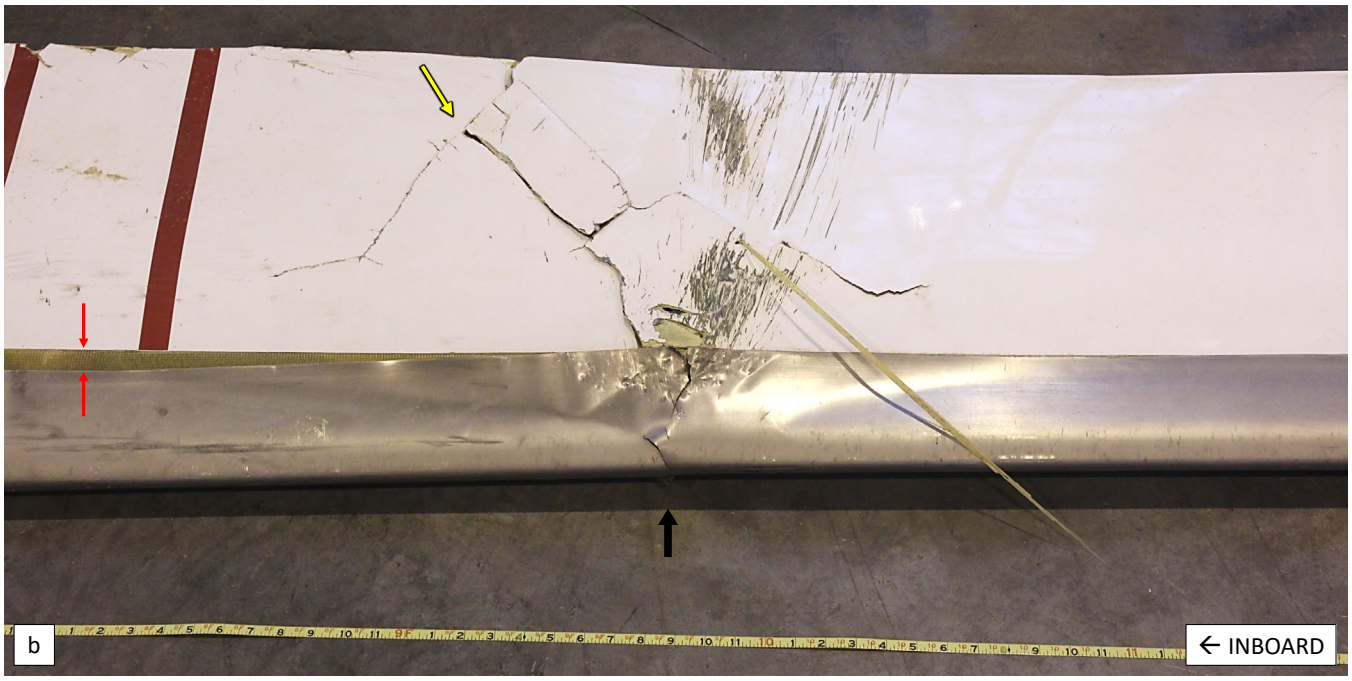

Figure 22: Photograph of the white blade BS 148 (black arrow) leading edge cap and partial spar fracture location a) upper surface and b) lower surface. A branched crack feature is indicated by a yellow arrow and leading-edge cap separation is indicated between red arrows.

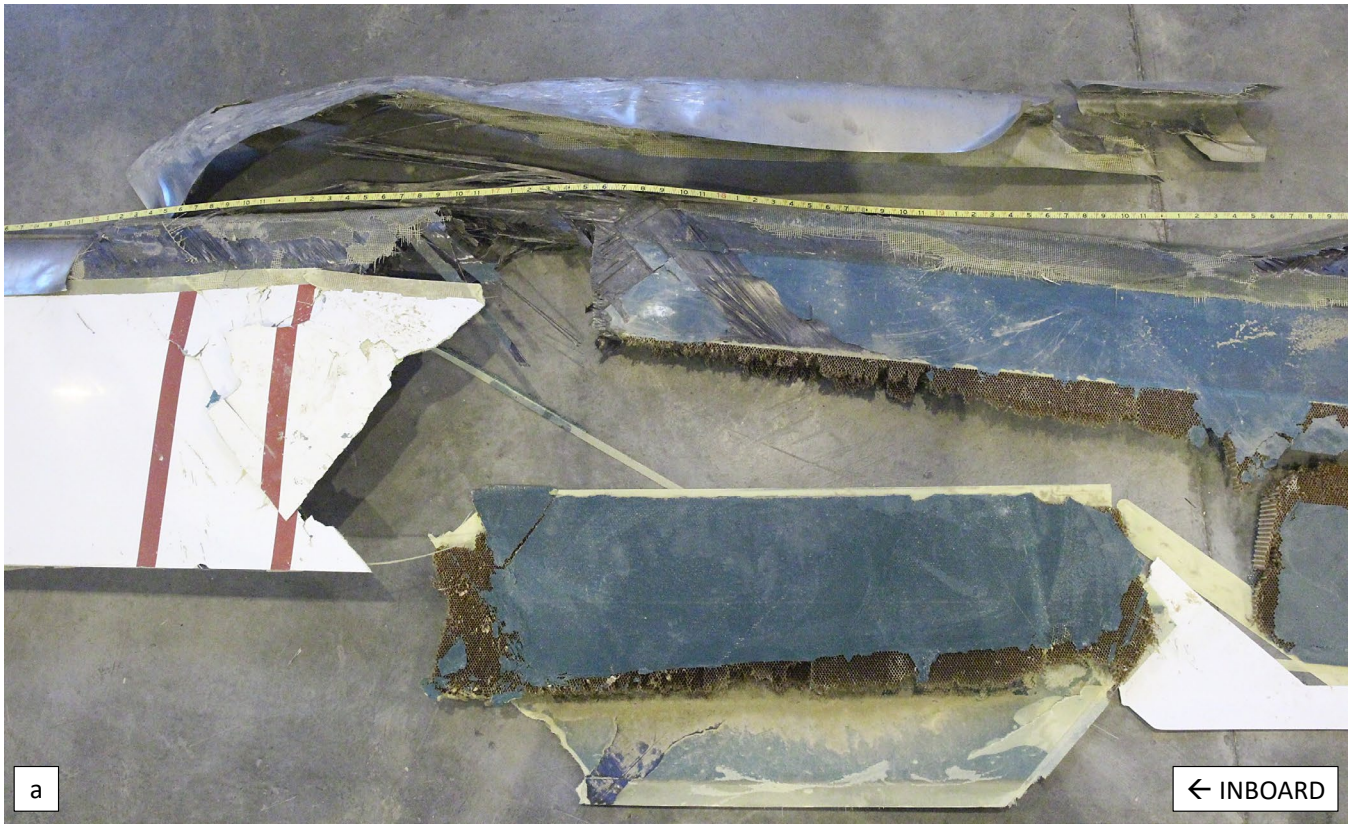

Figure 23: Photograph of the white blade BS 228 fracture location a) upper surface and b) lower surface.

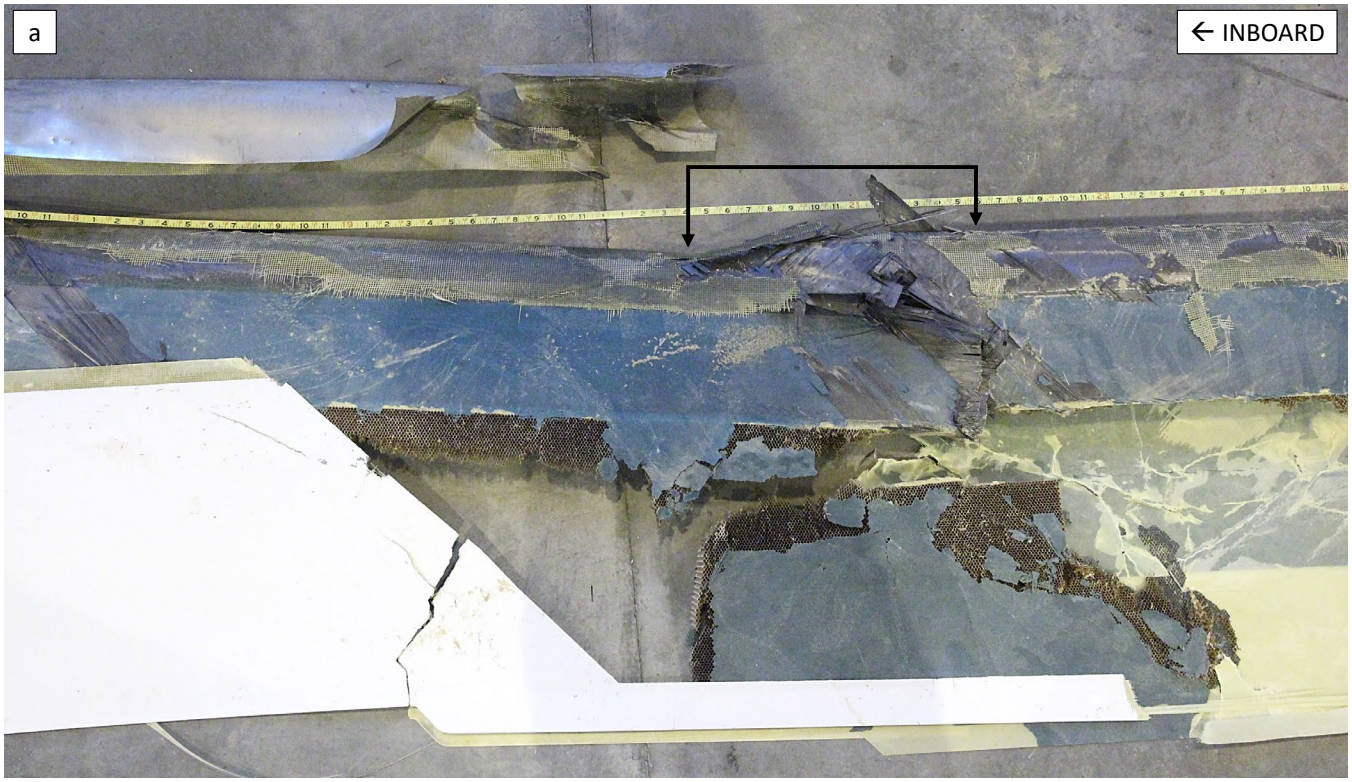

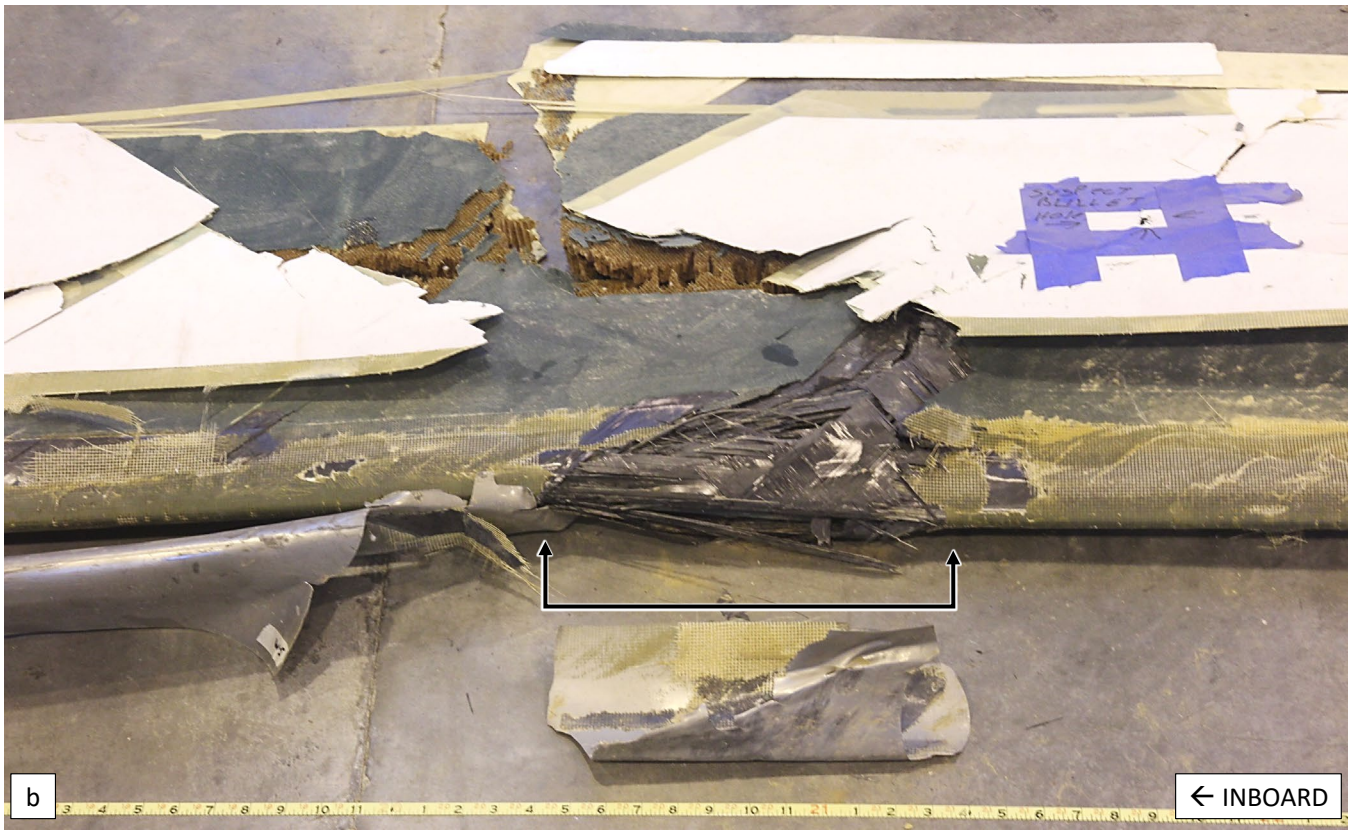

Figure 24: Photograph of the white blade BS 263 – 276 fracture location a) upper surface and b) lower surface.

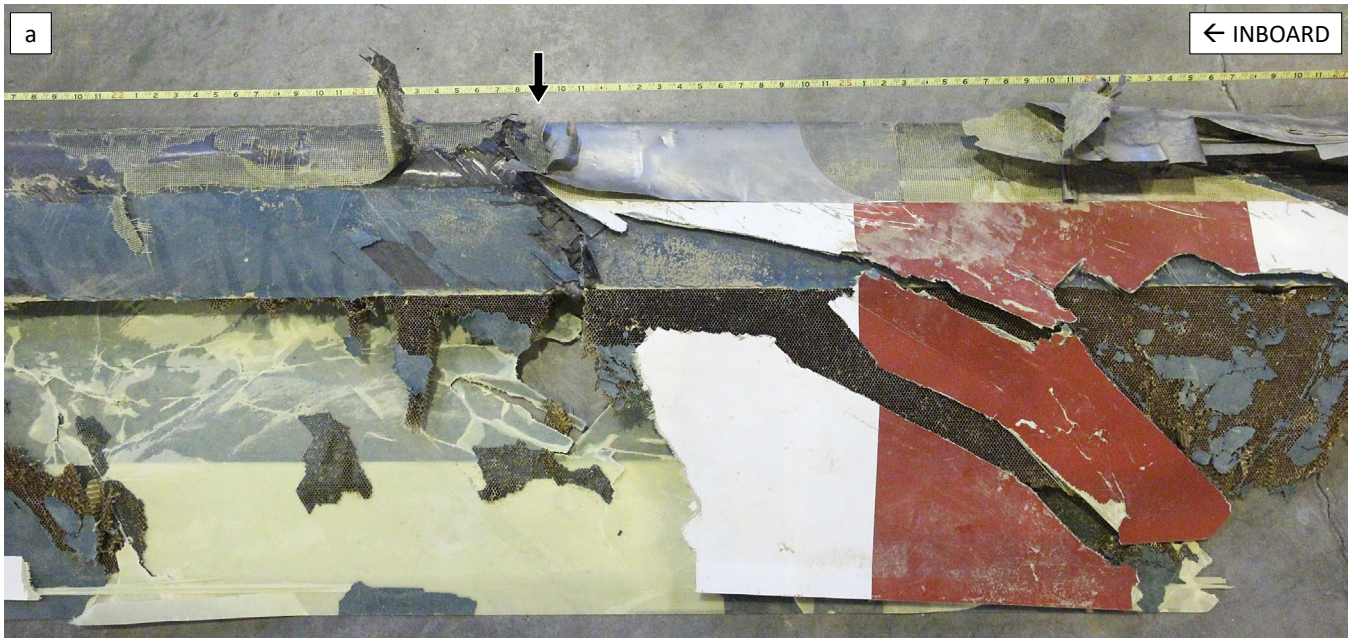

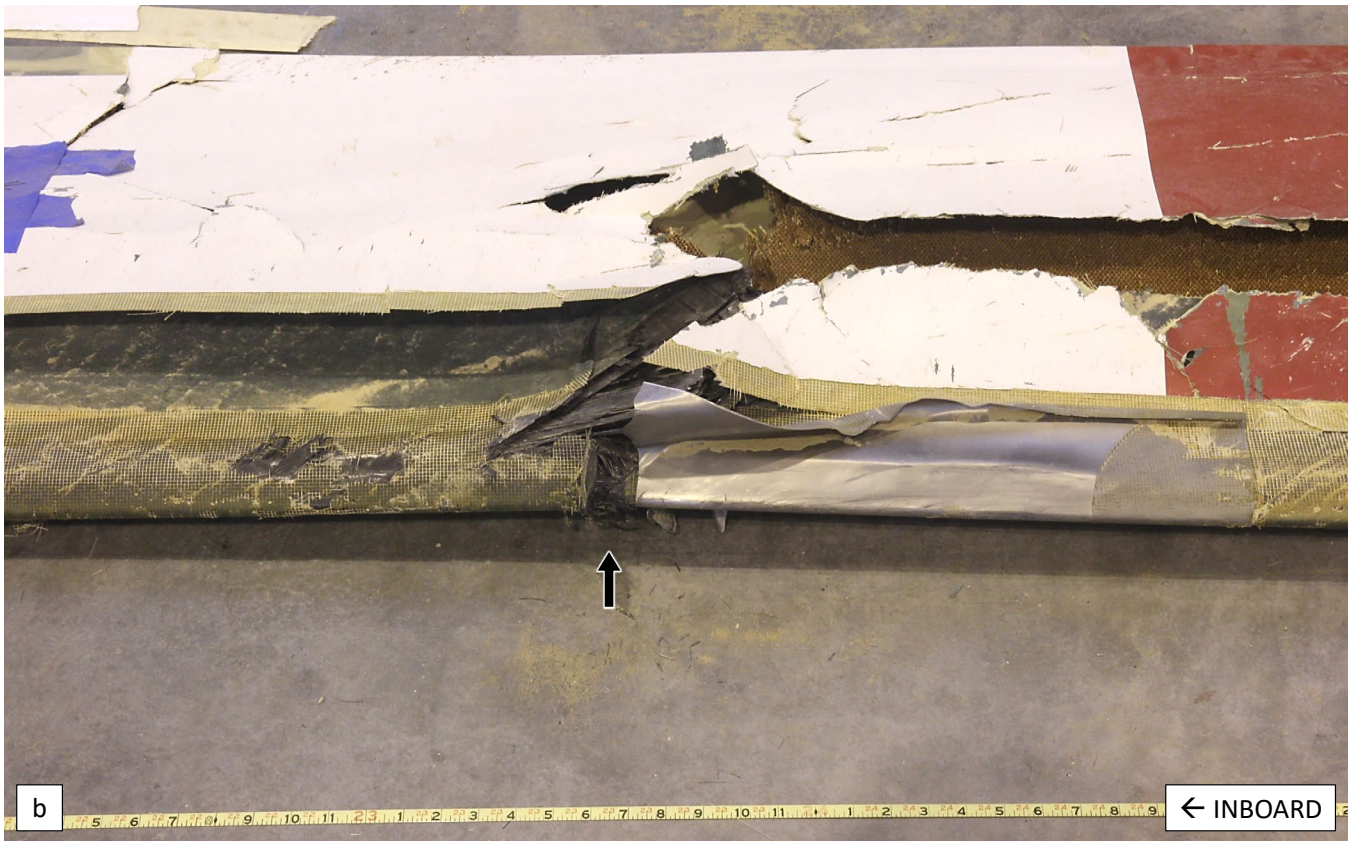

Figure 25: Photograph of the white blade BS 299 – 307 (black arrow) fracture location a) upper surface and b) lower surface.

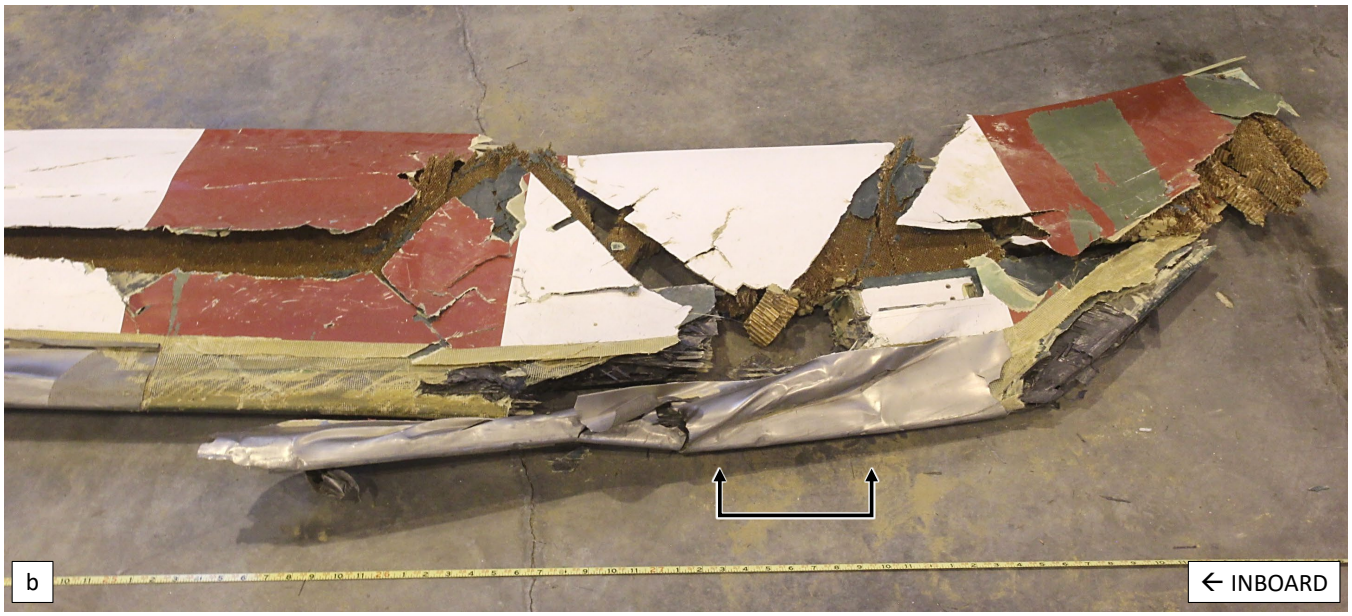

Figure 26: Photograph of the white blade BS 347 (between black arrows) fracture location a) upper surface and b) lower surface.

Figure 27: Photograph of the reconstructed white blade upper surface (top image) and lower surface (bottom image) viewed from tip to root.

Figure 28: Photograph of the yellow blade identification placards and lower surface of the attached blade cuff.

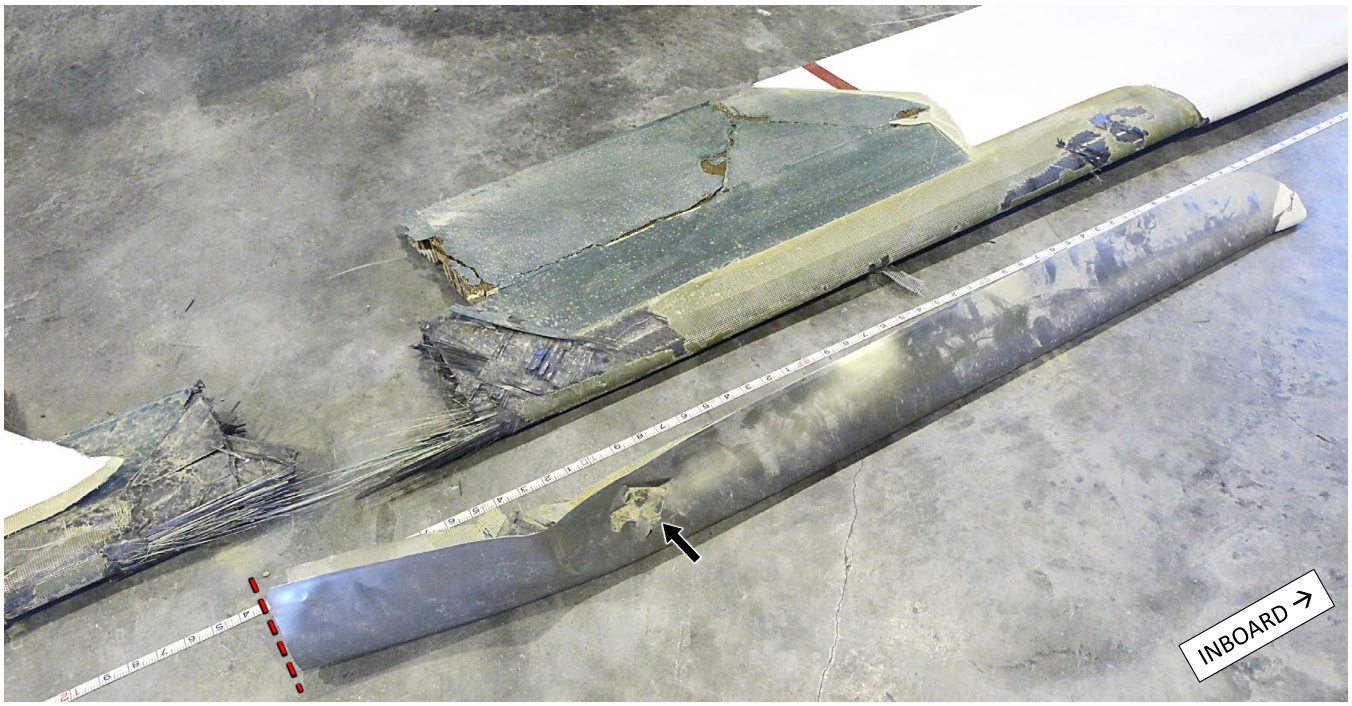

Figure 29: Photograph of a fractured (red dashed line) and separated piece of leading-edge cap from the yellow blade which spanned the BS 153 fracture location as viewed from the upper surface. A hole was observed in the leading-edge cap, indicated by the black arrow.

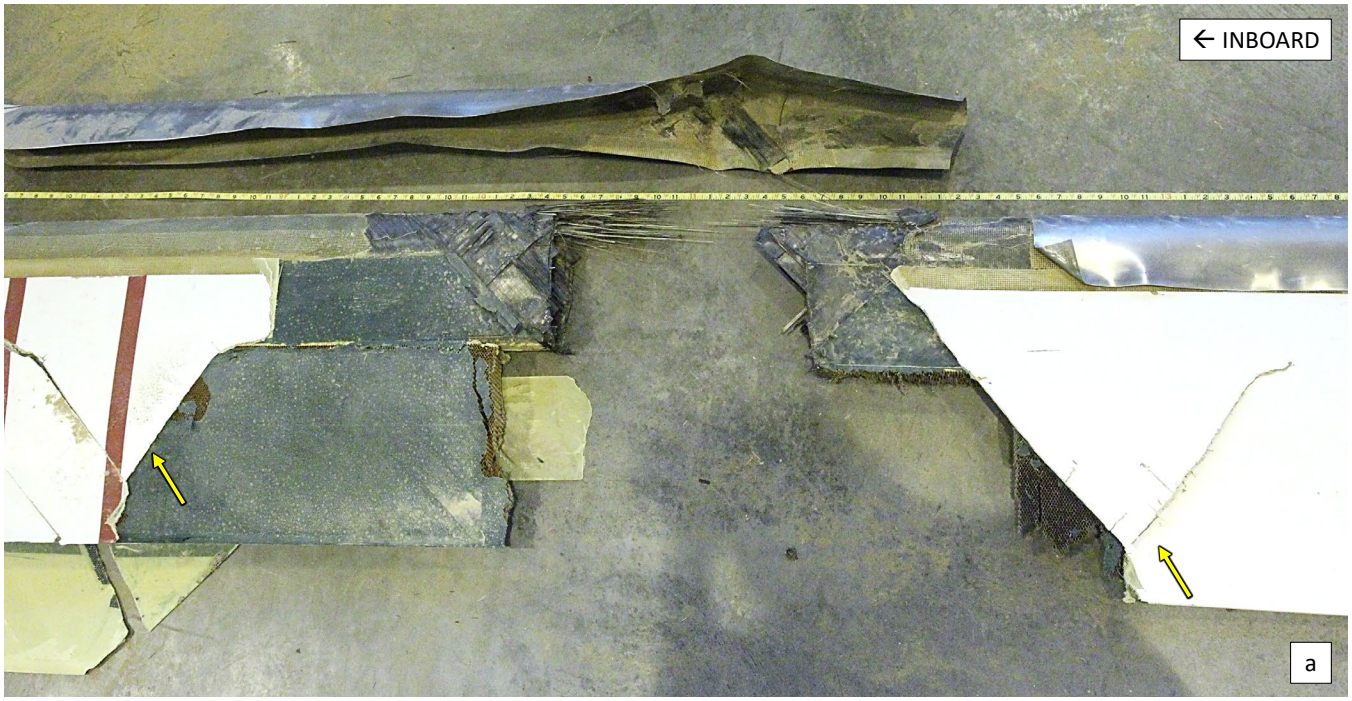

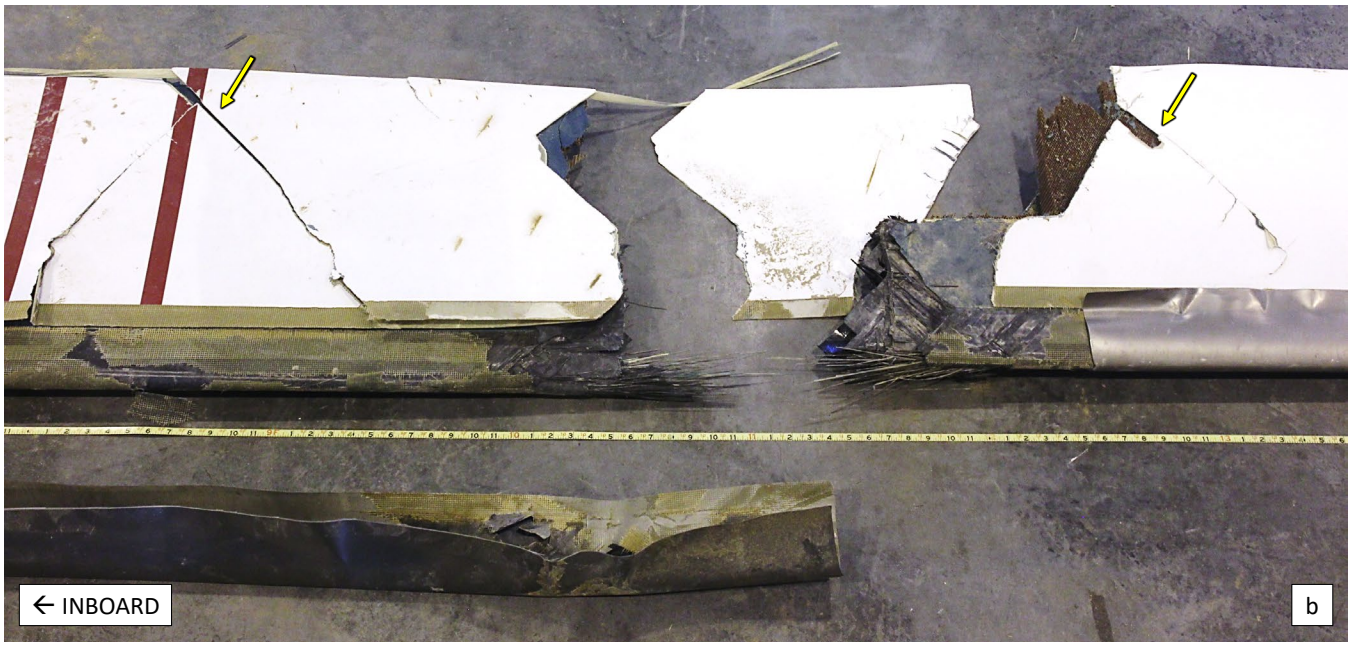

Figure 30: Photograph of the yellow blade BS 153 fracture location a) upper surface and b) lower surface. Branched crack features are indicated by yellow arrows.

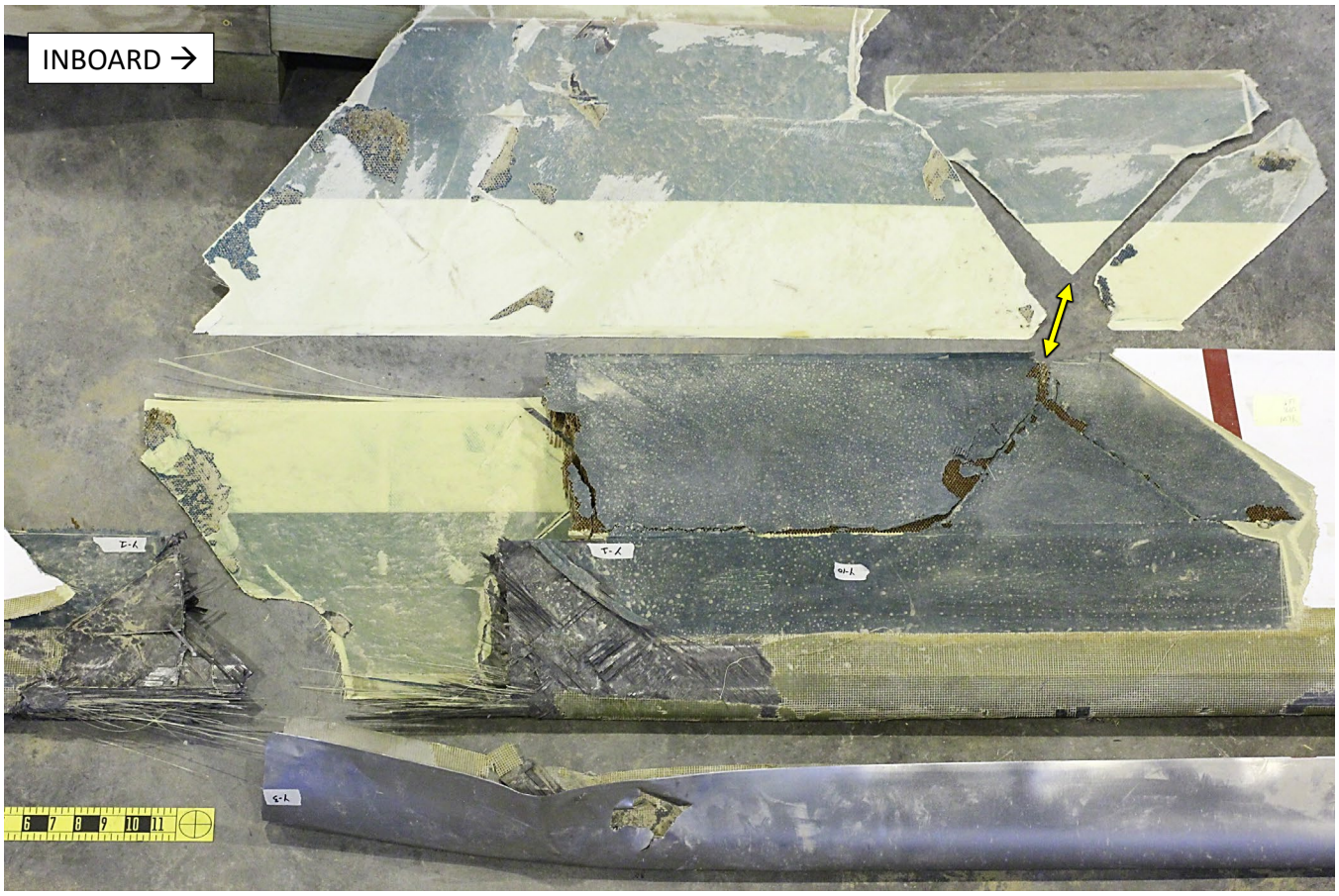

Figure 31: Photograph of the yellow blade BS 153 fracture location (upper surface) with separated blade skin laid open to reveal the disbonded interface. A branched crack feature is indicated by yellow arrows.

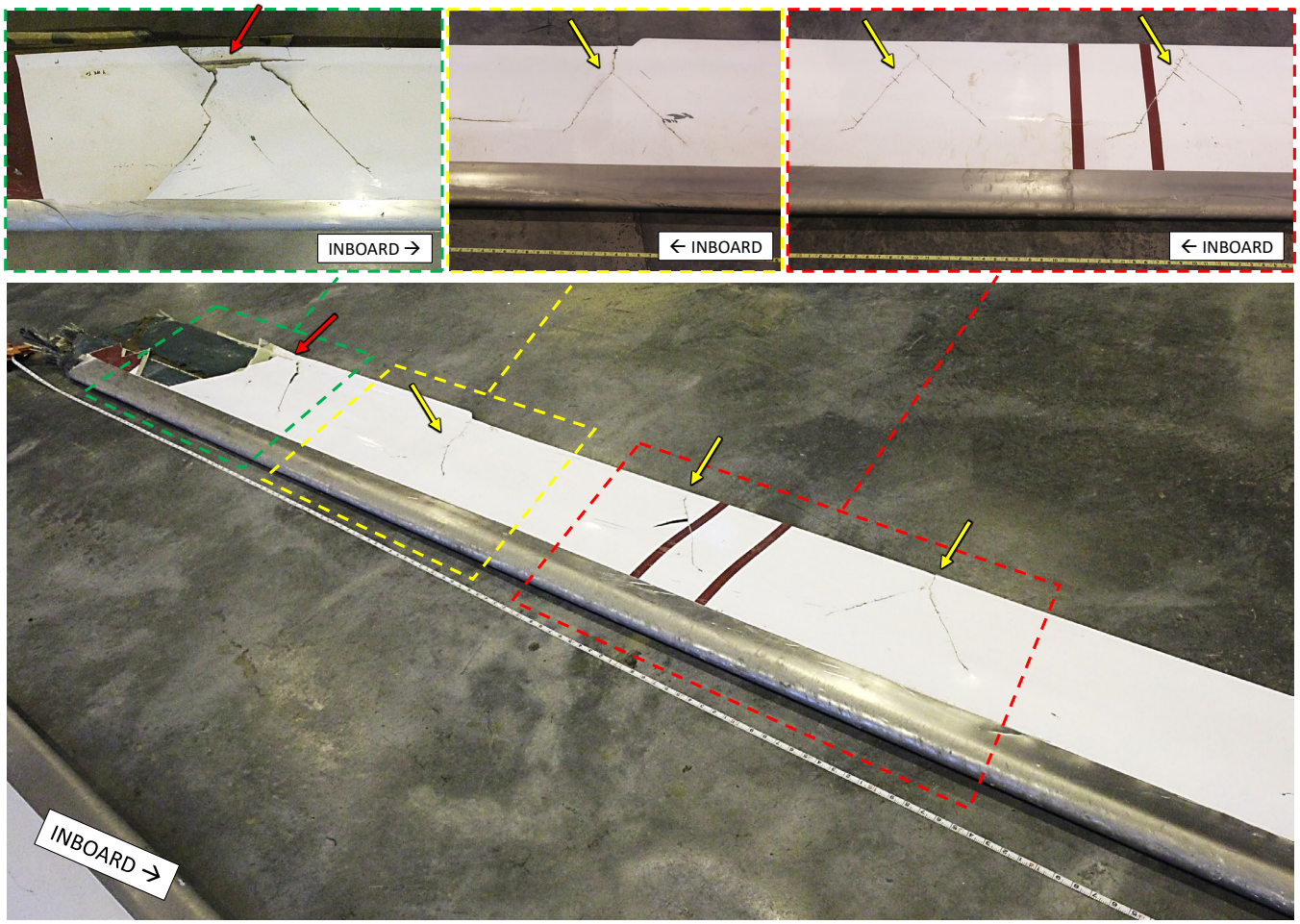

Figure 32: **Bottom Image:** Photograph of branched crack features observed on the upper surface of the outboard piece of yellow blade. Red and yellow inset images above show the coordinating branched crack feature on the lower surface. The green inset image above shows a closer view of the upper surface branched crack feature.

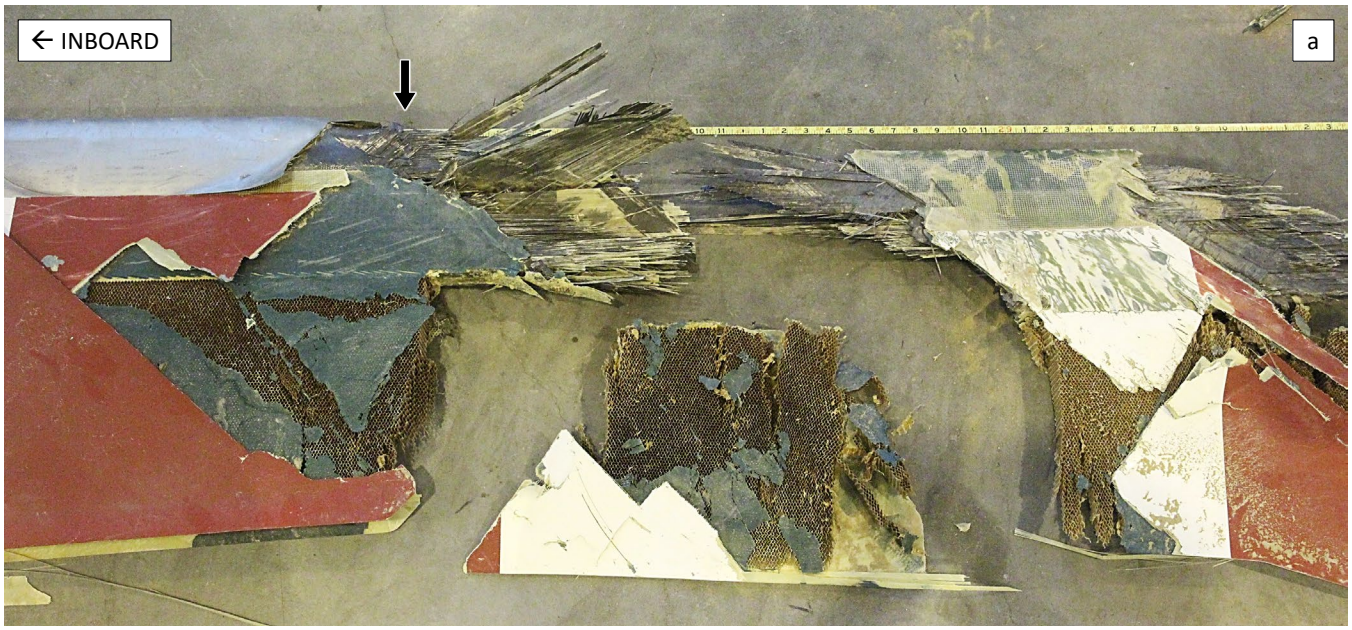

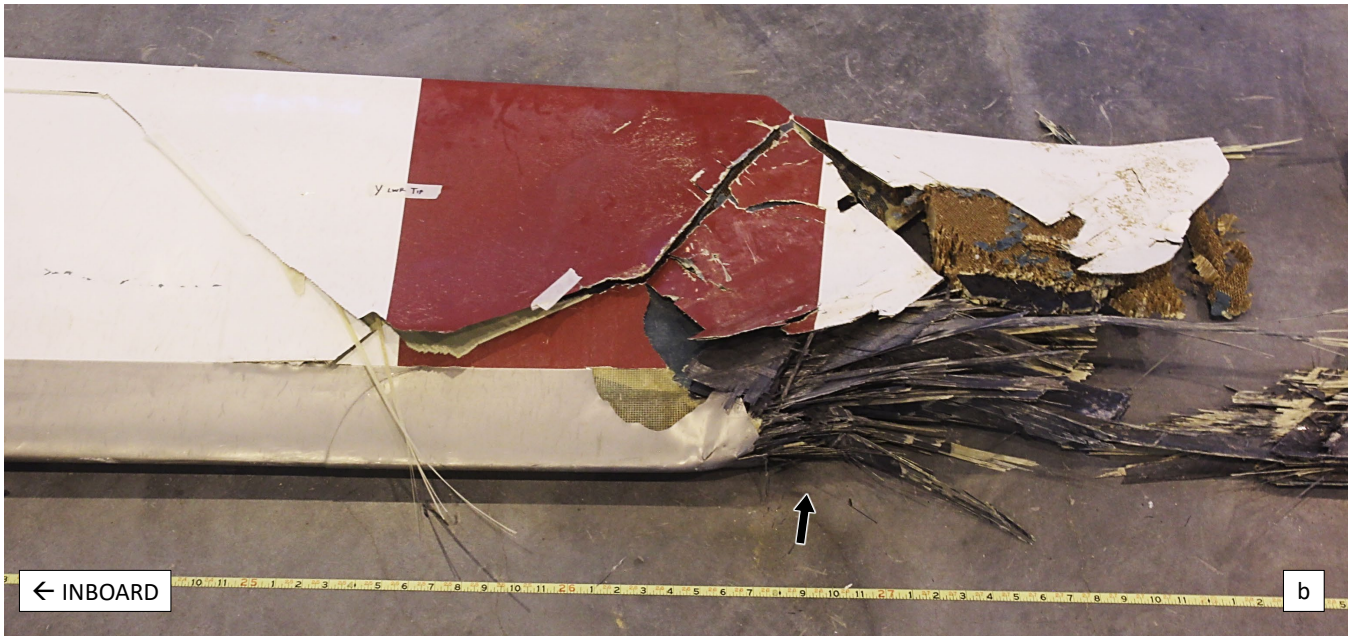

Figure 33: Photograph of the yellow blade BS 332 – 336 (black arrow) fracture location a) upper surface and b) lower surface.

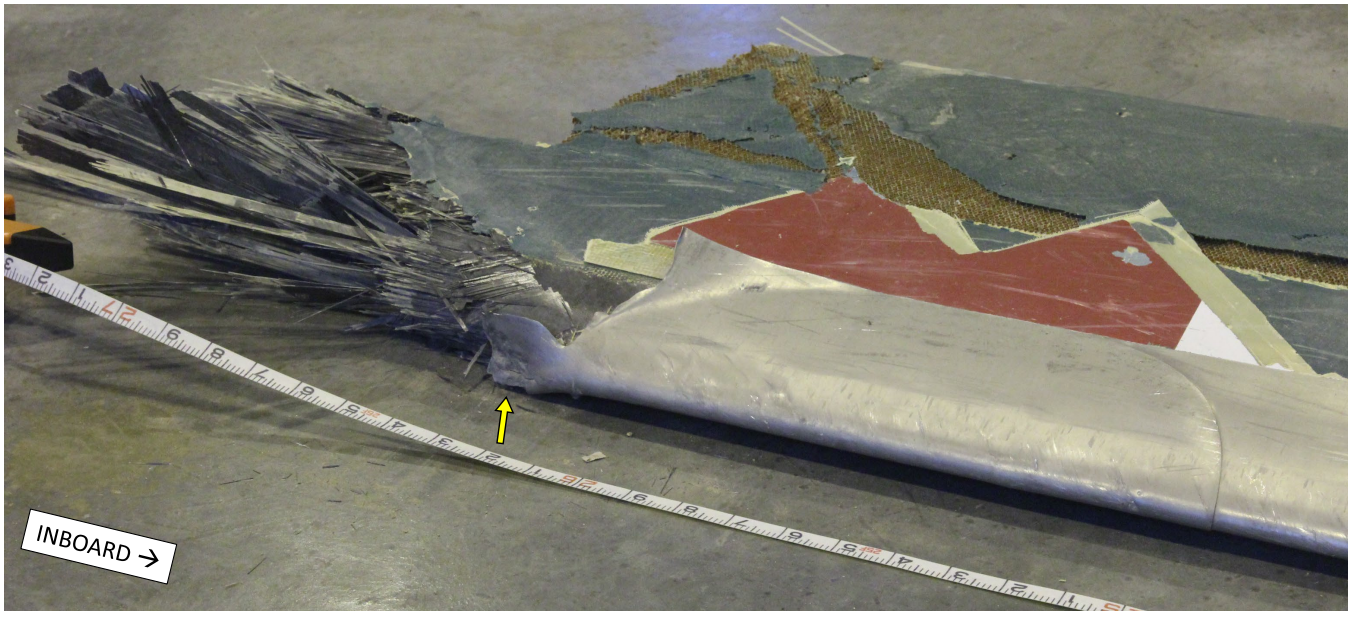

Figure 34: Photograph of the yellow blade BS 332 – 336 fracture location (upper surface) with impact witness mark on leading-edge cap indicated by a yellow arrow.

Figure 35: Photograph of the reconstructed yellow blade upper surface (top image) and lower surface (bottom image) viewed from tip to root.

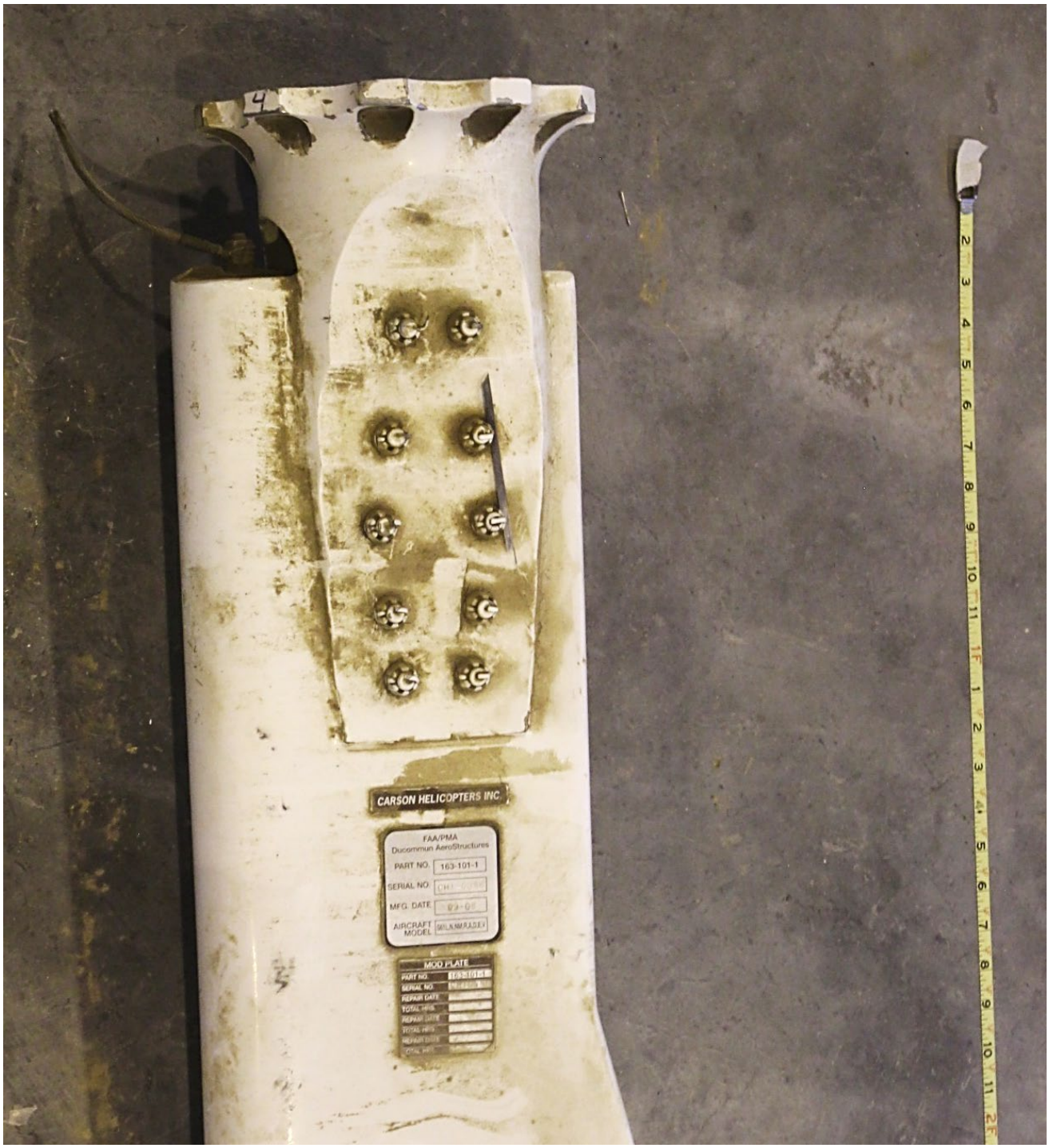

Figure 36: Photograph of the blue blade identification placards and lower surface of the attached blade cuff.

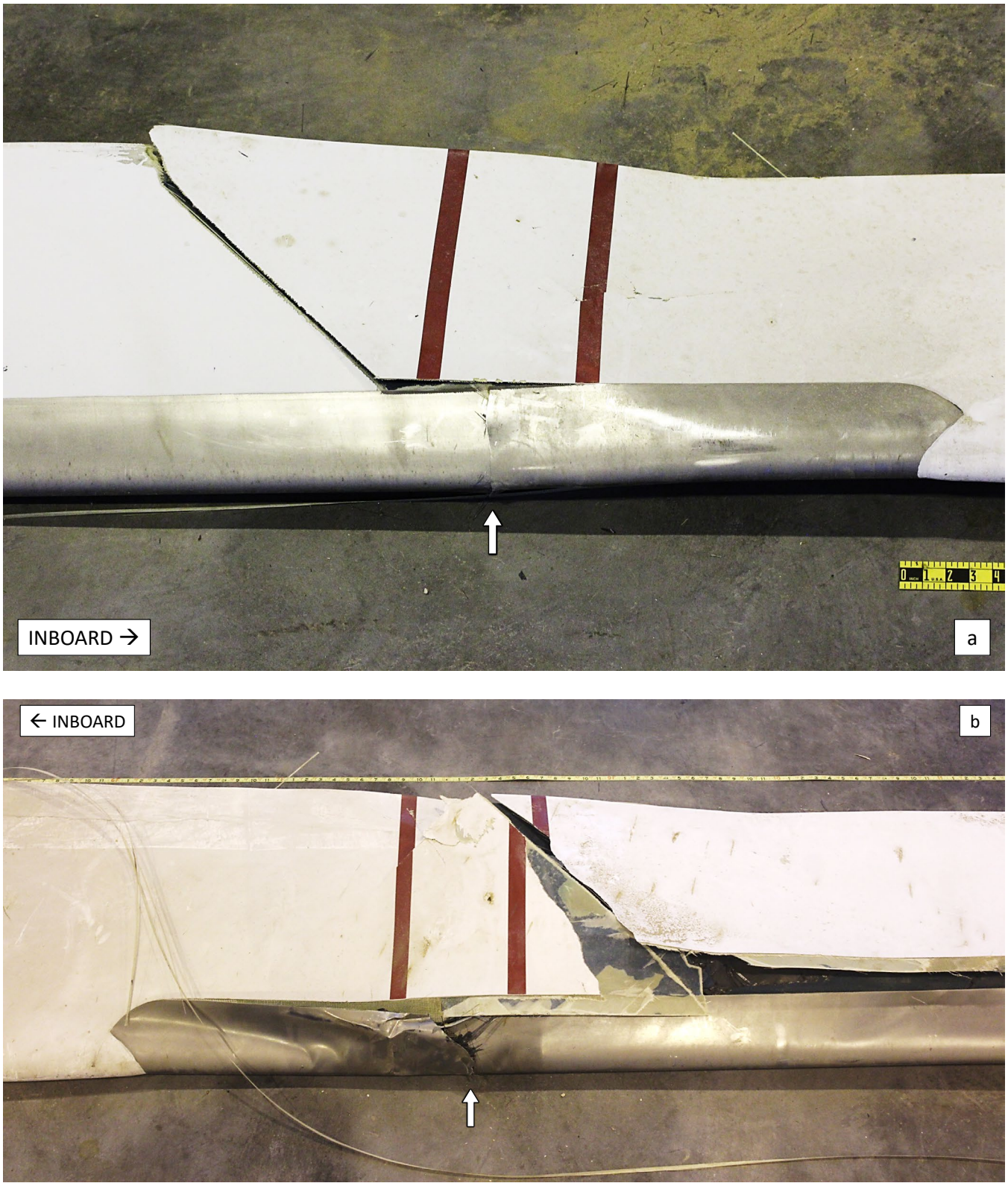

Figure 37: Photograph of the blue blade BS 126 (white arrow) fracture location a) upper surface and b) lower surface.

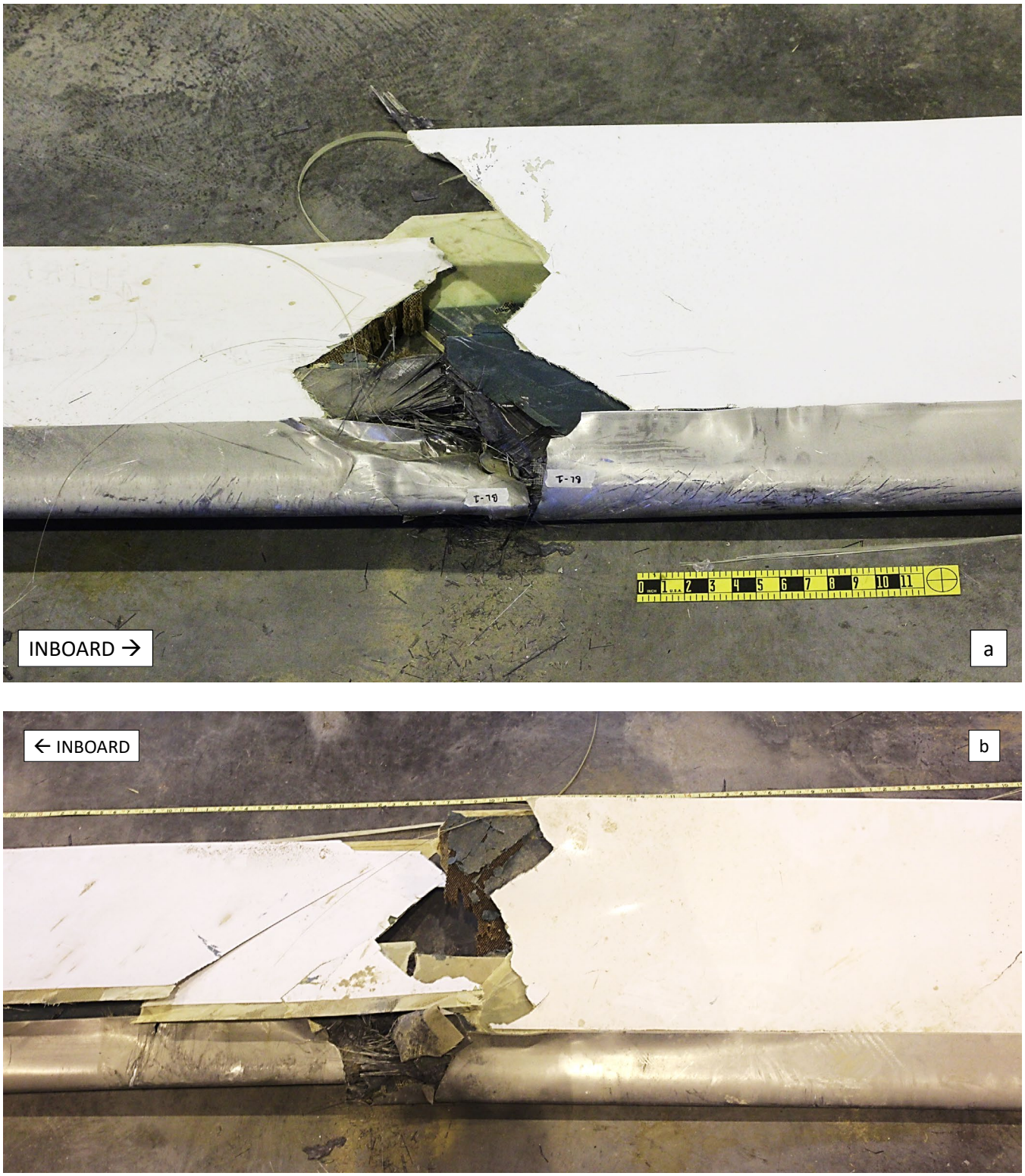

Figure 38: Photograph of the blue blade BS 177 fracture location a) upper surface and b) lower surface.

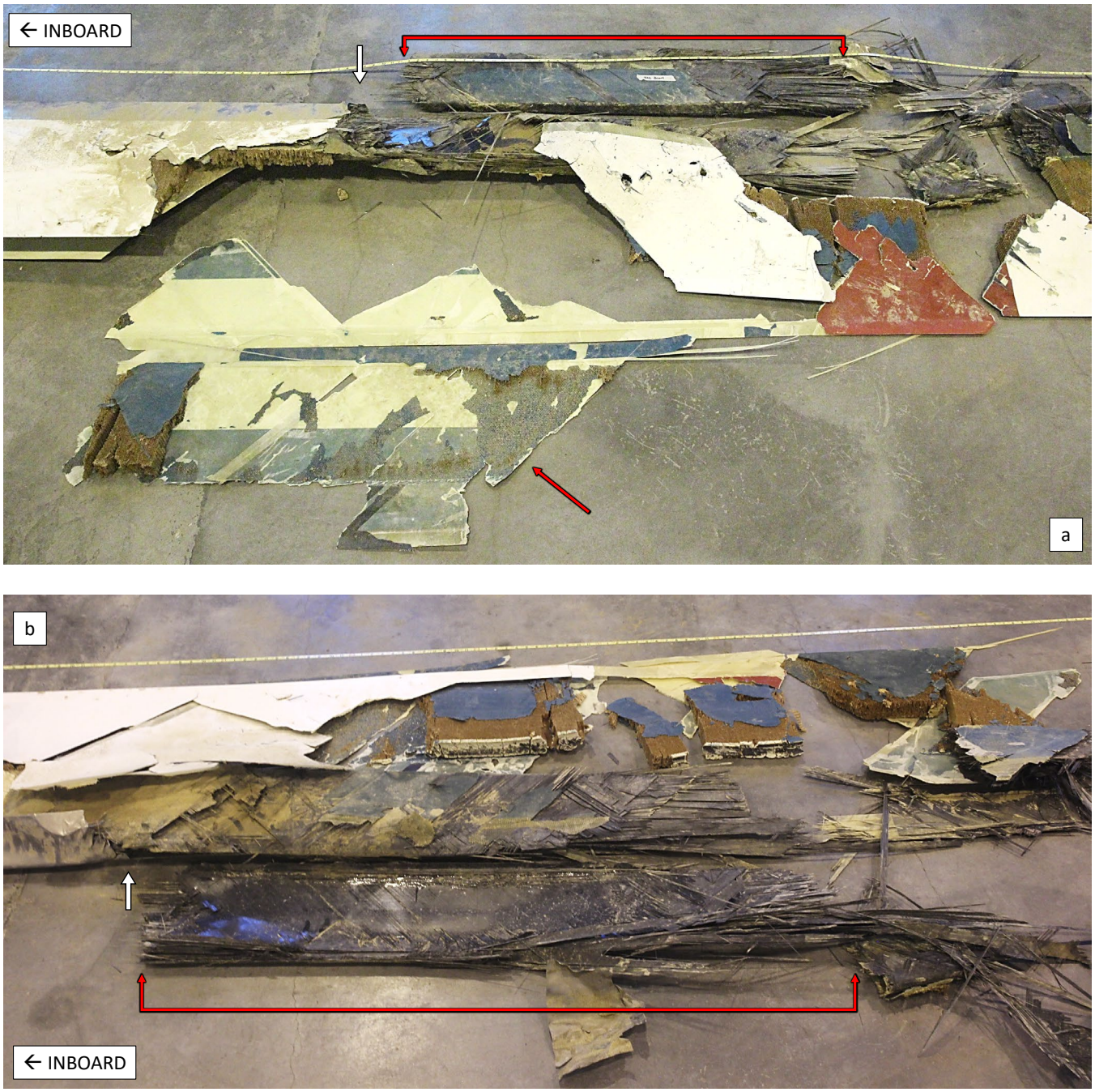

Figure 39: Photograph of the blue blade BS 277 (white arrow) fracture location a) upper surface and b) lower surface. Red arrows indicate pieces of the spar and blade skin that was received labeled “these pieces came from inside the tail boom.”

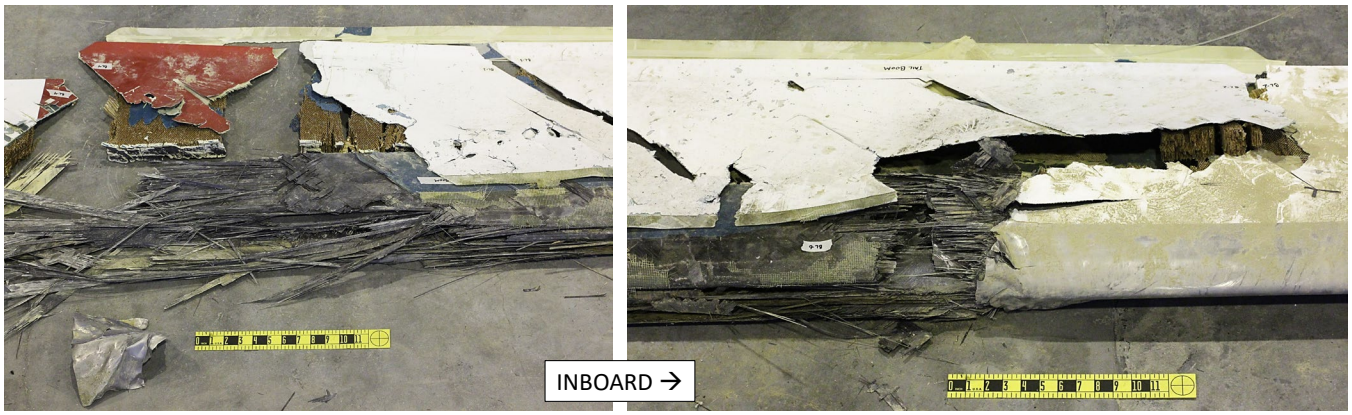

Figure 40: Photograph of the upper surface of the blue blade BS 325 fracture location (left) and the BS 277 fracture location (right) with spar and skin pieces partially reconstructed.

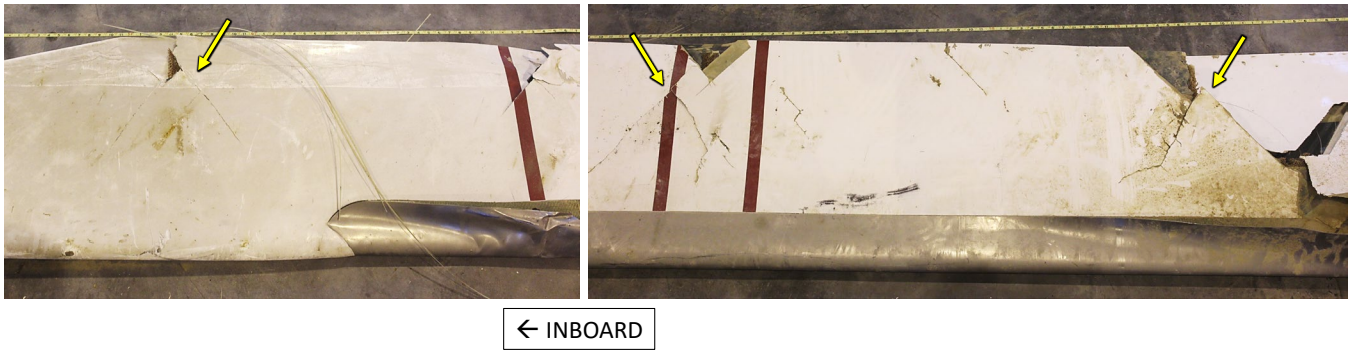

Figure 41: Photograph of branched cracking sites, indicated by yellow arrows, observed on the blue blade, lower skin.

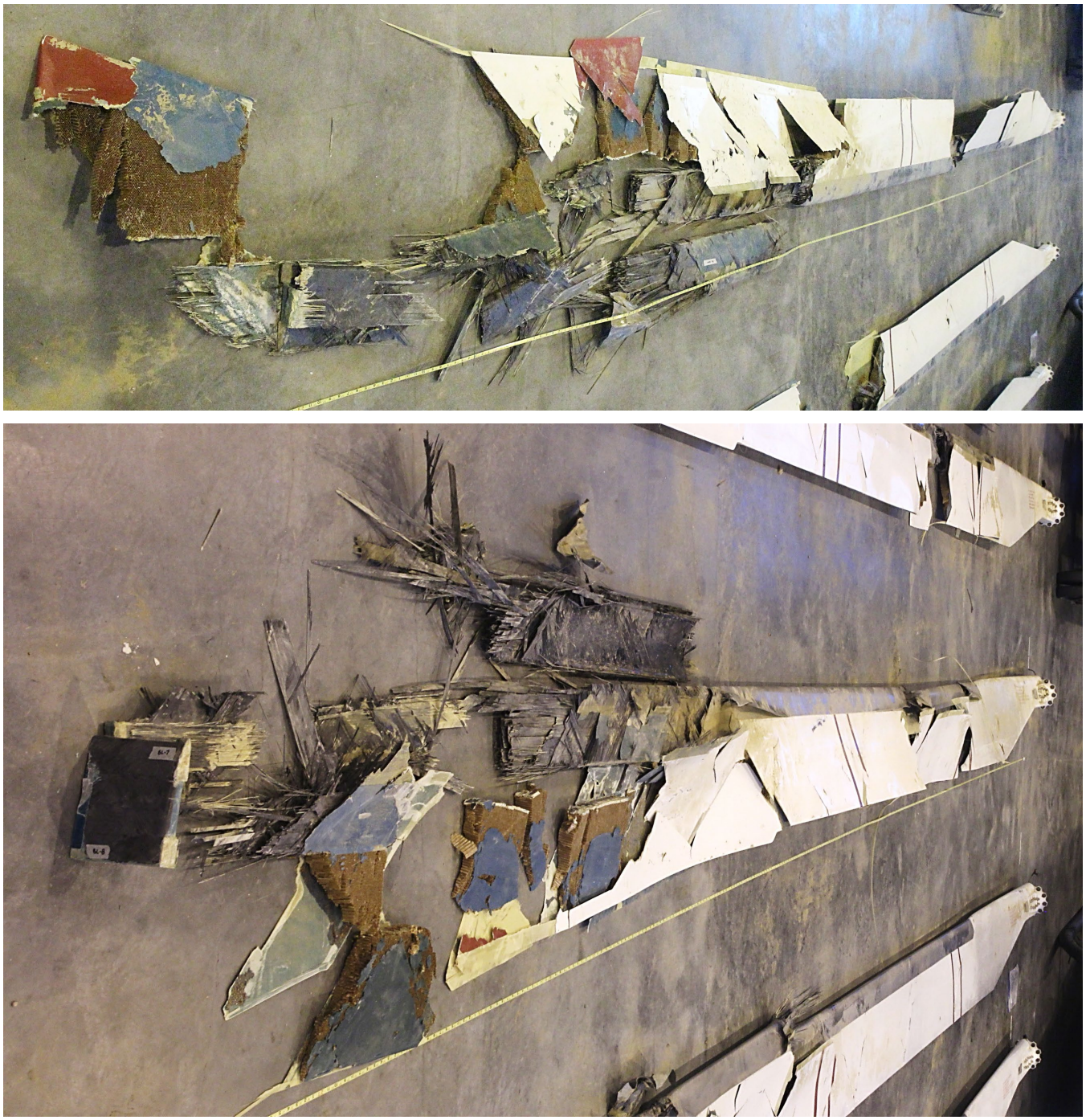

Figure 42: Photograph of the reconstructed blue blade upper surface (top image) and lower surface (bottom image) viewed from tip to root.

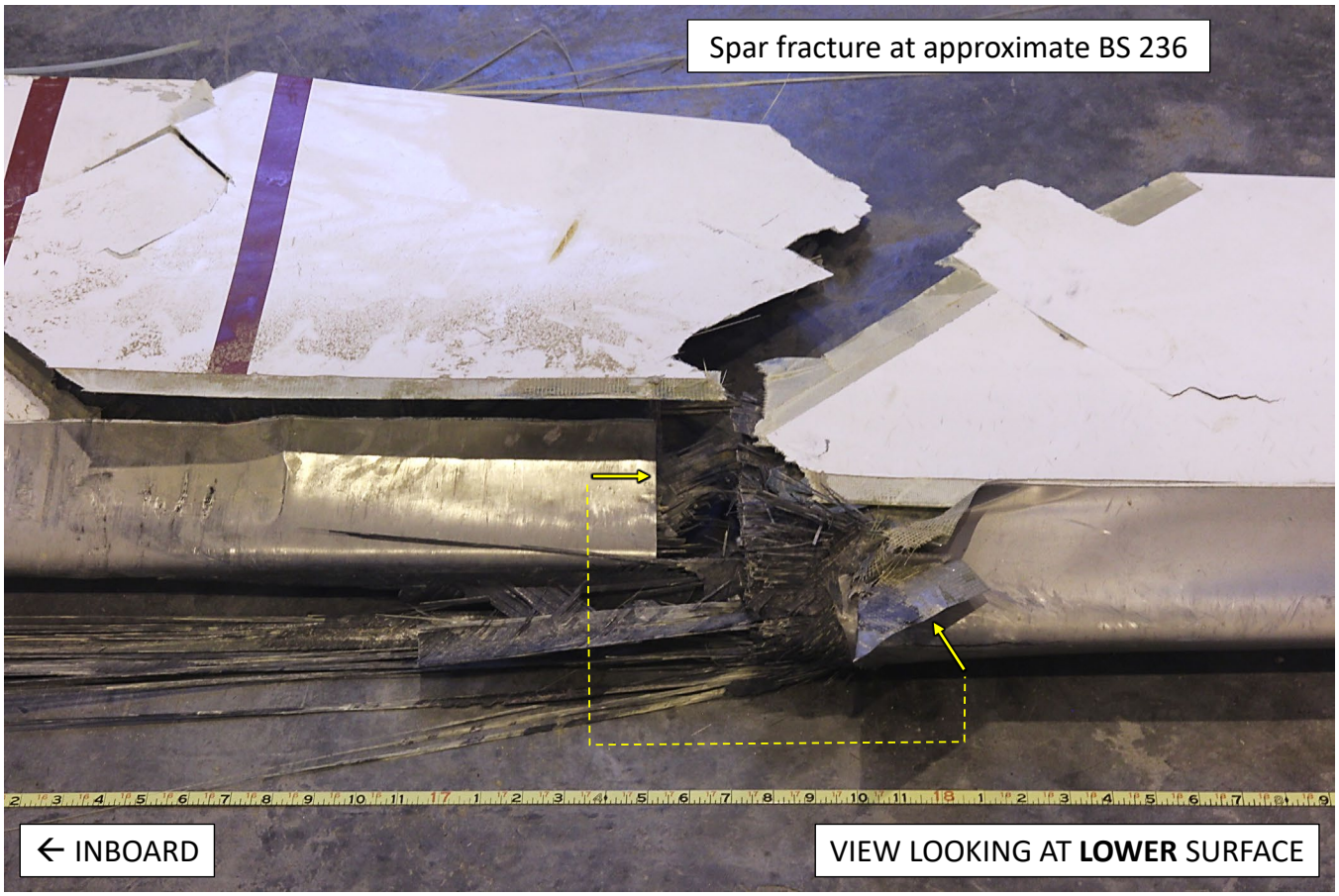

Figure 43: Photograph of the red blade leading-edge cap flat fracture at the BS 236 fracture location viewed from the lower surface. Yellow arrows indicated mating leading-edge cap fracture surfaces.

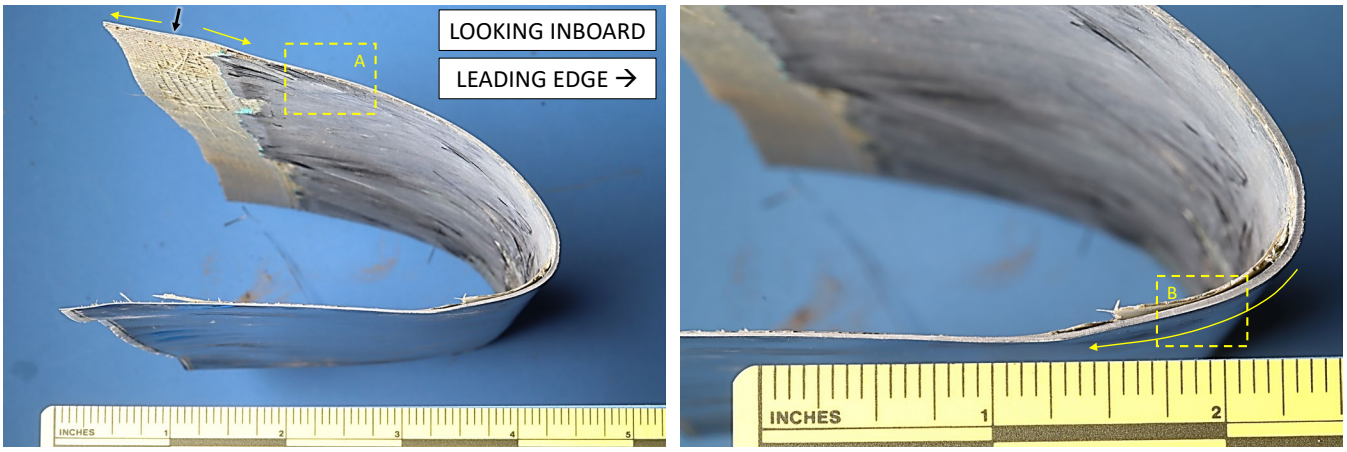

Figure 44: Photograph of the inboard red blade leading-edge cap flat fracture surface (left) with the origin area indicated by a black arrow. A closer view of the lower surface near the highlight is shown on the right. Crack propagation direction is indicated by yellow arrows. Closer views of the origin area and the areas boxed in yellow are shown in subsequent figures.

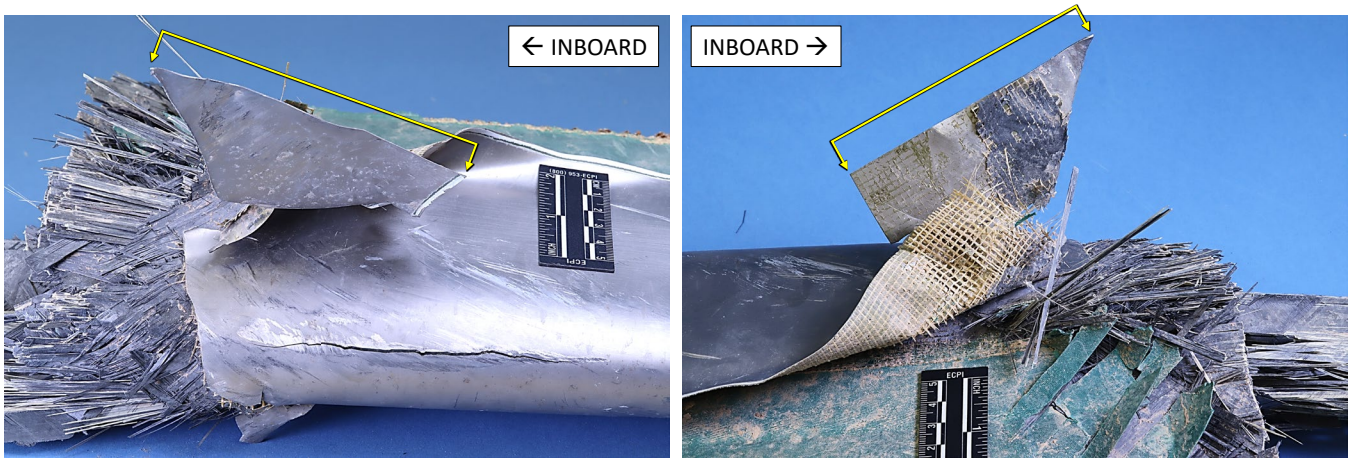

Figure 45: Photographs of the mating outboard red blade leading-edge cap flat fracture surface indicated by yellow brackets.

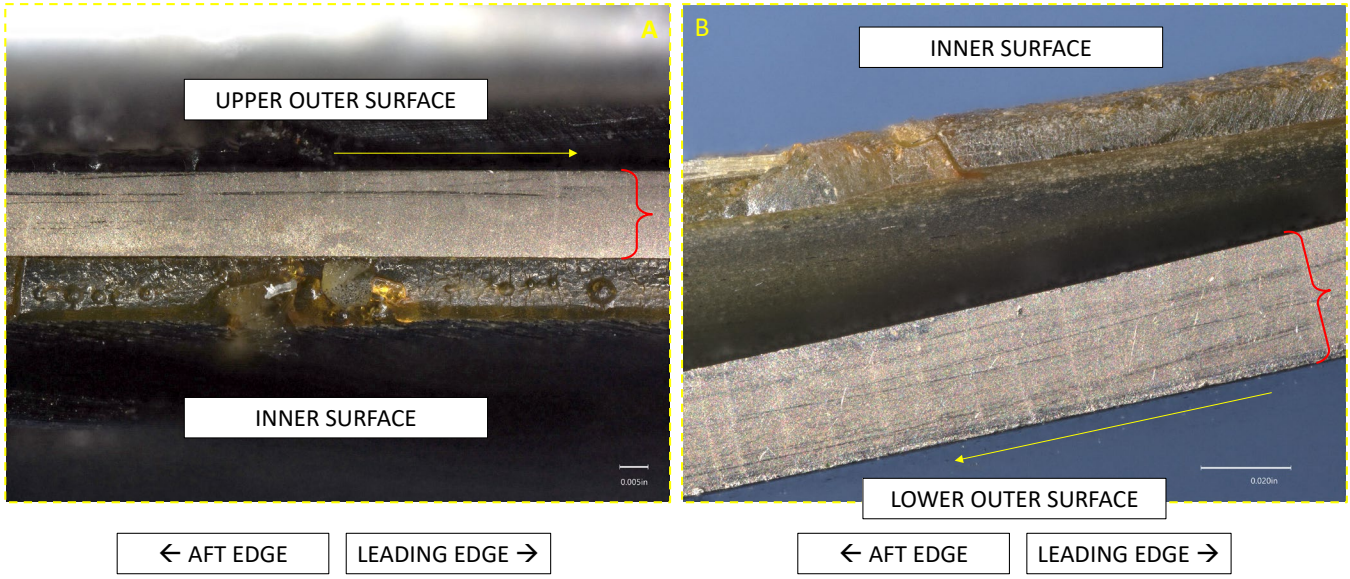

Figure 46: Digital microscope images of area A (left) and area B (right) as marked in figure 44. Visible crack arrest marks are oriented approximately vertically on the fracture surface bracketed in red. Yellow arrows indicate propagation direction.

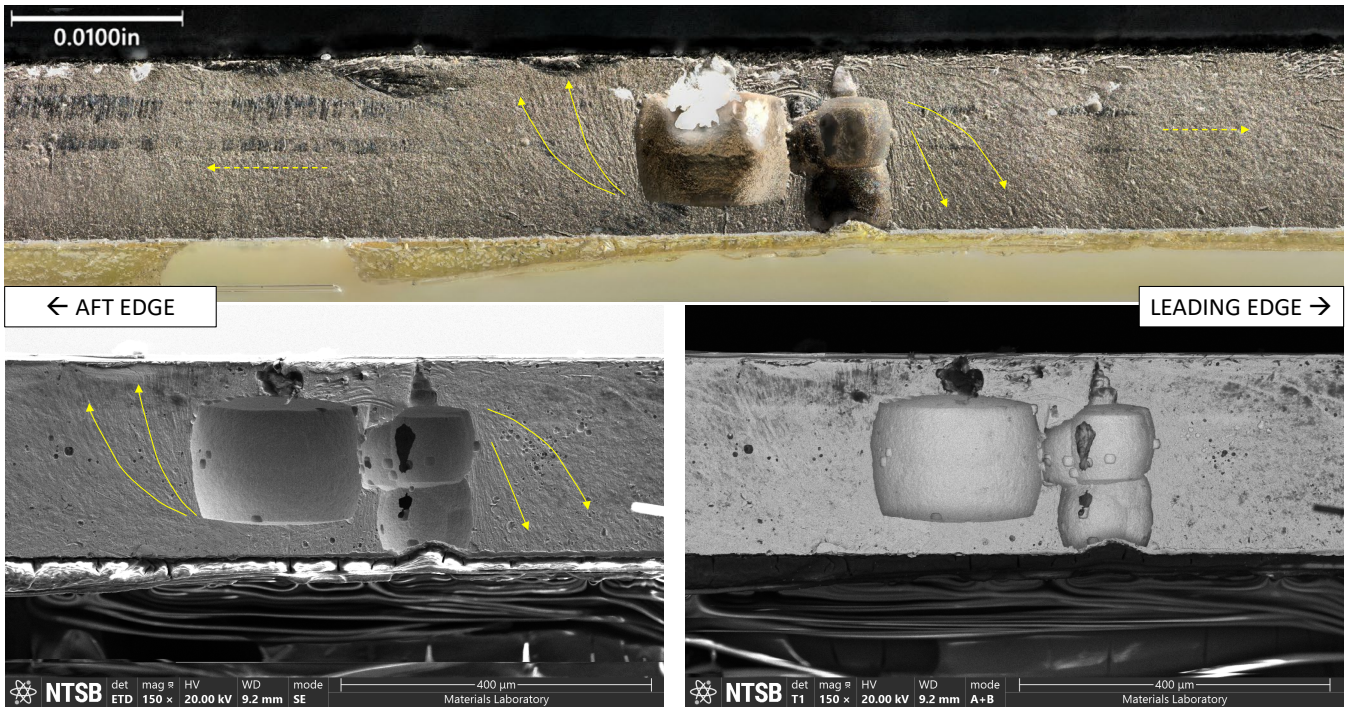

Figure 47: A digital microscope image (top), a secondary electron image (bottom left) and a backscattered electron image (bottom right) of the red blade leading-edge cap flat fracture origin area showing internal voids. Solid yellow arrows indicate radial marks observed emanating from the voids in opposite directions. The dashed yellow arrows indicate the general crack propagation direction from the origin area.

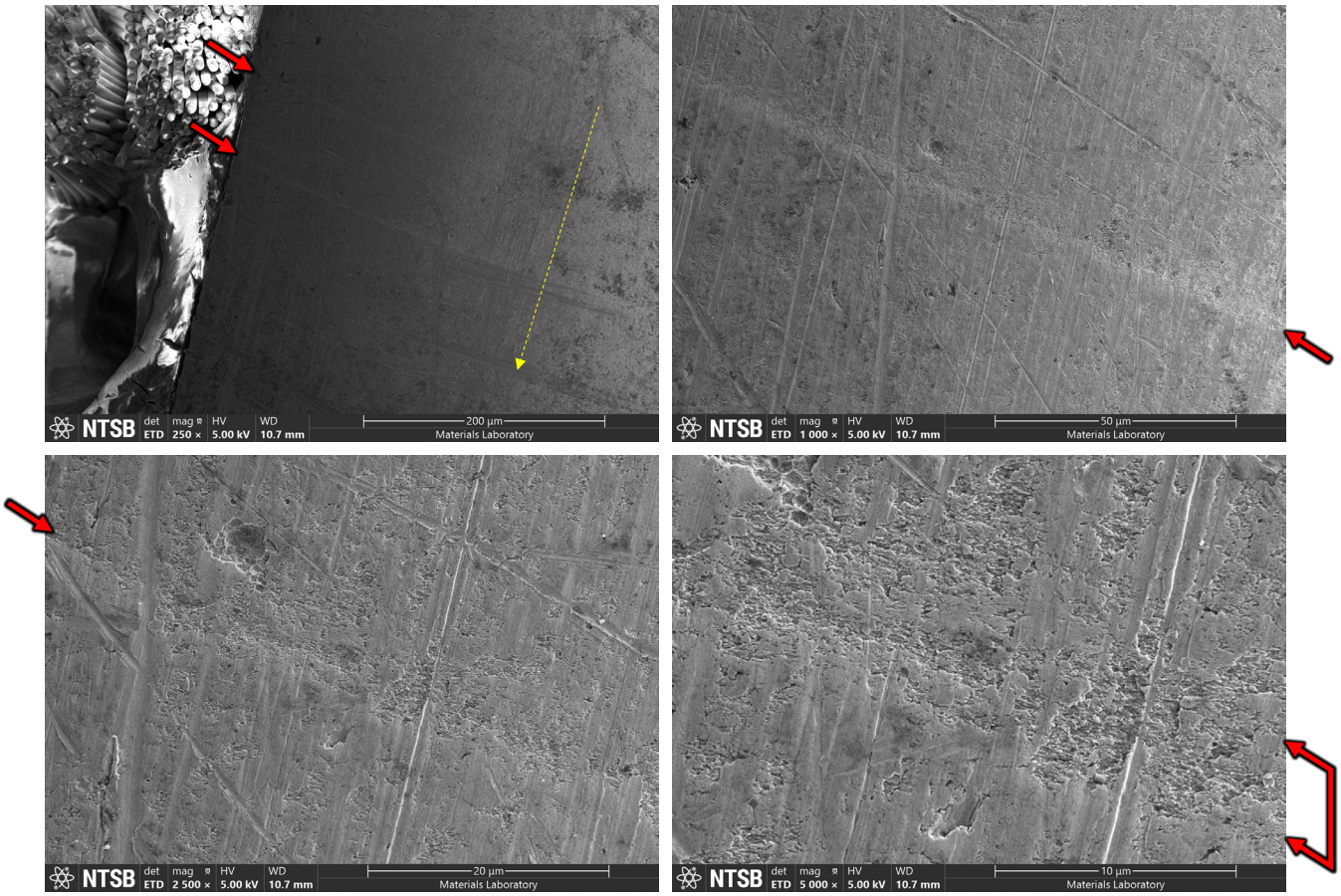

Figure 48: Secondary electron images of the red blade leading edge cap flat fracture surface showing crack arrest marks indicated by red arrows at progressively higher magnification. The crack propagation direction is indicated by the yellow arrow and applies to all images. The fracture surface was generally scratched and smeared.

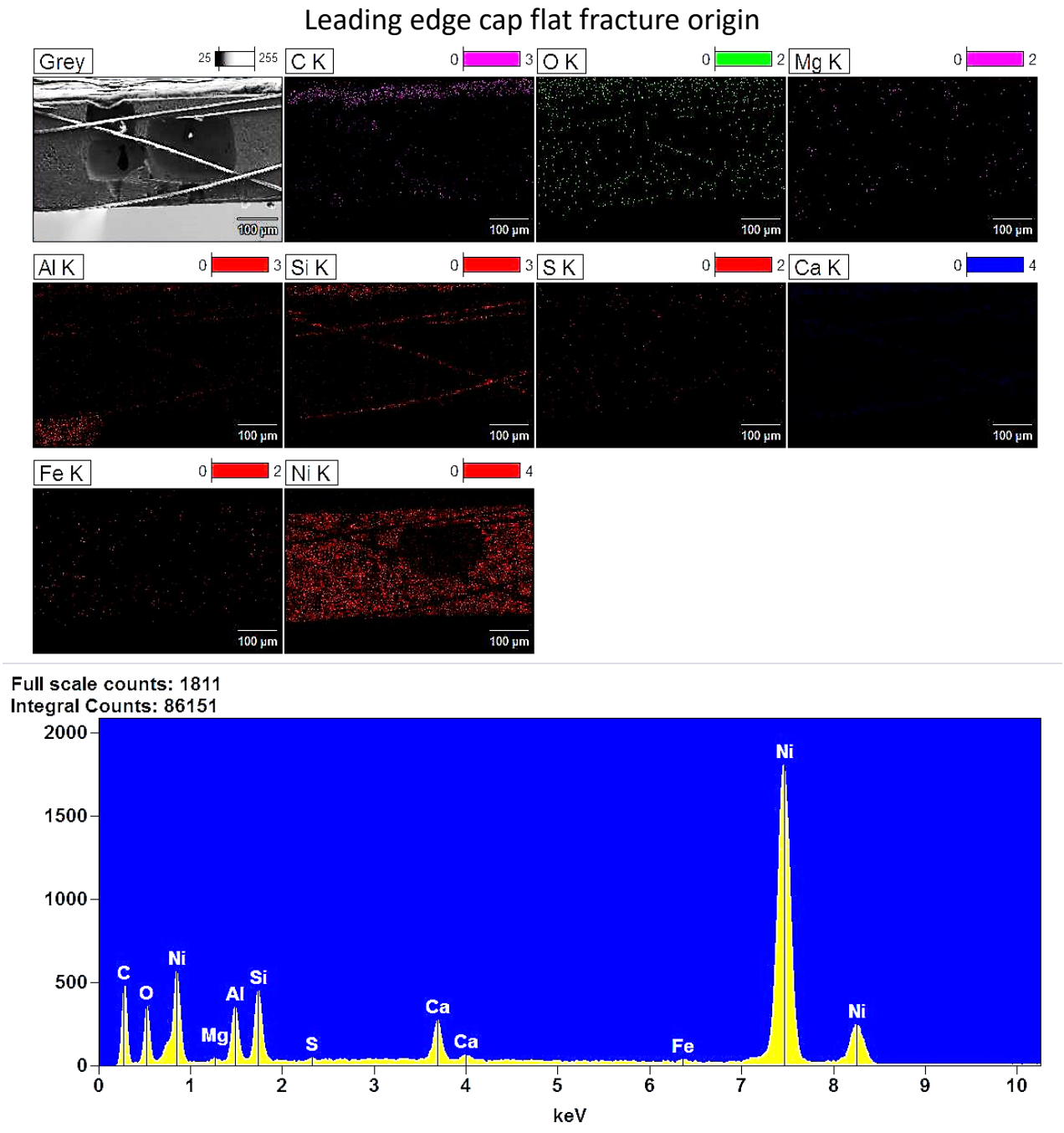

Figure 49: An EDS compositional mapping of the red blade leading-edge cap flat fracture origin area and the associated EDS spectrum.

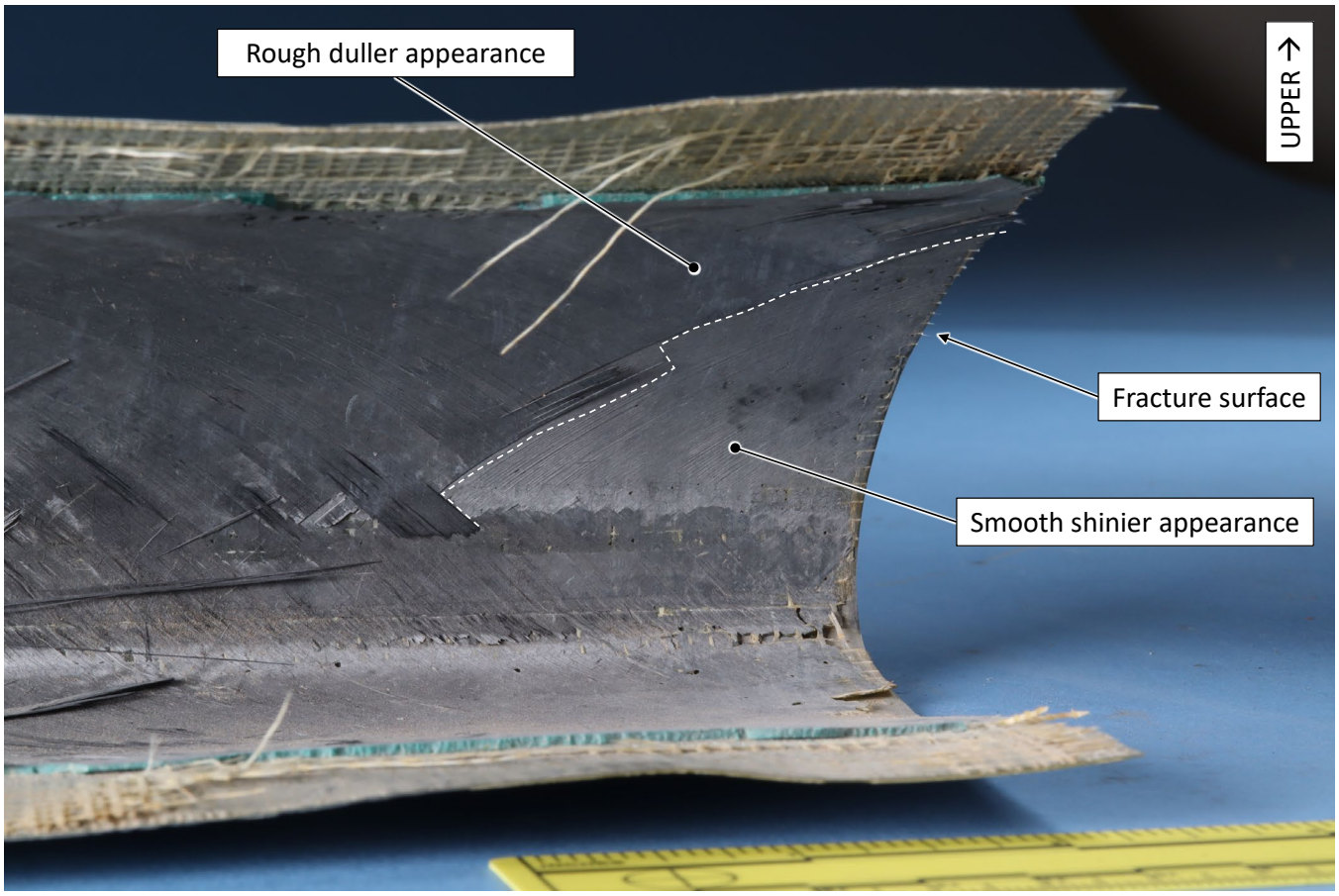

Figure 50: A photograph of the internal adjacent surface of the inboard red blade leading-edge cap flat facture after removal from the spar.

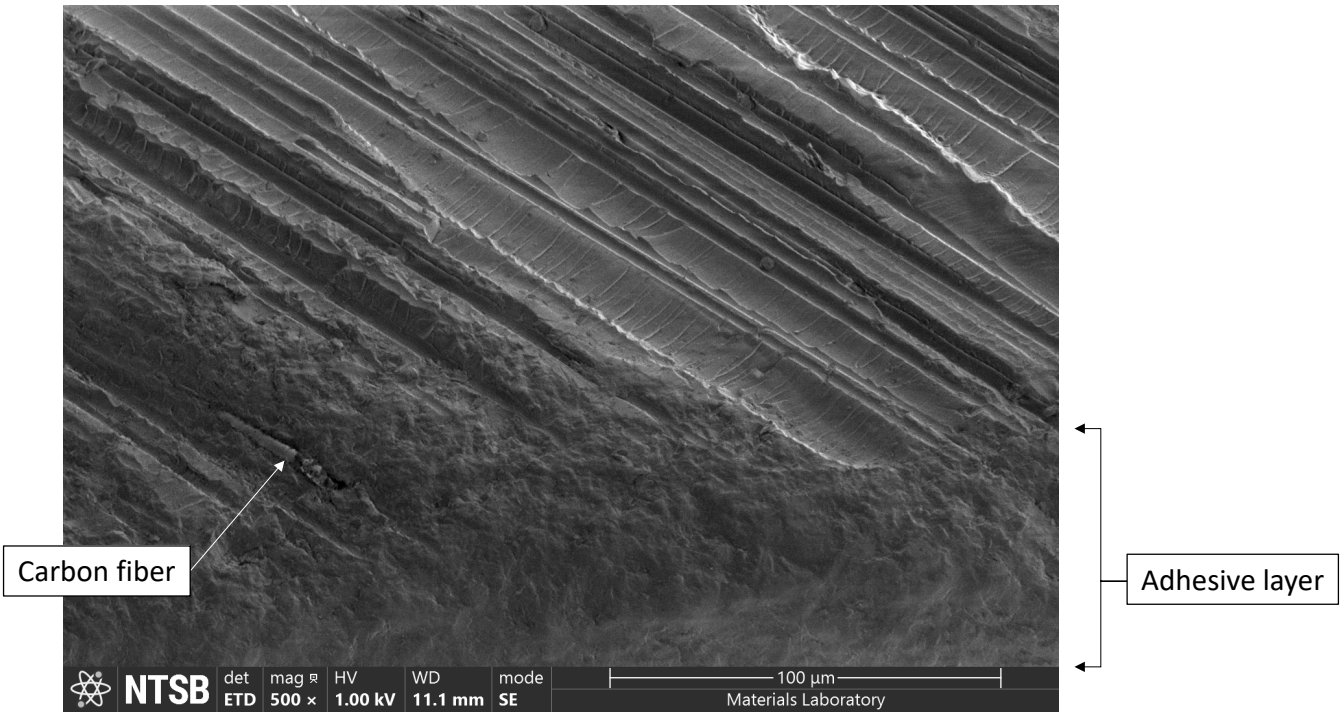

Figure 51: A secondary electron image of the tilted internal adjacent surface of the inboard red blade leading-edge cap flat facture. Fiber tracks were observed and are oriented upper left to lower right with river line features extending between tracks. The fracture features on the adhesive layer between the leading-edge cap and spar were obliterated.

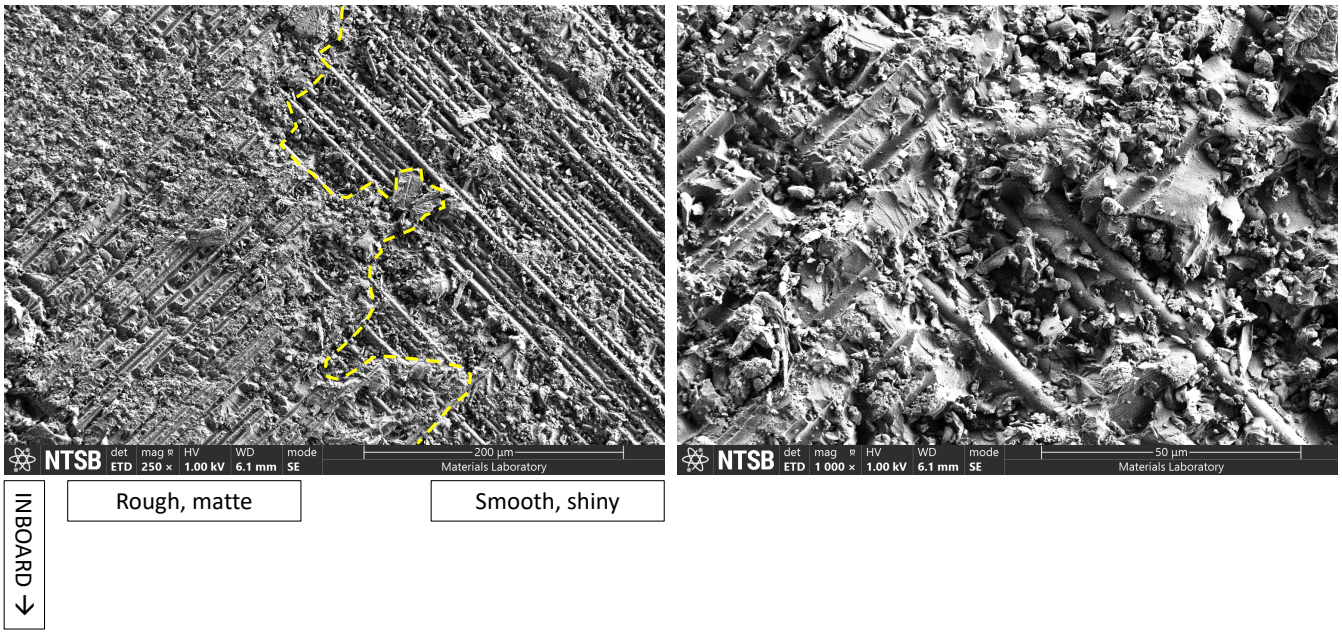

Figure 52: **Left:** A secondary electron image of the boundary (yellow dashed line) between smooth/shiny and rough/matte appearing areas on the spar fracture surface adjacent to the red blade flat fracture surface. **Right:** A higher magnification view at the boundary.

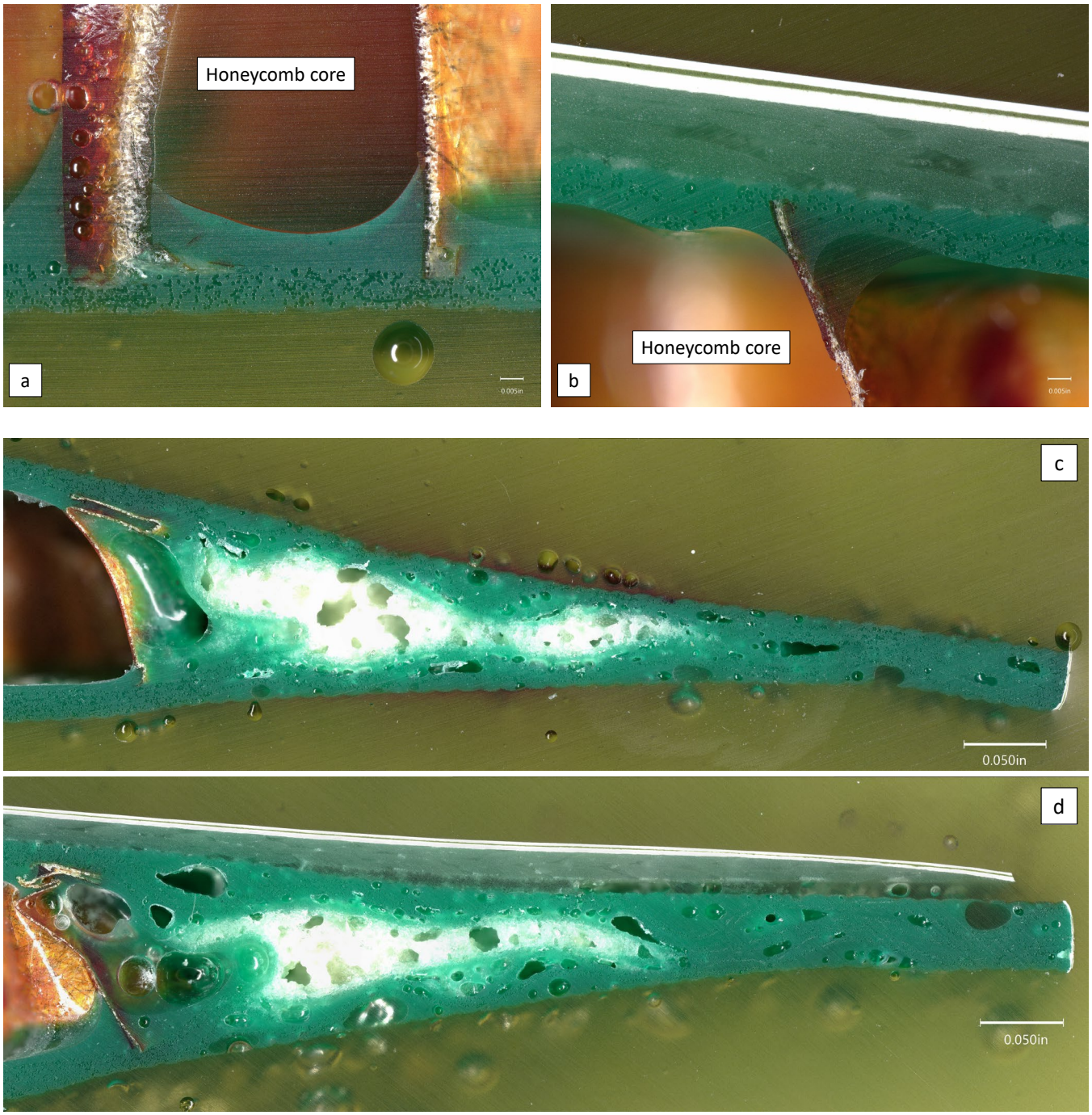

Figure 53: Digital microscope images showing typical cross section views of the yellow blade film adhesive where a) adhesive separation between core and skin was observed, b) skin remained bonded to core, c) both upper and lower skins had separated from the trailing edge, and d) one skin had separated from the trailing edge.

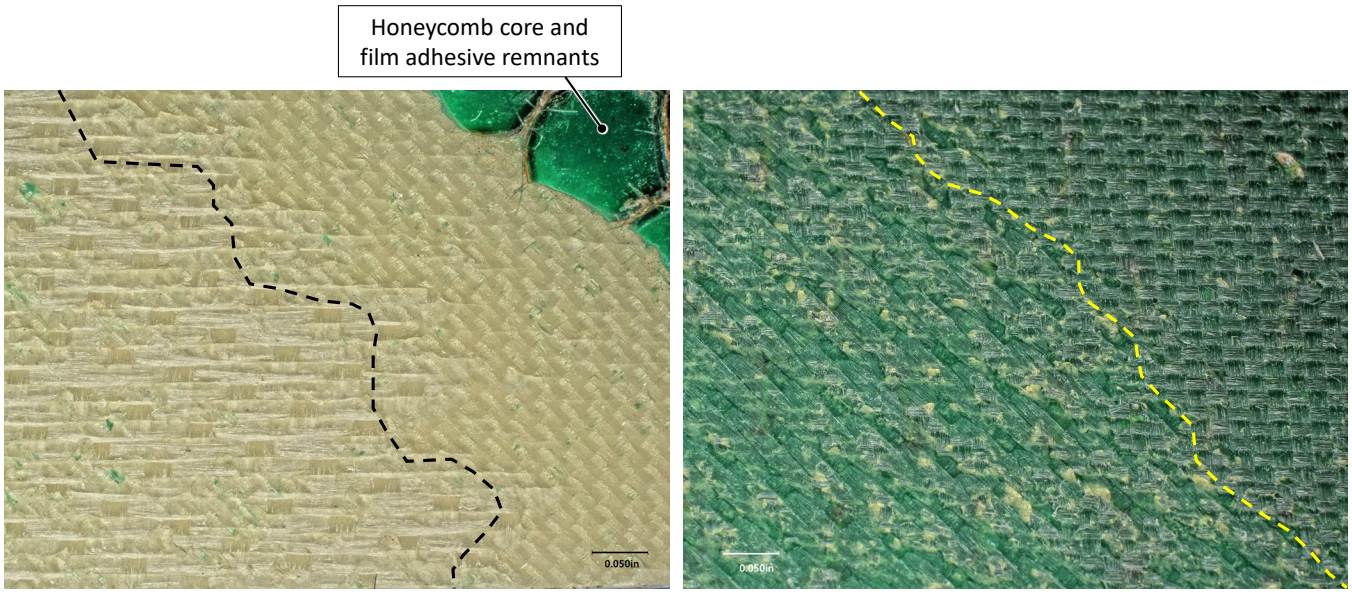

Figure 54: **Left:** A digital microscope image of the internal surface of the blade skin at a boundary (black dashed line) between a 5-harness satin weave pattern (left) and a plain weave pattern (right). **Right:** A digital microscope image of the film adhesive surface on the honeycomb core afterbody at a boundary (yellow dashed line) between a 5-harness satin weave pattern (left) and a plain weave pattern (right).

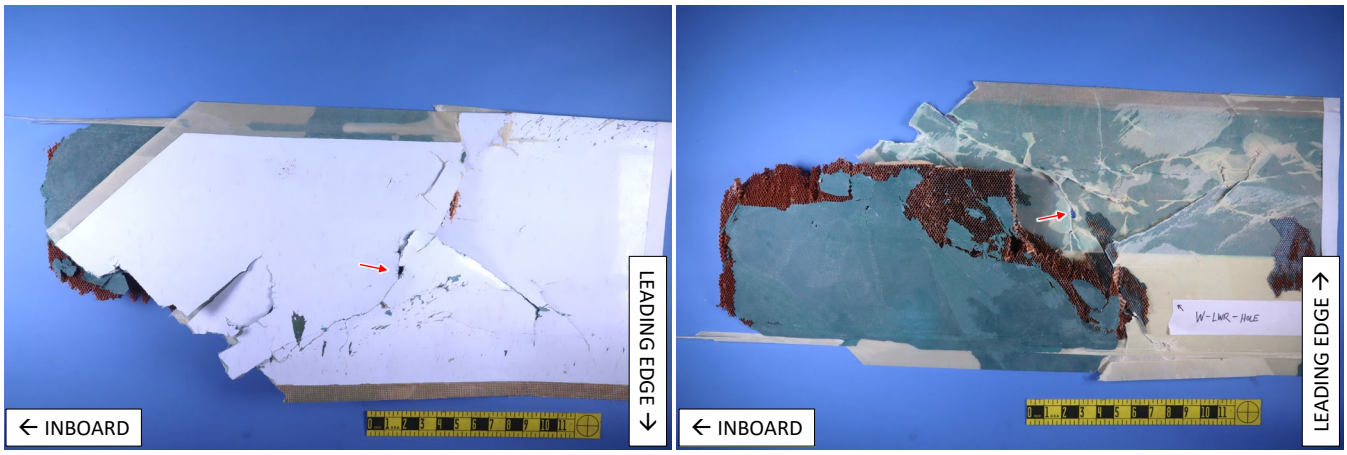

Figure 55: Photograph of the outer surface (left) and inner surface (right) of a piece of separated white blade lower skin with a hole feature (red arrow).

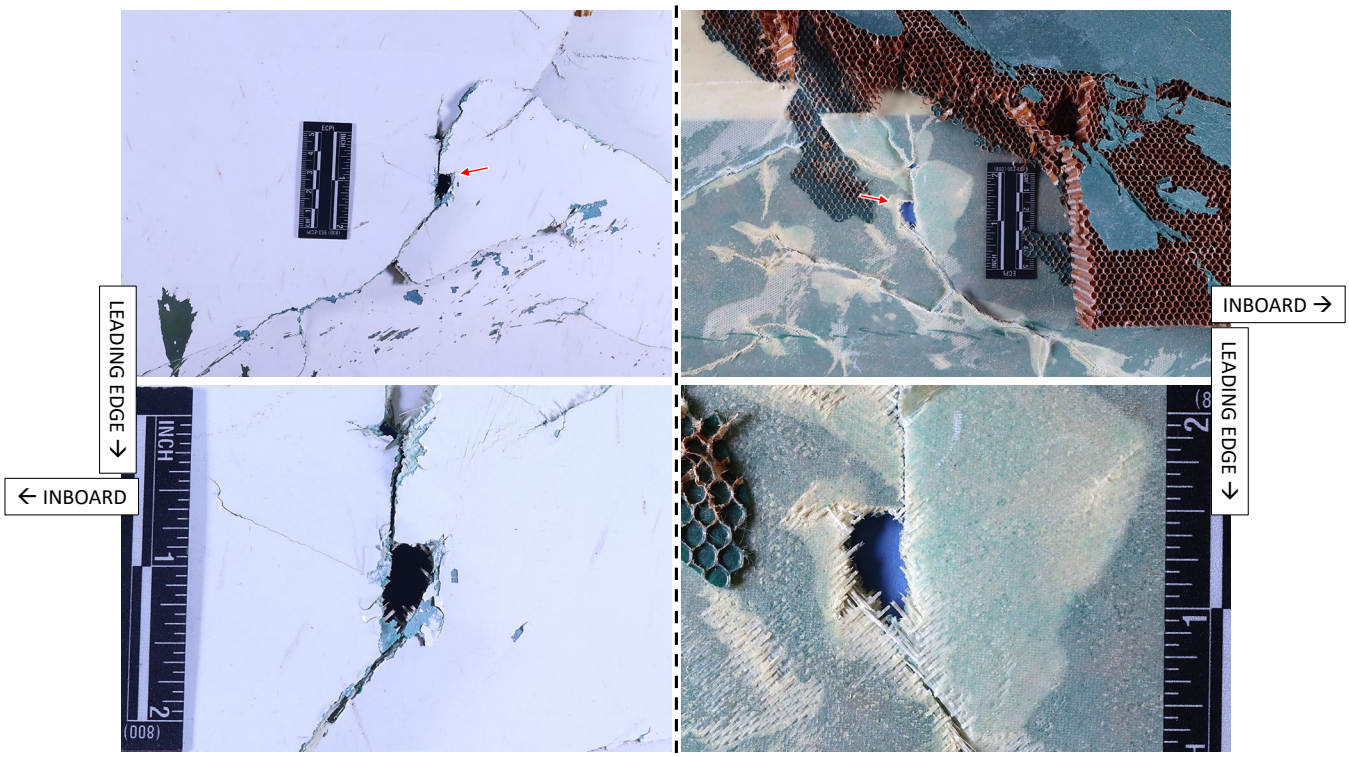

Figure 56: Closer photographs of the white blade lower skin hole feature (red arrow) viewed from the outer surface (left) and inner surface (right).

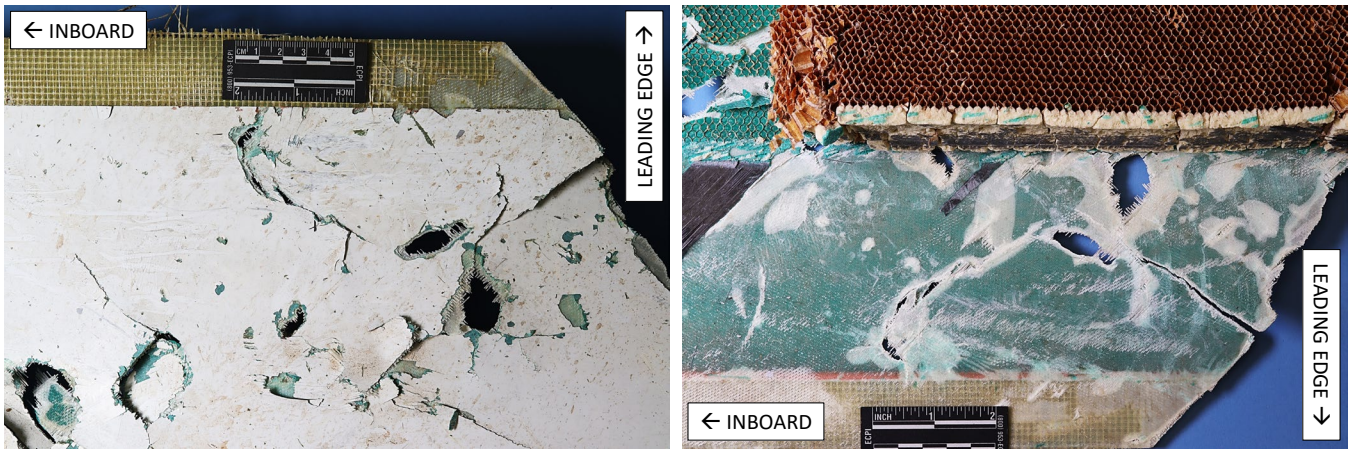

Figure 57: Photograph of the outer surface (left) and inner surface (right) of a piece of separated blue blade skin received from the accident site labeled “these pieces came from inside the tail boom.”